TECHNISCHE UNIVERSITÄT WIEN

VIENNA UNIVERSITY OF TECHNOLOGY

D I S S E R T A T I O N

Analysis and Visualization of Industrial CT Data

Dipl.-Ing.(FH) Christoph Heinzl
Matrikelnummer: 0426441
Altschwendt 84/6
A-4721 Altschwendt, Österreich
geboren am 16.08.1978

Altschwendt, im Dezember 2008

Analysis and Visualization
of Industrial CT Data
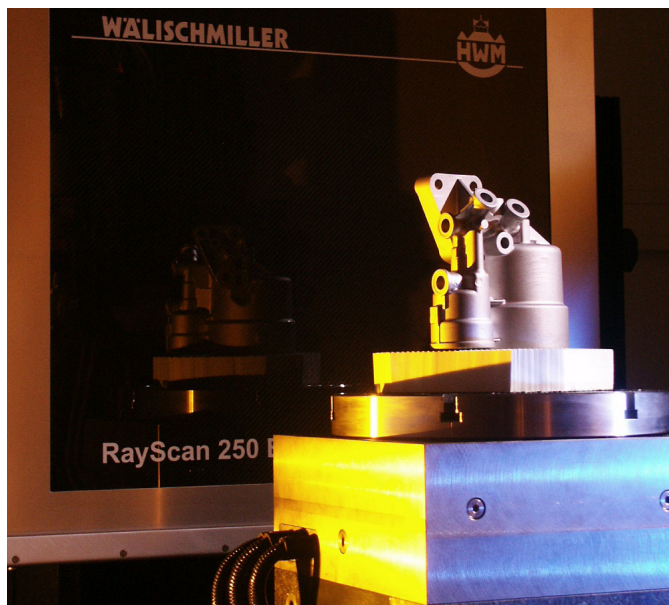
Christoph Heinzl

Institute of Computer Graphics and Algorithms
Vienna University of Technology, Austria

c.heinzl@gmail.com

Visibile facimvs qvod ceteri non possvnt

Abstract

Industrial X-Ray 3D computed tomography (3DCT) is on the edge of advancing from a non destructive testing method to a fully standardized means of dimensional measurement for every day industrial use. Currently 3DCT has drawn attention especially in the area of first part inspections of new components, mainly in order to overcome limitations and drawbacks of common methods. Yet an increasing number of companies is benefitting from industrial 3DCT and sporadically the first pioneers start using industrial 3DCT for quality control in the production phase of a component. As 3DCT is still a very young technology of industrial quality control, this method also faces severe problems, which seriously affect measurement results. Some of the major drawbacks for quality control are the following:

Artefacts modify the spatial greyvalues, generating artificial structures in the datasets, which do not correspond to reality.

Discrete sampling introduces further irregularities due to the Nyquist-Shannon sampling theorem.

Uncertainty information is missing when extracting dimensional measurement features.

Specifications and limitations of the components and the special setup a 3DCT constrain the best achievable measurement precision.

This thesis contributes to the state of the art by algorithmic evaluation of typical industrial tasks in the area of dimensional measurement using 3DCT. The main focus lies in the development and implementation of novel pipelines for everyday industrial use including comparisons to common methods. Convenient and easy to understand means of visualization are

evaluated and used to provide insight into the generated results. In particular three pipelines are introduced, which cover some of the major aspects concerning metrology using industrial 3DCT. The considered aspects are robust surface extraction, artefact reduction via dual energy CT, local surface extraction of multi-material components, and statistical analysis of multi-material components. The generated results of each pipeline are demonstrated and verified using test specimens as well as real world components.

Kurzfassung

Die industrielle 3D Röntgencomputertomographie (3DCT) steht derzeit an der Schwelle von einer zerstörungsfreien Werkstoffprüfmethode hin zu einer genormten Methode für dimensionales Messen. 3DCT wird vor allem im Bereich der Erstmusterprüfung von neuen Komponenten eingesetzt, um die Nachteile und Einschränkungen bisheriger Methoden zu überwinden. Eine steigende Anzahl von Firmen vertraut daher auf 3DCT und sporadisch wird 3DCT bereits von einigen Pionieren für die Qualitätskontrolle in der Produktion eingesetzt. Dennoch ist die 3DCT eine sehr junge Methode mit einigen Nachteilen, die großen Einfluss auf das Messergebnis haben. Einige der größten Nachteile von 3DCT im Bereich der Qualitätssicherung sind:

Artefakte ändern die Grauwerte im Datensatz und generieren künstliche Strukturen, die in Realität nicht vorhanden sind.

Diskretisierung bewirkt Unregelmäßigkeiten in den Grauwerten entsprechend des Abtasttheorems von Nyquist-Shannon.

Informationen bezüglich Unsicherheit der Daten gehen bei der Extraktion von dimensionalen Messmerkmalen verloren.

Spezifikationen and Einschränkungen der einzelnen Komponenten und der Bauweise des 3DCTs limitieren die erreichbare Messgenauigkeit.

Diese Dissertation trägt zum Stand der Technik durch algorithmische Lösungen von typischen industriellen Problemen im Bereich der Metrologie mittels 3DCT bei. Das Hauptaugenmerk der präsentierten Arbeit liegt in der Entwicklung und Implementierung von neuen Prozessketten, die für den täglichen industriellen Einsatz im Bereich der Qualitätssicherung

optimiert sind. Geeignete, einfach verständliche Visualisierungsmethoden werden evaluiert und angewendet, um einen Einblick in die generierten Messdaten zu ermöglichen. Im Speziellen werden drei Prozessketten präsentiert, die einige der wesentlichen Aspekte der Metrologie mittels 3DCT abdecken. Die betrachteten Aspekte sind robuste Oberflächeextraktion, Artefaktreduzierung mittels Dual Energy CT, lokale Oberflächeextraktion von Multimaterialkomponenten und statistische Analyse von Multimaterialkomponenten. Die generierten Ergebnisse jeder Prozesskette werden anhand von Testteilen und typischen Industriebauteilen demonstriert und verifiziert.

Contents

*If I have seen further than others, it is because I've stood
on the shoulders of giants.*

Isaac Newton

Preface

THIS thesis results from a collaborative work of the Institute of Computer Graphics and Algorithms, Vienna University of Technology and the Upper Austrian University of Applied Sciences - Wels Campus from 2005 - 2008 under the great guidance and support of Meister Eduard Gröller. I would like to thank him and also Johann Kastner for mentoring, their trust and their expertise, which was essential to finish this thesis.

Furthermore I would like to express my gratitude to all my collaborators, coauthors and colleagues. I want to thank the CT-group of the Upper Austrian University of Applied Sciences - Wels Campus for the friendly working environment and especially Dietmar Salaberger, Erwin Schlotthauer, Michael Reiter and Franz Pfeiffer for fruitful discussions and their inspirations, contributing to this thesis. Thanks to the vis-group of the Institute of Computer Graphics and Algorithms, Vienna University of Technology, for support, suggestions and valuable advice in designing the different techniques and also for critical comments when preparing conference talks. This work is dedicated to my dearest supporters, my wife Romana, who encouraged me to never give up, supporting me especially in stressful phases of my PhD, and my son Jakob, who reminds me of focusing on the important issues in life, considering problems in an unbiased, childlike way. Thank you!

The purpose of computing is insight, not numbers.

Richard Hamming

1

Introduction
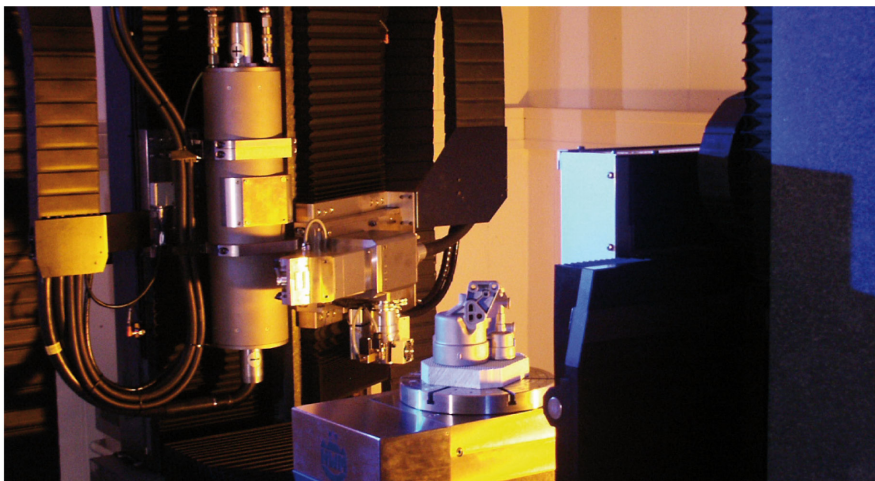
Micro focus source < 225kV	Macro focus source < 450 kV	a-Si Flatpanel detector
Focal spot: > 5 µm	Focal spot: 2.5 mm	Pixel: 1024²
Voxelsize: 5...323 µm	Voxelsize: 150...323 µm	Pitch: 400 µm

Figure 1.1: *Dual source X-ray computed tomography device at Upper Austrian University of Applied Sciences - Wels Campus. Detail images of the main components: X-ray sources and detector (images are courtesy of Viscom, Comet and Perkin Elmer).*

V ISUALIZATION constitutes one of the most exciting enhancements of modern engineering, providing insight using unique and undreamed-of means for transporting information. In an almost inexhaustible multitude of possibilities, it allows to illustrate highly complex problems by means of clear and easy to understand renderings.

Especially engineering benefits from visualization in conjunction with new imaging technology. Novel ways of testing provide unique insight into complex components, which allow precise, fast and after all inexpensive characterizations. Thus, especially in the preproduction phase of a new component these new technologies significantly reduce the design costs, development time as well as time to market. In consequence, the fast return on investment of new developments stimulates research activity in the field of analysis and visualization using novel imaging methods.

1.1 Quality Control

In state-of-the-art engineering, the complexity of a new component is strongly determined by the demanded characteristics. Function integration, weight reduction, stability, flexibility and economic issues are some of the major issues, which have direct influence on complexity. Within the last decades, especially automotive and aeronautic industry formed the new trend of constantly driving the industrial research in the direction of new materials and function-oriented, highly integrated, energy-efficient and lightweight components. As a consequence of the these high demands, also the efforts for quality control of new components are rising.

"Quality" is defined as a degree of excellence or the lack of it [Wik08b], measurable by means of quality control. The output of quality control is a classification as "pass" or "fail" in accordance to the custom requirements of a process. Especially in the preproduction phase of new components quality control is important, in order to assure and enhance the required tolerances of the production process or the component itself. In the production phase, quality control guides the compliance of components to the required level of acceptance.

1.2 Metrology

A major branch of quality control is metrology, the science of measurement [Wik08a], which is used to study the surface and the geometric structure of a component, *e.g.,* by measuring distances, wall-thicknesses or diameters. Common means of metrology permit the evaluation of dimen-
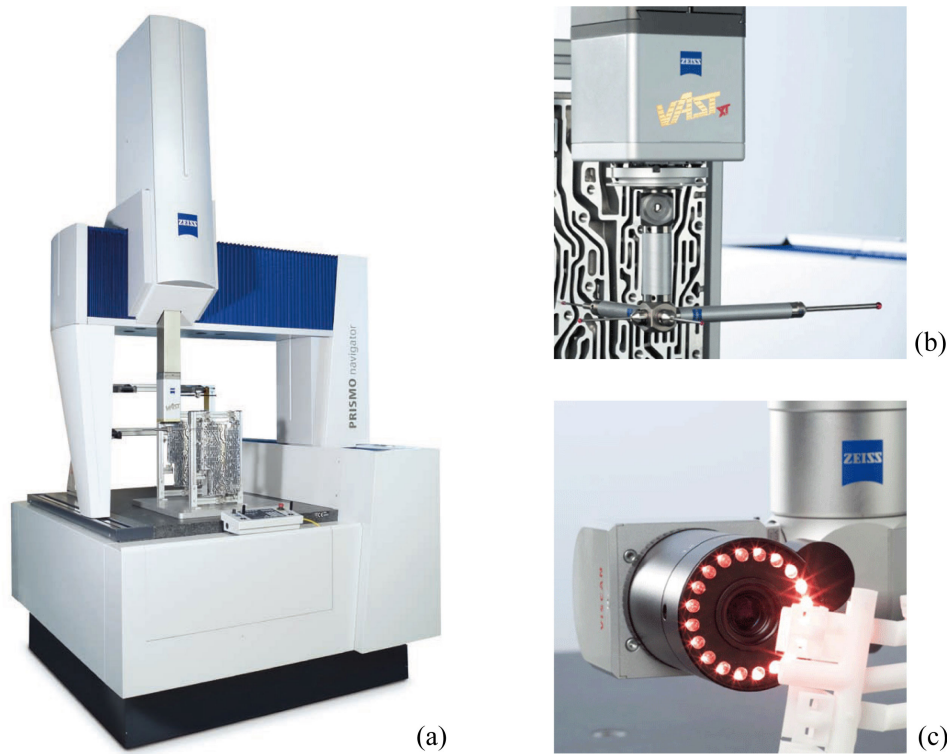
Figure 1.2: *(a) Bridge-type coordinate measurement machine with changeable probe holder. (b) Tactile and (c) optical sensor. Tactile sensors use a stylus for contacting the surface of a component. Optical sensors measure the geometry without touching the surface but are exposed to the optical properties of a specimen (images are courtesy of Carl Zeiss).*

sions at a calibrated precision over a defined measurement area with predefined environmental conditions considering the specimen and the measurement device. To facilitate metrology of industrial components, coordinate measurements are usually carried out using tactile or optical sensors. Figure 1.2 shows a typical bridge-type coordinate measurement machine (CMM) with a changeable probe holder, which may be equipped with custom sensors for the different measurement tasks.

The principle of tactile coordinate measurement is to contact surface points via a stylus, recording high precision position coordinates along a predefined pathway. The position coordinates are evaluated by a software tool, which accumulates the measured position coordinates to geometric features. The demanded measurement features are finally derived from the geometric features and documented in a measurement protocol. The second major branch of coordinate measurement is optical coordinate measurement, which in contrast allows a non touching characterization of a component's surface. Based on the principle of triangulation, the sen-

sor unit projects different patterns on the surface of the component to be measured. Cameras record these projected patterns on the component's surface. The position coordinates are subsequently derived using optical image equations.

While optical and tactile methods have the advantage of permitting high precision calculations of surface dimensions at a calibrated precision within a predefined measurement area, there are also severe disadvantages: Optical sensors are facing problems, when scanning reflecting or transparent probes. Tactile methods produce erroneous results, if the touching force deforms the specimen. Both methods are limited to measuring accessible and visible parts of a specimen. For complex components the programming and evaluation of inspection features is a timeconsuming process. To overcome these limitations new imaging methods are required [Kas08], [Bar07].

1.3   Industrial 3D X-ray Computed Tomography

With its origins in medical X-ray CT, which has been used in clinic routine for decades, 3D X-Ray computed tomography (3DCT) in the industrial context is a rather young method. Industrial 3DCT became popular in the field of non-destructive-testing (NDT) in the last decade. NDT was the first and is still one of the largest application areas using 3DCT [HMMW03].

Compared to medical CT, industrial 3DCT uses a different principle. The principle of common industrial 3DCT, also referred to as cone beam CT, is explained in Figure 1.3: At each angular position of a 360 degree turn a 2D penetration image of the specimen is recorded, which represents the X-ray attenuation generated by the specimen in the form of greyvalue images [KSBS04]. The complete series of penetration images allows to reconstruct the three dimensional distribution of spatial X-ray attenuation in a resulting greyvalue dataset of the measurement area. Figure 1.4 shows the 3DCT devices at the Upper Austrian University of Applied Sciences - Wels Campus. In the lower section the specifications of the main components are listed giving insight into application areas.

In recent years, industrial 3DCT devices were continuously advanced in order to achieve higher resolutions, facilitating highly detailed measurements. Highly detailed measurements are the basis for studying the surface geometry of a component concerning tolerances in distance, shape, profile or position. Currently, the first industrial 3DCTs are passing the frontier to a nanometer resolution, which makes the technology highly attractive for metrology. Consequently, industrial 3DCT was successfully introduced for industrial metrology applications. Especially in this application area, 3DCT gained importance within the last five years because 3DCT allows to overcome current limitations of conventional optical and tactile measure-

X-ray source   Flatpanel detector

Specimen
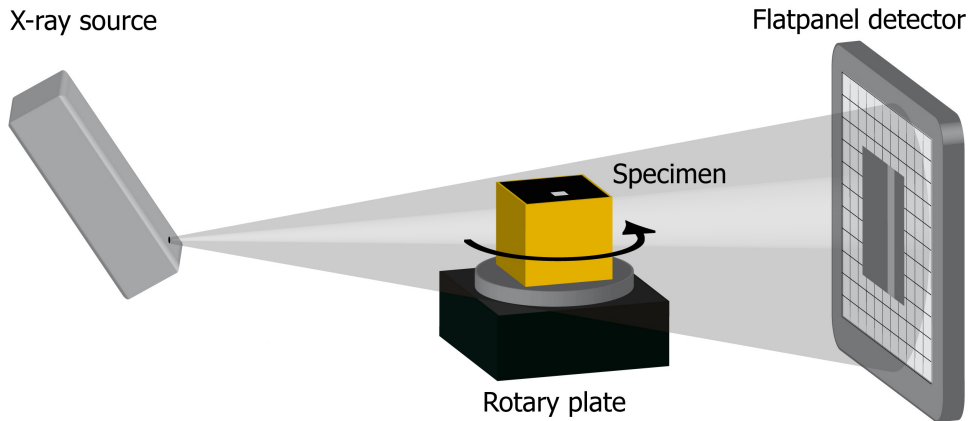
Rotary plate

Figure 1.3: *Principle scheme of industrial 3D X-ray computed tomography: X-ray source (left), rotary plate with specimen (center), matrix detector (right). A single rotation of the specimen is sufficient for full characterization concerning material and geometric features.*

ments in case of reflecting or transparent probes as well as probes with deformable surfaces. Figure 1.5 shows a diagram of different industrial 3DCT types, which depicts the typical object diameter and achievable resolution of each method.

The main characteristics and advantages of 3DCT compared to conventional metrology are summed up in the following enumeration:

Fast Compared to conventional means of metrology and non destructive testing 3DCT is a fast method. Typical scan times are about 30 minutes. Although the evaluation of the scans is computationally expensive, typical evaluations take about 2-3 hours.

Non-touching 3DCT allows a non-touching characterization. Even flexible or soft parts can be measured.

Non-destructive 3DCT non-destructively penetrates the specimen with X-rays. The X-ray attenuation is measured by a flat panel detector. If the absorption of materials differs, the materials are distinguishable.

Measurement of hidden or internal features 3DCT is the only method, which fully characterizes a specimen including the complete outer and inner structure of a specimen. Also hidden structures (*e.g.,* inner holes, voids or cooling channels) within the component can be measured without disassembling or destroying the specimen.

Despite of all these advantages, currently only optical and tactile coordinate measurements are capable of extracting measurement results at a

Sub-μCT
(phoenix|x-ray nanotom)

Dual Source CT (μCT, mCT)
(HWM RayScan 250 E)

|	Sub-μCT:	μCT:	mCT:
X-ray power :	< 180 kV	< 225 kV	< 450 kV
Detector:	2300 * 2300 Pixel	1024 * 1024 Pixel	1024 * 1024 Pixel
Voxelsize:	0.5 - 30 μm	5 - 323 μm	150 - 323 μm
Objectdiameter :	max. 120 mm	max. 600 mm	max. 600 mm
	smaller specimens		larger specimens
	higher resolution		lower resolution
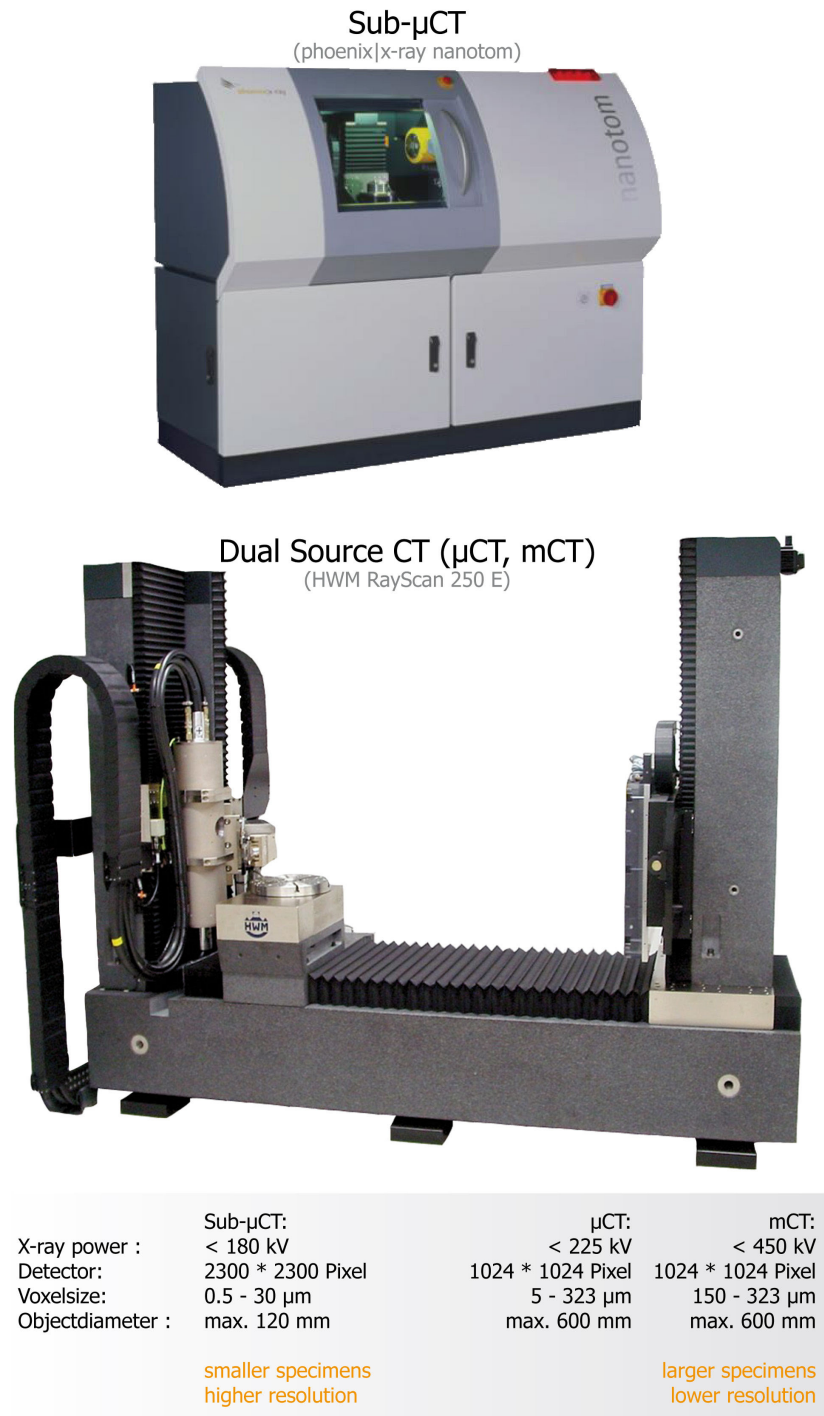
Figure 1.4: *Industrial 3DCT devices at the Upper Austrian University of Applied Sciences - Wels Campus including the specifications of each CT modality.*
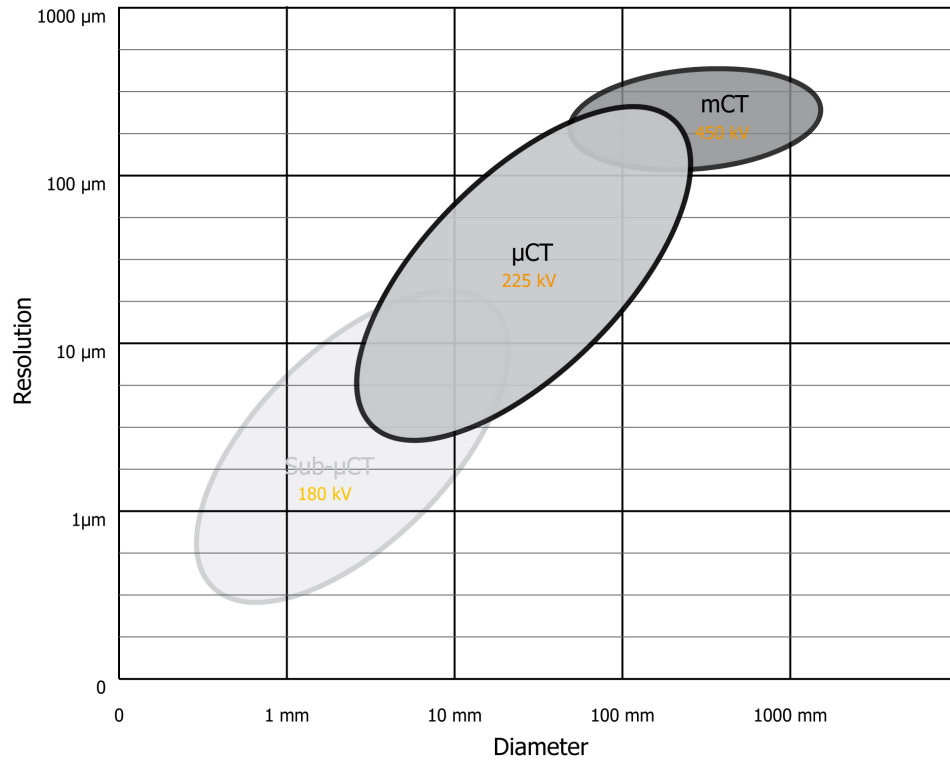
Figure 1.5: *Diagram of achievable resolution and object diameter for the different CT types at the Upper Austrian University of Applied Sciences - Wels Campus.*

calibrated precision in accordance to valid standards. Currently a standardization committee is working on regulations for metrology using 3DCT. For the moment no standard exists in the area of 3DCT, neither for non destructive testing, nor for metrology. For this reason absolute dimensional measurement results depend on the calibration procedure of the device manufacturers.

The special design of the dual source 3DCT device at the Upper Austrian University of Applied Sciences - Wels Campus (see Figure 1.1 and 1.4), which was used for all scans in the presented work, combines two different X-ray sources in a single CT system. The 225 kV micro-focus source has a very small focal spot with a size of 5 - 300 μm in diameter, depending on the used energy setting. This setup (micro-focus CT, μCT) allows characterizing small objects down to 5 mm in diameter, reaching a spatial resolution of up to 5 μm. The 450 kV macro-focus source produces X-ray radiation at a significantly higher level. Due to the higher energy level and a different design, this source has a fixed spot size, which is about 2.5 mm in diameter. So this setup (macro-focus CT, mCT) is suitable for specimens with higher penetration lengths and higher densities. The disadvantage
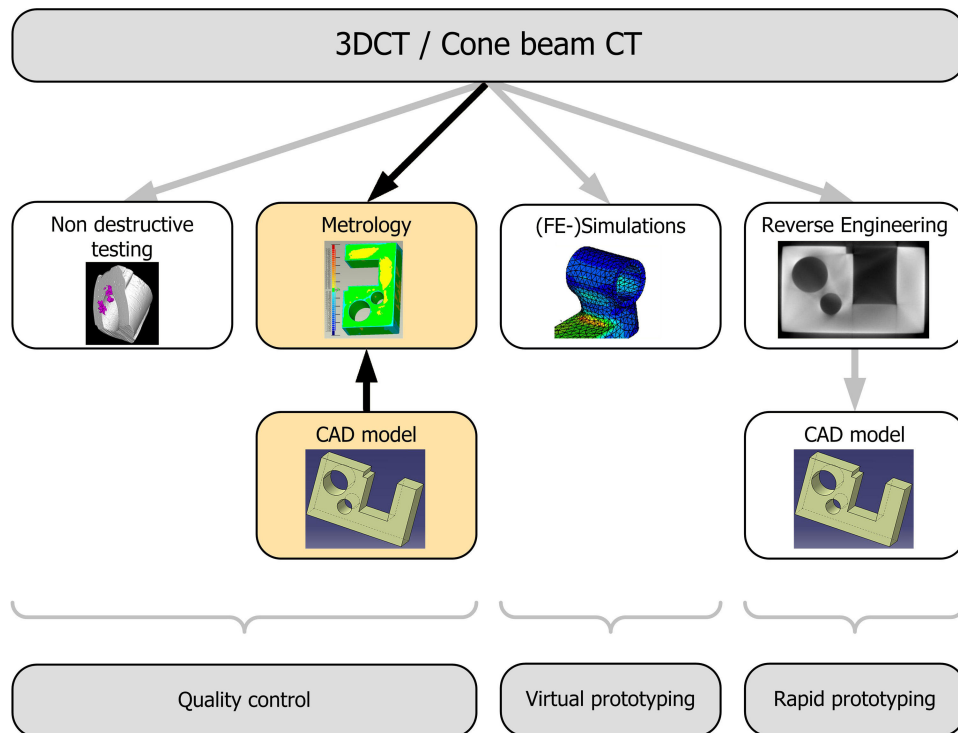
Figure 1.6: *Applications of industrial 3DCT in the areas of quality control, virtual and rapid prototyping (FE-simulation image is courtesy of CAE Simulation & Solutions).*

of the macro-focus compared to the micro-focus setup of this dual source system is that the best achievable spatial resolution is just about 150 μm compared to 5 μm using the micro-focus setup. However, the combination of two different X-ray sources allows a significant expansion of the application areas of this 3DCT device. Furthermore it allows to combine scans of both sources to facilitate novel scanning technologies, *e.g.,* dual energy CT which chapter 3 and chapter 4 are based on.

The main application areas of 3DCT are shown by Figure 1.6: The original and still the largest application area of 3DCT is non-destructive-testing (NDT). In NDT, especially internal structures, *e.g.,* shrink holes, material enclosures or cracks, are of interest. The presented work is focussed on the second major application area of 3DCT: Metrology for dimensional measurements of 3D geometry features. In this context the evaluation of critical measurement features is of interest, *e.g.,* distances, wall thicknesses or diameters. Especially for the following types of components, 3DCT outperforms conventional means of metrology:

Small parts While for small parts of 5 mm in diameter and below, conventional tactile and optical coordinate measurement is timeconsum-

ing, difficult and in several cases impossible, 3DCT is the method of choice in this application range.

Deformable components The touching force of tactile methods deforms the specimen. Therefore either the extracted dimensional feature is erroneous or the stylus is not even able to record touch points from the surface of flexible or soft parts.

Inner geometry / hidden structures As X-rays penetrate the measured specimen, 3DCT also evaluates hidden and internal structures without destroying the specimen. Conventional methods are limited to measuring accessible and visible parts of the specimen.

Optical reflective or transparent components Optical methods usually fail when scanning reflective or transparent components. Using non reflective contrast sprays a measurement may be feasible, but also the specimen gets contaminated.

Applied in the area of NDT and metrology, 3DCT is able to cover a large part of quality control.

3DCT is also beneficial in the field of virtual and rapid prototyping. In virtual prototyping using 3DCT, surface models of scanned prototypes are generated, which allow to directly and non-destructively consider and improve the geometry of prototypes in the preproduction phase. Another highly interesting application area of 3DCT is reverse engineering and rapid prototyping: A CAD model is extracted out of a 3DCT scan, which allows to reproduce and duplicate components. All in all, the application spectrum of 3DCT is widespread and diversified.

1.4 Artefacts

The most critical problem, which industrial 3DCT is facing these days are artefacts and their effects on the quality of the resulting dataset. Artefacts are artificial structures in the scan result, which do not correspond to reality. Industrial 3DCTs, which are based on cone beam geometry and matrix detectors, are prone to artefacts like noise-induced streaks, aliasing, beam-hardening, partial volume and scattered radiation effects [Hsi03]. Therefore the quality of the datasets is easily affected by the environmental conditions of the measurement. Some of the parameters which have a major contribution to the dataset's quality are: the specimen's geometry, the penetration lengths, the positioning of the specimen in the cone beam, the measurement parameters and the specimen's material combination. Down to lower resolutions of emerging sub-μCT, also thermal expansion may come into play, generating unsharp and distorted 3D datasets. In Table 1.1 some of the most common artefact types in 3DCT are depicted.

Table 1.1: *Most common artefact types in 3DCT*

Artefact	Image	Physical background
Beam hardening		For polychromatic radiation the correlation between attenuation and penetration length is nonlinear. Therefore thicker objects seem to reduce radiation by a smaller amount compared to thinner objects, resulting in grey-value modifications in the reconstructed dataset towards inner regions of the specimen.
Scattered radiation		Physical effect of Compton scattering and other scattering processes in the material. Greyvalues in the inner material areas and in air regions are elevated. Edges are blurred and contrast gets worse.
Streaking artefacts		High density objects are not fully penetrated by radiation. Too low detector dynamic range. Insufficient number of projections used while scanning.
Ring artefacts		Inhomogeneities of neighboring detector pixels. The rotation of the specimen produces circular artefacts.
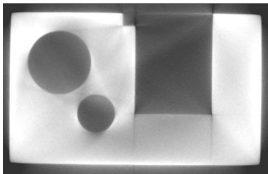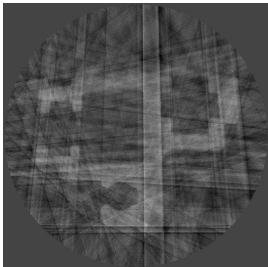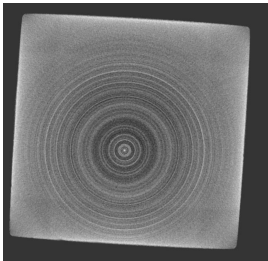
Artefact	Image	Physical background
Partial volume effect		Too low spatial resolution modifies greyvalues.
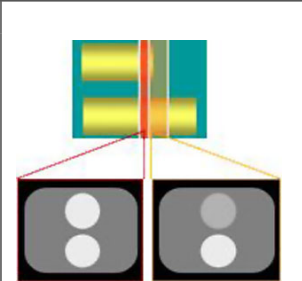
For single material components there are several methods on compensation of artefacts. Olson et al. [OHP81] and Fuchs [Fuc98] use prior information on the material characteristics and the spectrum of the X-ray source in order to compute reprojections of the reconstructed scan. However the material information and especially the spectrum of the X-ray source is in most of the cases unavailable. Kasperl [Kas05] proposed an algorithm, which is widely used in industrial 3DCT, called Iterative Artefact Reduction (IAR). The IAR is based on the linearization technique of Herman [Her79], which applies a nonlinear characteristic correction curve on the volume dataset (see Figure 1.7). This correction curve is directly extracted from the dataset without using a calibration object. Projection images are pre-processed applying the correction curve, which is extracted from the post-processing step of the reconstruction. Therefore the correction curve is enhanced in each iteration and consequently the artefacts in the datasets may be reduced. A related method was introduced by Hopkins et al. [HDL*04]. The major disadvantage of these methods is that for each specimen and material a new characteristic curve has to be extracted. Furthermore the quality of the correction curve depends to a large extent on the quality of the segmentation of a considered material.

For multi-material components, common artefact reduction methods are not applicable and currently there is no multi-material artefact reduction method available. Nevertheless a huge amount of industrial components consist of more than one material, at least after assembly. In this application area 3DCT currently suffers from the introduced artefacts, which prevent a reliable dimensional measurement. Accordingly, the 3D reconstruction of the component's surface produces inaccurate and erroneous surface models, which can not be used in the area of prototyping. To circumvent artefacts due to multi-material components, a disassembly into single material components and subsequent separate scans are helpful. The negative point is that the component gets modified and in several cases destroyed. Furthermore, scanning time and memory consumption are multiplied in accordance to the number of disassembled materials.
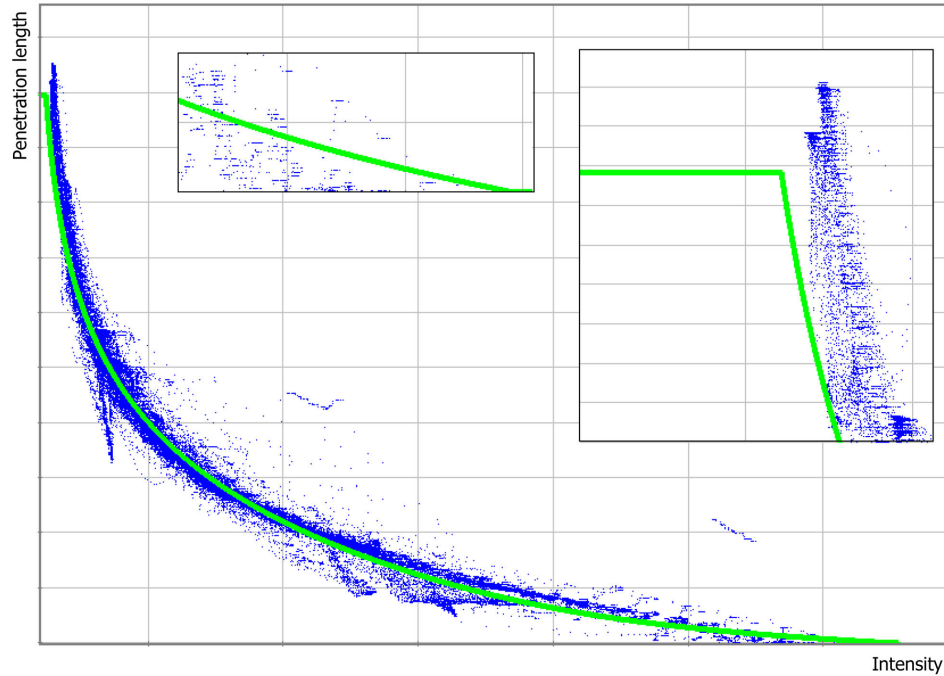
Figure 1.7: *Typical artefact correction curve extracted using Iterative Artefact Reduction (IAR). The IAR is based on a linearization technique applying a nonlinear characteristic correction curve on the volume dataset. The detail images zoom into the start and the end of the curve (images are courtesy of Fraunhofer IIS/EZRT).*

1.5   Scope of Thesis

Despite of being a rather young technology, which is in addition still exposed to severe problems, 3DCT has attracted the interest of major companies in automotive, aeronautic, electronics, leisure industry as well as many other industrial fields. Driven by the advantages of 3DCT, of non destructively and fully characterizing a specimen including geometrical structure, material composition and defects, these companies invest in the technology of 3DCT to overcome current limitations of conventional quality control. Especially in the preproduction phase of a new product, 3DCT is already an inexpensive and fast means of quality assurance, which allows significant reduction of development costs and time to market.

This thesis aims at taking the next step from visual inspection of 3DCT scans in non destructive testing towards qualitative evaluation of 3DCT datasets in dimensional measurement. The main focus lies in the algorithmic evaluation of 3DCT datasets and in providing insight using convenient and clear visualizations. Application scenario is metrology of typical industrial components, which are affected by artefacts because of their complexity, material decomposition or limitations of the used 3DCT devices.

Three novel approaches are presented, which focus on some major draw-
backs of metrology using industrial 3DCT:

Robust Surface Extraction for Dimensional Measurement deals with the
problem of extracting surfaces from artefact-affected scans of
complex, homogeneous material specimens.

Surface Extraction from Multi-Material Components using Dual Energy CT
addresses the topic of metrology for multi-material components
using the novel data acquisition technique of dual energy CT.

Statistical Analysis of Multi-Material Components using Dual Energy CT
aims at analyzing the spatial uncertainty of datasets from multi-
material components.

What this thesis is not about is development of the CT device, *e.g.*, cali-
bration and analysis of the base dimensional measurement precision of CT
devices. These issues are considered to be out of scope and are therefore
not treated in this work.

The trouble with measurement is its seeming simplicity

Unknown

2

Robust Surface Extraction
for Dimensional Measurement

Volumetric data   Watershed segmentation   Surface mesh
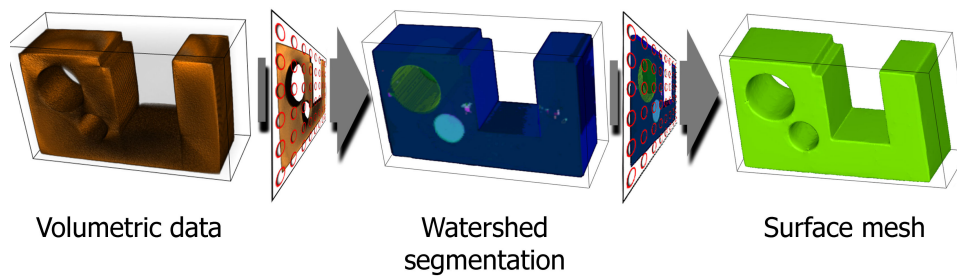
Figure 2.1: *Homogeneous industrial work piece segmentation based on 3D watershed and constrained elastic-surface nets for local surface extraction.*

SURFACE extraction constitutes one of the main chal-
lenges in the area of metrology using industrial 3DCT
data. As the extracted surface is used as ground truth for
each further dimensional measurement evaluation, the surface
extraction algorithm has a major influence on the quality of the
extracted measurement results.

This chapter addresses the topic of surface extraction of ho-
mogeneous industrial components. A robust method is pre-
sented for creating surface models from volume datasets with
distorted density values due to artefacts and noise. The sur-
face extraction pipeline uses a pre-filtering step to reduce noise
and artefacts without blurring edges in the dataset. A wa-
tershed filter applied on the gradient magnitude information
of the smoothed dataset creates a binary dataset. Using con-
strained elastic-surface nets, a smooth but feature preserving
mesh is created from the binary volume.

The major contribution of this method is the development of a
specific processing pipeline for homogeneous industrial com-
ponents to handle large resolution datasets of industrial 3DCT
scanners. The pipeline is crucial for the following visual inspec-
tion of deviations.

2.1   Introduction

In modern engineering the complexity of industrial products is continu-
ously increasing, while development times have to be as short as possi-
ble [SS00]. To meet these short periods in rapid product development, the
requirements in terms of quality assurance are very high.

Actual/nominal comparison is a common means of quality assurance,
used to compare the measured geometry of a specimen with reference ge-
ometry data. The aim of this process is to get an overview of the deviation
at each location of the specimen. In dimensional measurement primarily
crucial distances are of interest, in order to compare a component's dimen-
sions with the specifications of a computer aided design (CAD) model. Es-
pecially the automotive industry is interested in actual/nominal compari-
son and dimensional measurement to verify the quality of prototypes and
samples. For example in the case of an oil filter housing, shape distortion
may occur while cooling down the melted material. So it is essential to
adapt the production process to guarantee specified tolerances and finally
to reach an optimal shape of the component. Other application areas can
be found in aeronautics, electronics, and leisure industry.

For common surface-model extraction-tasks in industrial applications,
usually a single isovalue is specified to distinguish between material and
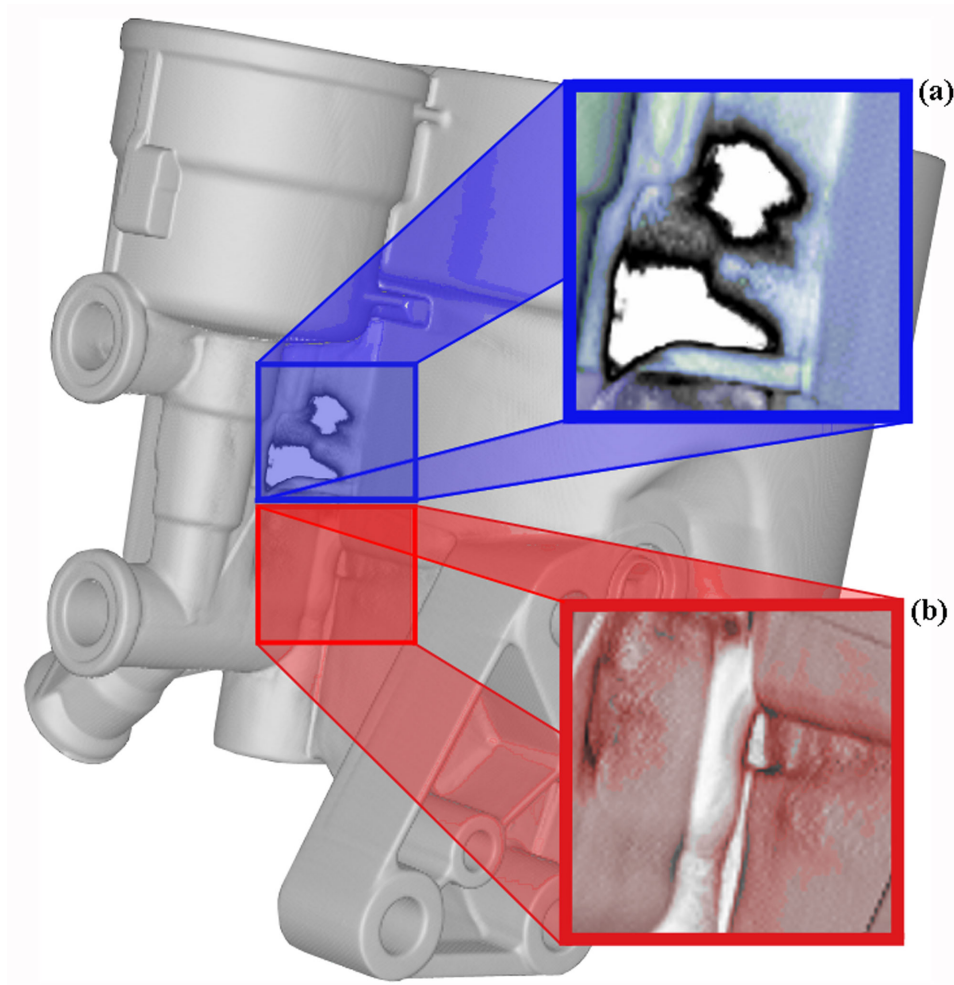
Figure 2.2: *CT dataset of an industrial filter housing, large penetration lengths and complex geometry result in heavy artefacts. (a) thinning and holes, (b) additional volume through thickening.*

air [Vol04]. A polygonal mesh is extracted along the selected isovalue using a surface creation algorithm. For example the marching cubes algorithm creates triangle models of constant density surfaces from 3D volume data [LC87]. However, in datasets with distorted density values, the classification of material with a single, global threshold is difficult and sometimes impossible. Artefacts modify the greyvalues in areas of complex geometry and large penetration lengths. With a global isovalue, structures are added due to artefacts in certain areas, while in other regions the structure is thinned and even holes appear. In Figure 2.2 these cases are depicted showing a 3D view of a complex die-cast component with a global isovalue. The blue detail image (a) still shows big holes emerging in the

structure, while in the red detail image (b) volume is already added.

To avoid getting a falsified surface through unprocessed densities, it would be better to have a modified dataset, which works with just one global threshold. In this case a surface creation algorithm would lead to results with sufficient accuracy. As 3DCT is prone to produce artefacts, a mechanism is required, which enhances the dataset, so that a single threshold is sufficient.

As CT datasets always contain artefacts to a certain degree, this chapter concentrates on designing a new method, that locally adapts contours [HKKG06] (see Figure 2.1 and Figure 2.3). Therefore a pipeline is created, which considers the greyvalues of the volume dataset as "ground truth". The major aim is to extract as much information of the dataset as possible. The pipeline has to be robust with respect to artefacts and it has to be applicable in actual/nominal comparison or dimensional measurement tasks. Furthermore, it has to be practicable in terms of data-processing speed and quality.

2.2   Related work

There are several methods in the area of industrial computed tomography, that try to improve on artefact-affected data. Generally they can be grouped into two sets. Either the dataset is enhanced by artefact reduction, *e.g.* see the work of Kasperl [Kas05], so that a single threshold is sufficient. Or the dataset is considered as "ground truth" and the best possible surface is extracted.

Steinbeiss [Ste05] developed an algorithm that locally adapts a global threshold setting. First, an initial isosurface is generated using a suitable global threshold. Along the direction of the surface normal of a considered vertex, the algorithm creates a greyvalue profile. The vertex location is then moved to the position with the maximal gradient magnitude. In a further refinement, the local greyvalue level of material and background is determined. The vertex location is adjusted to the position of the mean of local material and background grey values. The method is sensitive to noise of real CT-scans, which Steinbeiss tries reduce by considering neighboring greyvalue profiles. Due to averaging of vertex positions the algorithm modifies the surface and it cannot distinguish between noise and small details.

Whitaker and Breen [WB98] introduced an approach that directly operates on voxel data. In this approach the intermediate step of converting data to another representation is not necessary. The basic idea is to consider the zero level-set of a volume as a deformable surface. The surface is then deformed in order to minimize the mean curvature on the surface. However this approach does not contain any data prefiltering to reduce arte-

facts. Furthermore it does not generate a surface mesh, which is necessary in common industrial reverse engineering tools like Geomagic Qualify.

Bischoff and Kobbelt [BK02] have presented algorithms on isosurface-topology simplification and isosurface reconstruction with topology control. They use a priori knowledge about the topology of the input data to eliminate the topological artefacts that arise from the noise. Let us assume that the desired topology and an approximating shape are known beforehand. An initial triangle mesh is then adjusted to match a given shape by applying topology-preserving operations. Bischoff and Kobbelt's approach is not suitable for our application scenario because topolocial information is not known a priori.

Gibson [Gib98] proposed a method which extracts a surface from binary data. This algorithm detects surface vertices depending on the eight greyvalues of a volume cell. After connecting the surface vertices, the surface net is relaxed minimizing an energy measure. The original segmentation is maintained by a constraint forcing each vertex to stay within its original volume cell. Triangulation of the surface points generates the final surface model. Gibson's method assumes binary segmented data as input. For our application it has to be extended with a mechanism for artefact reduction and for binarization. In the presented pipeline model these extensions are introduced.

2.3 Homogeneous industrial workpiece segmentation

In order to extract as much information from a dataset as possible, the use of fully three dimensional preprocessing algorithms is essential. This guarantees, that no information about the third dimension gets lost. An information loss may occur if one executes a segmentation algorithm just on two dimensional slice images. In the following subsections all components of the proposed pipeline (see Figure 2.3) are discussed in detail:

2.3.1 Anisotropic Diffusion Filter

As 3DCT scans are affected to a certain degree by ambient noise, postprocessing steps are subjected to uncertainty. To reduce ambient noise as well as smaller artefacts, a smoothing algorithm has to be applied. Standard isotropic diffusion methods, for example Gauss filtering, blur the input image with a filter kernel applied on each voxel. As each voxel is blurred, boundaries are moved. Therefore these methods are unacceptable for geometry-comparison tasks. In order to provide the segmentation with smooth input data without blurred edges, an anisotropic diffusion filter is applied.

VOLUME DATA

Anisotropic Diffusion Filter

Gradient Magnitude

Watershed Segmentation

Constrained Elastic Surface Nets

SURFACE MODEL
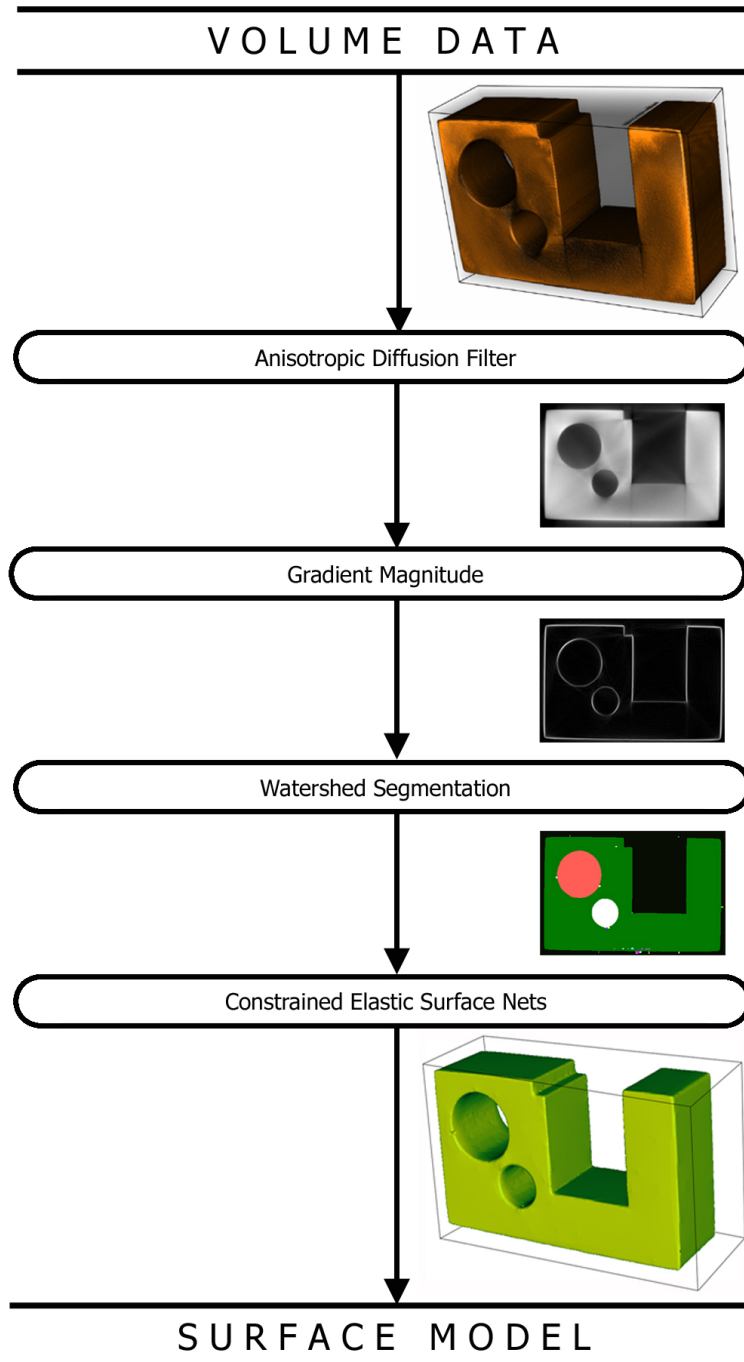
Figure 2.3: *Workpiece segmentation and surface extraction of homogeneous industrial components; Input: volume dataset with distorted greyvalues, Output: Surface mesh.*
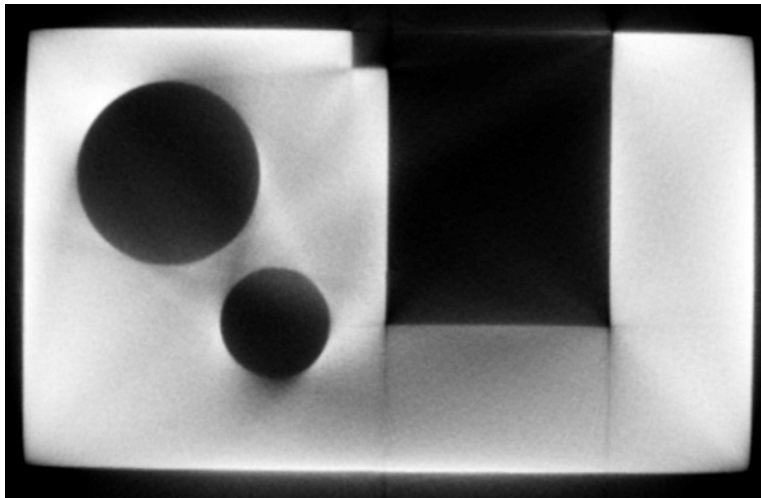
(a)
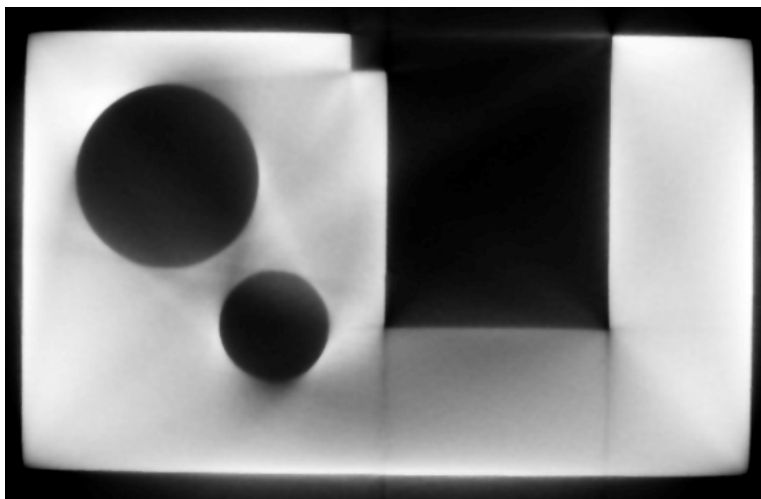
(b)

Figure 2.4: *Anisotropic diffusion filter, axial cross section through a testpart, (a) scattered radiation artefacts throughout the material, (b) after anisotropic diffusion filtering small artefacts, noise and other irregularities are reduced.*

Anisotropic diffusion methods are used to reduce noise in images while preserving specific image features [PM90], *e.g.*, edges, fine details or surface structure. Perona and Malik's method calculates multiscale descriptions of images. If an image $U(\mathbf{x})$ is embedded in a higher dimensional function of derived images $U(\mathbf{x}, t)$ then this higher dimensional function represents the solution of the heat diffusion equation,

$$\frac{dU(\mathbf{x}, t)}{dt} = \nabla \cdot C \nabla U(\mathbf{x}, t) \qquad (2.1)$$
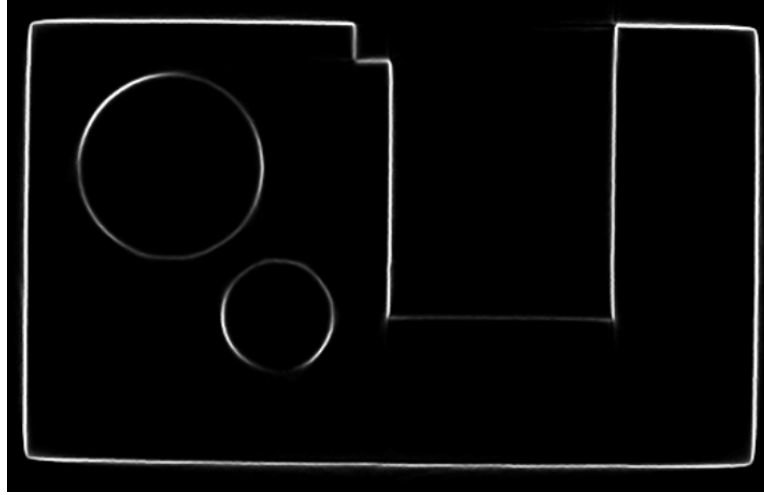
Figure 2.5: *Gradient magnitude filter, axial cross section through a testpart. Bright areas depict high gradient magnitudes while dark areas show low gradient-magnitude values.*

which is constrained by a constant conductance coefficient C and the initial condition $U(\mathbf{x}, 0) = U(\mathbf{x})$ representing the original image. If C is extended to a function of $\mathbf{x}$, the solution of the heat equation will then be

$$\frac{dU(\mathbf{x}, t)}{dt} = C(\mathbf{x})\Delta U(\mathbf{x}, t) + \nabla C(\mathbf{x})\nabla U(\mathbf{x}, t) \tag{2.2}$$

A variable conductance term C controls the way the diffusion process takes place. Typically, C is chosen as a function of image features. This allows to selectively preserve or remove features by anisotropically varying the diffusion strength. Specifying C as a nonnegative monotonically decreasing function as in

$$C(\mathbf{x}) = e^{-\left(\frac{\|\nabla U(\mathbf{x})\|}{K}\right)^2}, \qquad K = const \tag{2.3}$$

will force the diffusion to mainly take place in homogeneous interior regions and it will not affect the boundary regions [ISNC03].

Applying an anisotropic diffusion filter, the quality of the datasets can be significantly improved. Small artefacts, noise and other irregularities are reduced without blurring edges, which is essential for surface detection. Figure 2.4 shows a cross section before and after prefiltering the dataset.

2.3.2 Gradient Magnitude

After prefiltering, the greyvalues of material areas still vary to a certain extent due to beam hardening, scattered radiation, and other artefacts. Using varying greyvalues as input to the segmentation task results in misclassification of artefact-affected areas, which is undesirable.
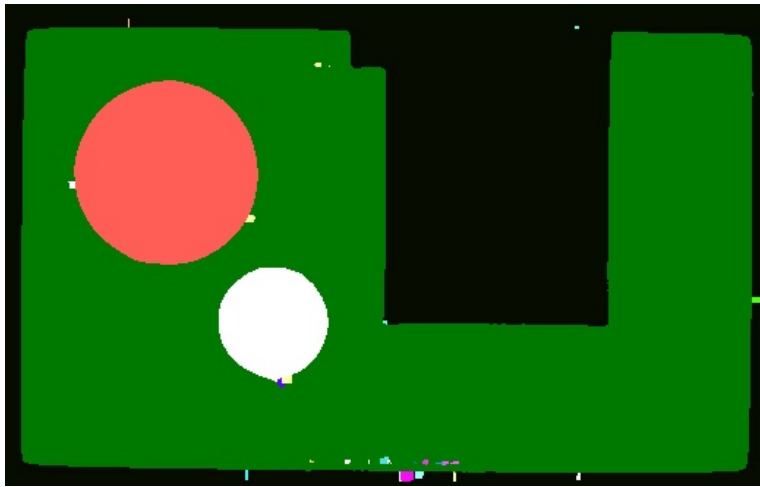
Figure 2.6: *Watershed segmentation, axial cross section through a testpart. Extracted regions are color-coded. Watershed segmentation allows to generate large connected regions but also a few smaller individual regions are extracted.*

As we are mainly interested in edges and material transitions, the gradient magnitude of the prefiltered datasets is computed in the presented application scenario. This is achieved by calculating the directional derivative at each spatial location of the dataset using a first order derivative operator. The result of gradient magnitude filtering is depicted in Figure 2.5.

2.3.3 Watershed Segmentation

For the segmentation task, a simple segmentation algorithm is not robust in terms of greyvalue deviations. Region growing for example, implicitly uses a global threshold. Therefore it produces similar thickening and thinning structures like global thresholding.

To avoid this effect, a region based segmentation algorithm is used. Watershed segmentation generates the binary volume by grouping regions with similar greyvalues. Watershed segmentation is a low-level image analysis algorithm producing a hierarchy of segmented and labeled regions from a scalar-valued input. In geography, a watershed region is bordered by the ridges of neighboring catchment basins. In image processing, images are depicted as height functions. A catchment basin is defined around each local minimum of the height function, such that each of its points may be connected with the minimum by a descending path [VS91].

To avoid oversegmentation, a flooding level is defined. The height function is flooded up to a certain level to decrease the number of extracted regions. Shallow segments with lower levels than the flood level will merge, eroding boundaries of adjacent regions (see Figure 2.6).

For the recombination of the extracted regions, Šrámek and Dimitrov [ŠD02] proposed a classification method, which is based on watershed hierarchies. In this approach a much simpler, faster and in most of the cases sufficient way for binarization is used. The mean greyvalues of the remaining regions are calculated and classified by a global threshold.

2.3.4 Constrained Elastic-Surface Nets

As soon as the binary segmentation is finished, the surface mesh is extracted. A marching cubes algorithm applied on a binary volume creates a jagged surface. This jagged surface accurately represents the binary volume but not the original surface of the specimen. Therefore a mechanism is needed to detect surfaces of binary segmented data.

Gibson [Gib98] proposed constrained elastic-surface nets, a technique to create a smooth surface model from binary datasets, which still preserves fine details. Gibson's algorithm consists of four steps: First, vertices of the surface are identified using volume cells. All volume cells intersected by the surface are identified. If every cell corner has the same binary value, then the volume cell has to be completely inside or completely outside the segmented object. Otherwise a surface cell has been found. In this case a surface vertex $p[i]$ is initialized by placing the vertex in the centre of the volume cell. In the next step surface vertices are linked and the neighborhood for each vertex is determined. Assuming only face-connected neighbor volume-cells, each vertex in the volume can have a maximum of 6 linked neighbors. In the relaxation step, the position of each surface vertex is modified according to the number of neighbors $N(i)$:

$$\hat{p}[i] = \frac{1}{\#\{N(i)\}} \sum_{j \in N(i)} p[j] \qquad (2.4)$$

An energy measure calculated from the edges controls the smoothing process. The energy is computed as the sum of the squared lengths of all edges in the surface net. To retain thin structures, a constraint is defined which forces every vertex to stay within its original volume cell. After several iterations of the smoothing procedure, the energy quickly reaches a minimum level where the surface turns out to be smoothest. At a higher number of iterations, the energy level converges to a slightly higher value and edges become sharper. In the final step the surface is being triangulated.

2.4 Results and discussion

In this section results are discussed, when applying our pipeline on homogeneous reference objects as well as on a real industrial die-cast component. All CT scans were performed on a HWM RayScan 250E system using a 225

kV micro-focus X-ray source. Reference measurements were performed on a Zeiss C400 coordinate measuring machine with an absolute accuracy of +/-2μm. Our demo application containing the presented pipeline was implemented in Visual C++ using the Insight Segmentation and Registration Toolkit (ITK) [ISNC03] for image processing and the Visualization Toolkit (VTK) [SML04] for visualization. All 3D views are rendered using raycasting.

2.4.1 Reference objects

Workpiece one is a regular aluminium testpart (Figure 2.7) developed by Kasperl [Kas05]. It has two cylindrical drill holes with different diameters and a rectangular milling. This object produces severe scattered radiation artefacts due to the different penetration lengths at a relatively high material thickness. Figure 2.7 shows a CT scan of workpiece one with strong artefacts changing the geometry of the smaller drill hole. Settings of this measurement are: 810 projection images, voltage 200 kV, current 620 μA, integration time 500 ms. To reduce artefacts, the X-ray beam is prefiltered using physical pre-filtering plates of 0.1 mm lead and 0.15 mm copper, in order to minimize low energetic radiation. The extent of the resulting 16 bit dataset is $339 * 525 * 169$ voxels with a voxelsize of 200 μm.

Workpiece two is an aluminium step cylinder (Figure 2.8). The step cylinder consists of 5 concentric rings with increasing outer diameters and a drill hole along the longitudinal axis. This object is used as reference for geometric and dimensional measurement in 3DCT, because it allows to classify different inner and outer diameters at different wall thicknesses. Due to the increasing wall thickness in the lower rings, artefacts affect the dataset so that it is difficult to distinguish between material and air in the drill hole. With this object the limitations of a 3DCT concerning geometric and dimensional measurements can be shown. The settings of this measurement are: 720 projection images, at 210 kV, 1000 μA, 500 ms integration time, 1mm copper pre-filtering resulting in a 16 bit dataset of $561 * 559 * 436$ voxels with a voxelsize of 236 μm.

Workpiece three is a real industrial component (Figure 2.2). The complex filter housing generates artefacts in the area of the bridge between the two joining parts. Measuring this object, severe artefacts appeared in the central area (see Figure 2.2). While in detail image (a) thinning and holes are shown, in detail image (b) structures are added through thickening. The dataset was measured with a voxelsize of 252 μm using 810 projection images at 210 kV, 830 μA, 500 ms integration time and 1mm copper prefiltering. These settings resulted in a dataset of over 1 GB in size. Our developed demo application cannot handle this amount of data yet. Therefore a representative subgrid of $529 * 771 * 100$ voxels was taken, which covers the artefact-affected area.
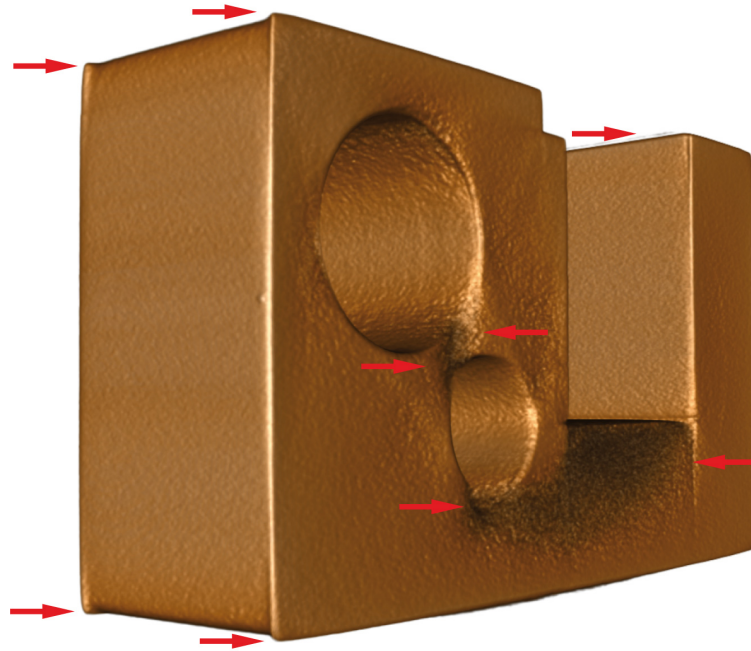
(a)
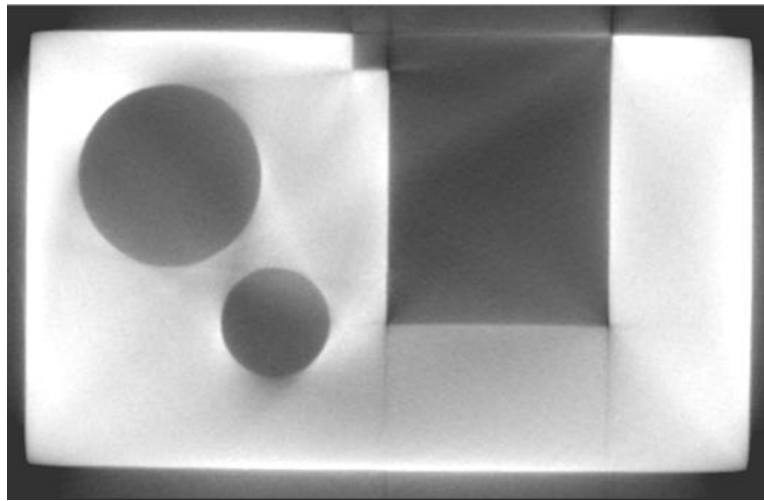
(b)

Figure 2.7: *CT scan of workpiece one. (a) Modifications of rendering of workpiece one due to scattered radiation and beam hardening artefacts (see red marked areas). (b) The sagittal cross-section shows severe artefacts in the area of the drill holes and the rectangular milling. In the artefact-affected areas the geometry is modified.*
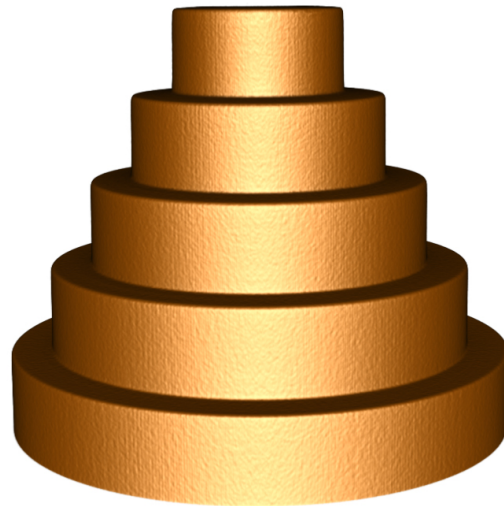
(a)
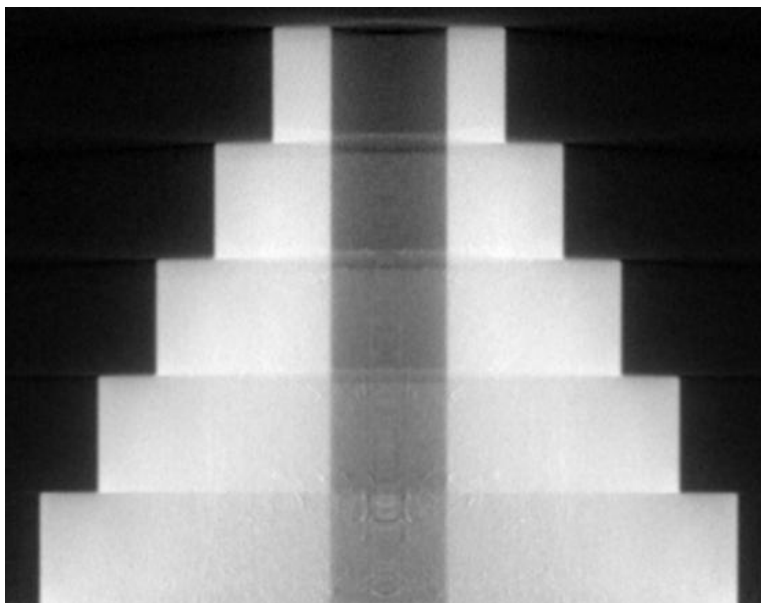
(b)

Figure 2.8: *CT scan of workpiece two. (a) shows the reference object which is used for geometric and dimensional measurement tasks. Along the horizontal axis the outer ring diameters and wall thicknesses increase, while the inner ring diameters remain constant. Small variations of the data values result in a fine texturing in the result images. (b) The sagittal cross-section shows increasing artefacts in the centre drill hole when wall thicknesses are increasing.*

2.4.2   Tuning the pipeline

To extract a usable surface model, the parameter setting of each step is crucial. The anisotropic diffusion filter is used to support the watershed segmentation in producing fewer and bigger regions. Excluding this filter would lead to oversegmentation or misclassifications in artefact-affected areas. General settings of 5 iterations at a conductance of 50 were used. For workpieces with severe artefacts, the number of iterations was increased to 7 and the conductance to 75. The anisotropic diffusion filter takes 65 - 70 % of the whole processing time. Therefore the number of iterations is a major factor in the overall processing time.

Applying the watershed segmentation, the flooding threshold influences merging of small regions with similar greyvalues. On the one hand oversegmentation is significantly reduced using a higher threshold. On the other hand, the regions of air will be misclassified, whose greyvalues are slightly below the surrounding material grey level. Especially in the lower rings of workpiece two, this effect can be found. So the flooding level has to be set individually for each dataset.

Generally, the processing time of the watershed segmentation is related to the smoothness of the dataset. A dataset which is not prefiltered either increases the overall processing time disproportionately or forces the program to crash due to memory limitations. Our findings are that for all three datasets, the processing time of the watershed segmentation was 25 to 30 % of the overall processing time.

For the constrained elastic surface nets, the same number of iterations is used for creating the surfaces of all three workpieces. The energy level reaches a minimum after 8 to 10 iterations. After 20 to 30 iterations the edges are further sharpened which improves the overall accuracy. Therefore the number of iterations is fixed to 30 iterations for all datasets. Increasing the number of iterations is not crucial for the overall processing time because the constrained elastic-surface nets take only 5 % of the processing time.

A general approach to tune the pipeline consists of the following steps: Firstly, the parameters of the diffusion filter have to be adjusted. To increase diffusion, the number of iterations is increased. The conductance parameter controls the sensitivity of the conductance term: the lower the conductance, the stronger the diffusion equation preserves image features. Secondly for the watershed segmentation the flooding level has to be set. To avoid unintended region merges the flooding level has to be set well above air grey level but below the lowest material grey level. For the binary classification of the remaining regions, the mean greyvalue of the material regions has to be found.
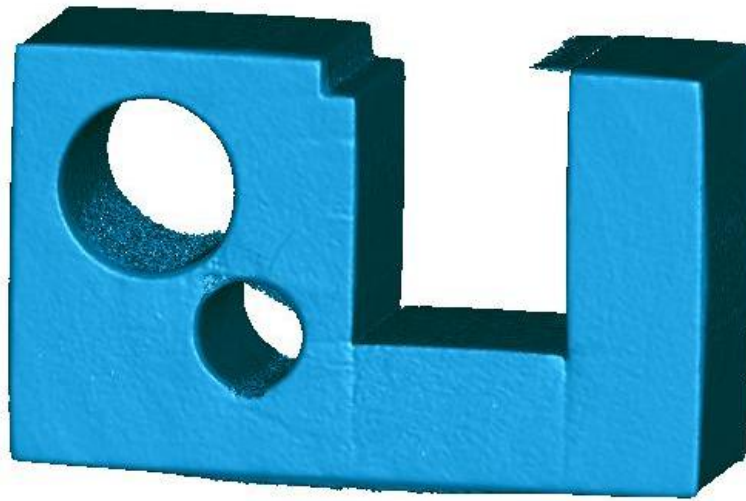
(a)

(b)

Figure 2.9: *Surface model of workpiece one: (a) best isosurface, (b) result of the presented method: geometric modifications, thinning and thickening artefacts are successfully removed.*

2.4.3 Analysis

In the case of workpiece one, severe artefacts distort the greyvalues of the dataset due to high material thicknesses (see Figure 2.4). In order to reduce oversegmentation and misdetections, prefiltering is increased. The desired result of a fully connected binary volume without artefacts could be achieved with the disadvantage of a higher overall processing time. As

(a)   (b)
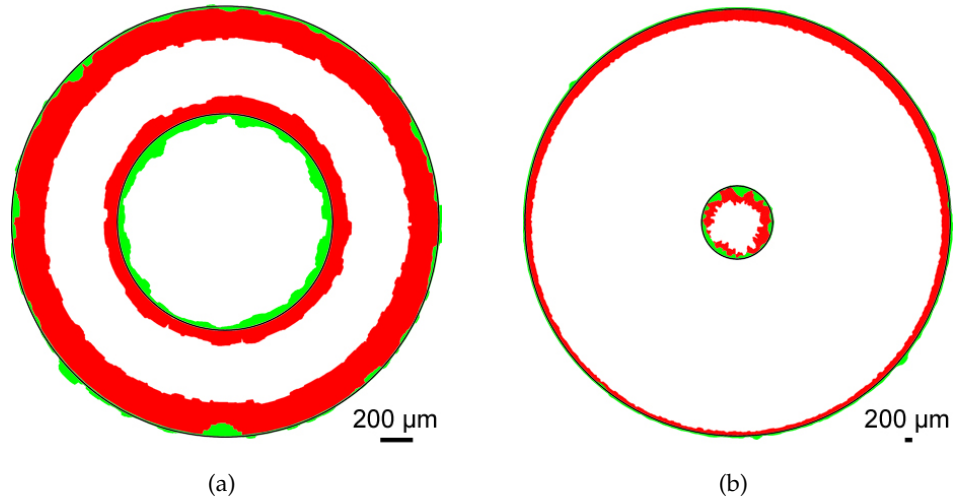
Figure 2.10: *2D actual/nominal comparison of the resulting surface models. Axial cross section in the middle of (a) first and (b) last ring. The CAD model was taken as reference (black). The best global isovalue of workpiece two is depicted in red and the output of the presented pipeline in green. Variations of the inner and outer contours are depicted 15 times scaled. Mind the different scales: the inner circles in both figures have the same size.*

depicted in Figure 2.9 the presented method is able to remedy the erroneously modified geometry in the area of the drill holes. Furthermore the scattered radiation effects in the area of the rectangular milling could be significantly reduced.

To verify the exactness of lengths, a surface representation of workpiece two was extracted using our pipeline. In this surface representation, five cross sections in the middle of each ring were specified. For each of these cross sections the inner and outer diameters are calculated using a circle fit. In Figure 2.10 conventional surface extraction with the best possible isovalue is compared to the output of the presented pipeline with the CAD model as reference. In order to double-check the calculated distances due to our pipeline, the diameters are measured with a coordinate measuring machine (CMM). Furthermore the distances are compared to an isosurface extracted using Otsu's global threshold method [Ots79]. Results are shown in Figure 2.11. Compared with the CMM a mean deviation of 9 μm for the outer diameters and 57 μm for the inner diameters could be reached.

Applying our pipeline on workpiece three, the geometry could be extracted without creating holes in the area of severe artefacts. In this area, where global thresholding produces holes, a mean deviation of +/- 36 μm between constructed surface and CAD model is achieved. For actual/nominal comparison, three visualization methods are applied. A common method for actual/nominal comparison is color coding. Each position
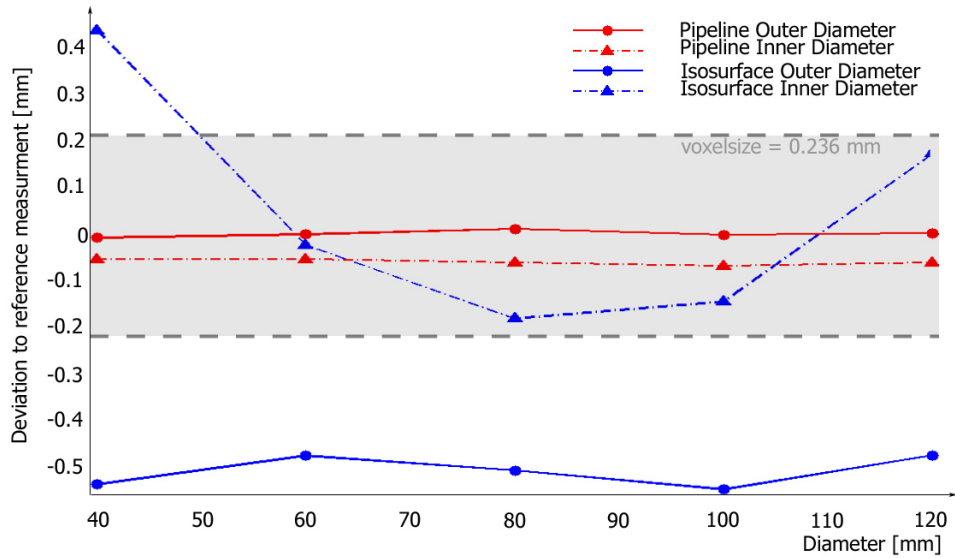
Figure 2.11: *Plot of deviations to reference measurement versus the diameter of the cylinders. Inner and outer diameters of workpiece two are considered. Otsu's global threshold method [Ots79] is compared to the extracted dimensions from our pipeline. Reference measurements were carried out using a coordinate measuring machine.*
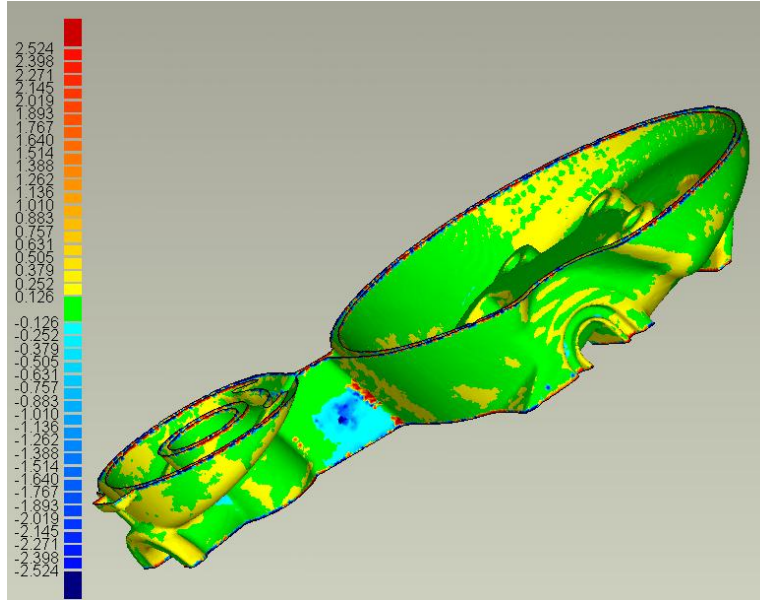
Figure 2.12: *Actual/nominal comparison for workpiece three (representative sub grid) between best isovalue and results from our pipeline. The colorscale denominates the deviations from the reference to test model in mm. Red refers to strong positive, blue to strong negative deviations, green depicts areas with low deviation.*
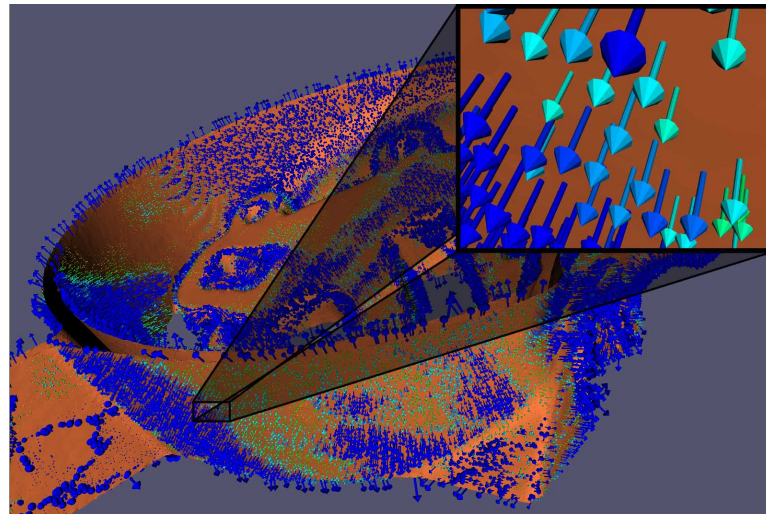
(a)
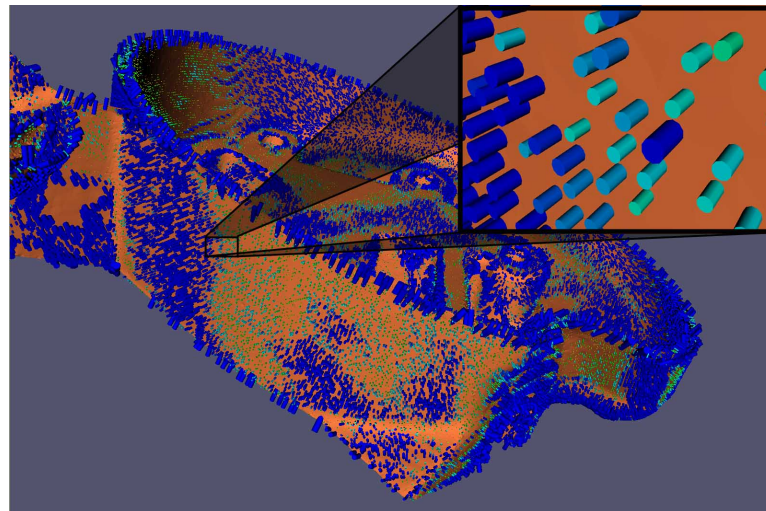
(b)

Figure 2.13: *Glyph-based visualization using (a) arrows, and (b) cylinders. The vector glyphs represent the deviation vector and are color-coded as well as scaled according to the absolute value of the deviation.*

of the reference object is coded with a color corresponding to the local deviation. In this visualization, a scalar is mapped onto a 3D object representation. The direction of the deviation vector is not considered. Figure 2.12 depicts a color-coded visualization generated using Geomagic Qualify.

If an arrow is placed at each vertex pointing in the direction of the corresponding deviation vector, three dimensional deviation information can be included (Figure 2.13(a)). In addition the vector glyphs are color-coded

and scaled according to the absolute value of the deviation. Due to scaling the glyphs, this representation allows to quickly identify areas of great deviations. Furthermore the directional information illustrates the alignment between reference and test object. A third visualization method maps cylinders to the surface model (Figure 2.13(b)).

The overall processing times were measured on an Athlon 64 4000+ system with 1GB RAM. On this system the processing times for extracting a surface are 4:58 minutes for workpiece one, 10:23 minutes for workpiece two and 4:44 minutes for workpiece three.

2.5 Summary

A new pipeline for industrial workpiece segmentation is presented which allows automated and effective actual/nominal comparisons. The discussed method offers the possibility to extract reproducible surface models from artefact distorted volumes. The proposed pipeline model is to a certain extent robust concerning common artefact types, which is of great importance for actual/nominal comparison and dimensional measurement tasks. Furthermore the accuracy for and the applicability on industrial components has been discussed.

I have learned to use the word "impossible" with the greatest caution.

Wernher von Braun

3

Surface Extraction from Multi-Material Components using Dual Energy CT
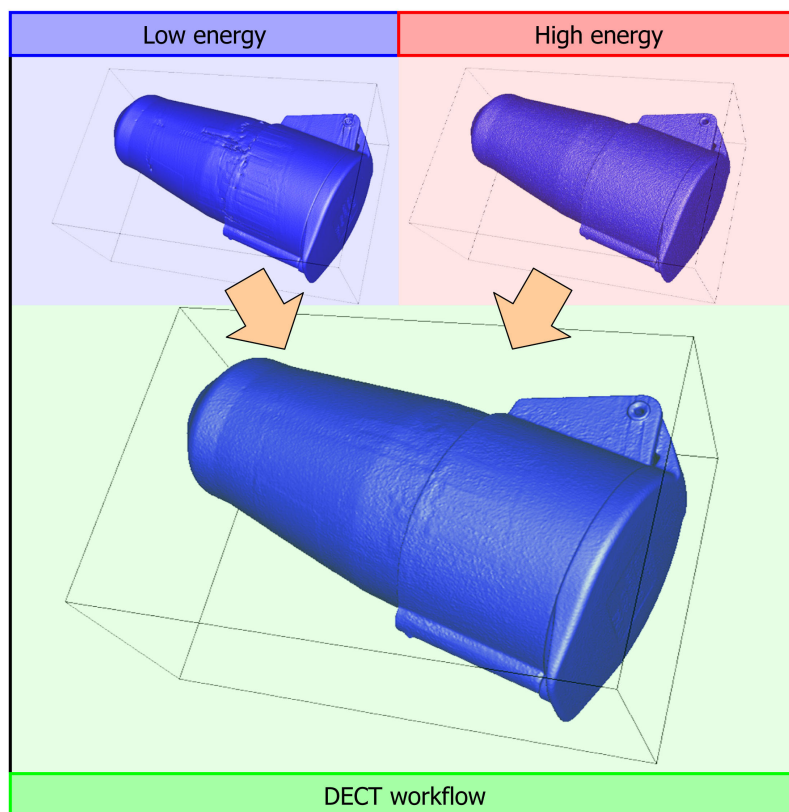

Figure 3.1: DECT workflow for surface extraction from multi-material components. A low energy (LE) and a high energy (HE) CT scan are fused to facilitate metrology on multi-material components.

MULTI material components with high density within low density material pose a major problem to dimensional measurement using 3DCT. The generated scans suffer from severe artefacts, which prevent reliable metrology. However a huge amount of industrial components consist of more than one material, at least after assembly.

This chapter describes a novel method for creating surface models of multi-material components using dual energy computed tomography (DECT). Based on the advantages of dual X-ray exposure technology, the presented workflow additionally uses image fusion and local surface extraction techniques. A prefiltering step reduces noise inherent in the data. For image fusion the datasets have to be registered. In the fusion step the benefits of both scans are combined. The structure of the specimen is taken from the low precision, blurry, high energy dataset. The sharp edges are adopted and fused into the resulting image from the high precision, crisp, low energy dataset. In the final step a reliable surface model is extracted from the fused dataset using a local adaptive technique.

The major contribution of this work is the development of a specific workflow, which takes two X-ray CT datasets with complementary strengths and weaknesses into account. As result, a significant improvement in overall measurement precision, surface geometry and mean deviation to reference measurement is facilitated.

3.1   Introduction

When scanning multi-material specimens with high differences in density and therefore in the attenuation coefficients of each material, severe streaking artefacts prevent a reliable dimensional measurement. Usually, technicians in measurement technology disassemble the multi-material components. Each material is measured in a separate scan using optimal X-ray parameters. This procedure is time consuming and in several cases the specimen has to be destroyed. For instance, in the special case of a pressure sensor from the automotive industry, the sensor is cast integral into the plastic body and can not be removed without destroying the specimen. The common workflow for dimensional measuring of single material industrial components can be summed up as follows: a prefiltering step reduces the reconstructed dataset's inherent noise in order to support surface detection. For common surface extraction tasks in industrial applications, usually a single isovalue is specified to distinguish between material and air [Vol04]. A polygonal mesh is extracted along the selected isovalue us-
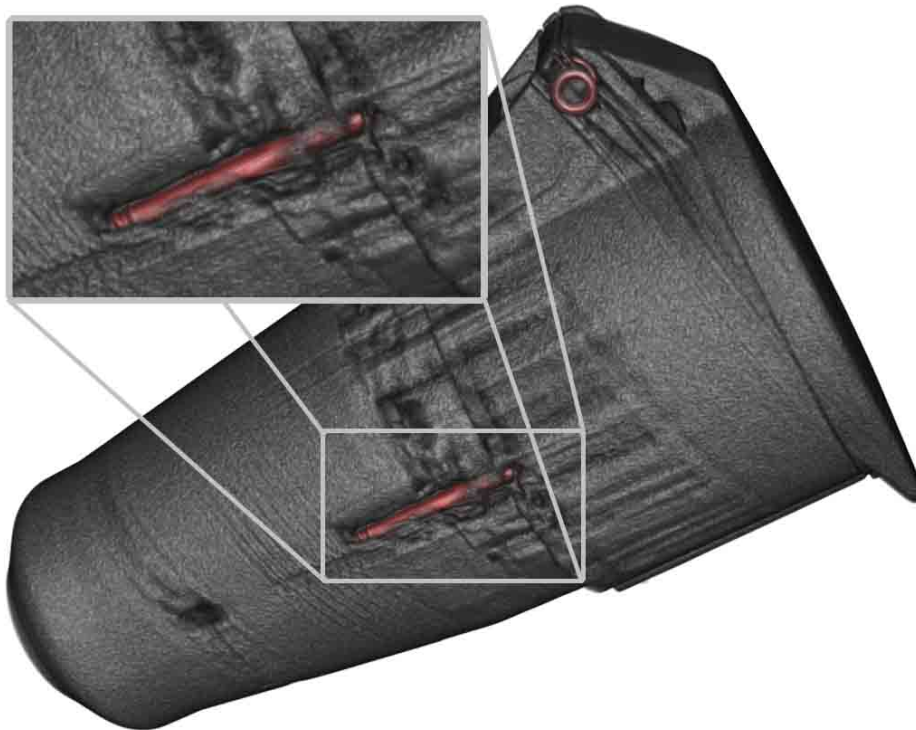
Figure 3.2: *Scattered radiation, beam hardening, and other physical effects generate severe artefacts, which modify the dataset and prevent a reliable global isosurface extraction. Artefacts manifest themselves as holes and artificial structures. In the rendering even a screw from the inside of the specimen becomes visible (high density objects are depicted in red, 3D view is rendered using raycasting).*

ing a surface creation algorithm, *e.g.,* marching cubes [LC87]. Finally the extracted surface model is compared to a computer aided design (CAD) model using actual/nominal comparison. The corresponding deviations between the reference and the test model are calculated and visualized by color-coding scalar deviations on the surface of the reference model.

Multi-material components with high density differences are not suitable for the common workflow of dimensional measurement using 3DCT. High density and highly absorbing materials (*e.g.,* steel) produce scattered radiation which is manifested in the reconstructed dataset. So the low absorbing material is simply covered by the different characteristics of artefacts from the strong absorbing material. If a global thresholding method for surface extraction is applied on an artefact-affected dataset, holes and artificial structures will be introduced by different artefact types which modify the surface models. A reliable dimensional measurement is in most cases impossible. In Figure 3.2 and Figure 3.10 these circumstances are depicted.

To improve measurement results, recent research activities have tried to exploit dual energy computed tomography (DECT). By scanning a specimen twice using different energies and therefore different energy spectra of the X-ray source, it is possible to quantify the different materials of a component by combining information from both scans.

This chapter introduces a new workflow to facilitate dimensional measurements of multi-material components [HKG07]. The reconstructed datasets of both X-ray CT scans are adaptively fused on a regional basis and a reliable surface model for dimensional measurement is locally determined. The major goal of our work is to design the workflow to follow typical dimensional measurement constraints. The method has to be applicable for typical dimensional measurement tasks and practical in terms of quality and data-processing speed on commodity hardware. The reconstructed datasets of the two scans are taken as ground truth, assuming no additional information of CAD models or additional specifications of primitives (*e.g.*, cylinders, cuboids) in the scanned data is available. The special setup of the industrial 3DCT at the Upper Austrian University of Applied Sciences - Wels Campus is used to facilitate the DECT scans. In this setup a dual X-ray source design was created using a 450 keV macro-focus source for the high energy scans and a 250 keV micro-focus source for the high precision measurements.

3.2 Related work

3.2.1 Dual energy computed tomography

Concerning data acquisition in DECT there are two different techniques: the dual exposure / dual source and the dual (layer) detector technique [RD06].

In medical CT, the dual exposure / dual source method has been launched in 2006 in order to facilitate the material-specific difference in attenuation in the resulting image for classification of tissue types [Sie08]. More recently the technology was transferred to industrial applications. Using the dual exposure / dual source technique, a specimen is measured twice using different X-ray energies. Usually a high energy measurement and a low energy measurement are carried out successively without moving the specimen on the rotary plate. In order to combine both measurements either the position of the specimen is not changed between the measurements or an accurate registration of the datasets has to be performed. Major disadvantages of the dual exposure / dual source technique are double the measurement time and also double the storage requirement. However, in the area of industrial 3DCT this method constitutes a novel en-

hancement for applications, which is usable on a widespread variety of existing 3DCTs.

Using the dual detector technique only a single measurement of the specimen is necessary. A modified detector consisting of two separate layers generates two penetration images at each angular position: the front layer detects low energy photons and the back layer detects high energy photons. The disadvantage of this method is that the energy separation of these detectors is rather poor [RD06]. Application areas for this technique are the characterization of organic and inorganic materials in baggage control systems for airport security and the examination of drilling cores concerning material properties [IDO*06], [IOR*05].

A considerable body of work on dual-energy 2D imaging is out of scope for our work and is therefore not treated. Due to specifications of our 3DCT equipment the dual exposure / dual source technique was used for our DECT measurements. Each component is scanned twice in two subsequent measurements without moving the specimen using a low energy (LE) and a high energy setup (HE).

3.2.2 Image Fusion

The general aim of image fusion is to combine a set of input images into a single output image. The output image preserves the salient information from each input image, suppresses noise and irrelevant parts of the input images, and should not generate distortions, artefacts, or inconsistencies [LON*04]. Image fusion techniques are used in a wide range of applications, *e.g.*, medicine, remote sensing, industry, surveillance and defense applications, which all benefit from the use of multiple images of a scene. Generally image fusion algorithms can be categorized into low, mid, and high level techniques. In some literature the levels are also referred to as pixel, feature, and symbolic levels.

Feature-level algorithms are usually more robust to noise compared to pixel-level algorithms. These algorithms typically segment the images into regions, fusing the regions using their various properties [LON*04]. Symbolic-level fusion algorithms try to combine image descriptions, *e.g.*, in the form of relational graphs [WWH99]. Feature and symbolic level fusion are out of scope for this work and are not considered any further.

In the area of pixel-level image fusion a considerable body of work has been done. Pixel-level algorithms either work in the spatial domain (*e.g.* the work of Li et al. [LMM94]) or in the transform domain (*e.g.* the work of Nikolov et al. [NHBC01]). Spatial-domain algorithms are able to focus on specific image areas limiting the influence of the fusion in other areas. As transform domain algorithms create the fused image globally, undesirable artifacts may be created in several image areas while enhancing properties

in others. For this reason transform domain algorithms are considered as not suitable in the proposed application area.

Multiresolution analysis constitutes another branch of pixel-level fusion. Burt [Bur84] created image pyramids by applying filters with increasing spatial extent in order to separate information at different resolutions. The value with the highest saliency is taken at each position in the transform image, *e.g.*, using the intensity gradients as saliency measure [PX04]. Finally the fused image is created by an inverse transform of the composite image. Furthermore various wavelet transforms can be used to fuse images. The discrete wavelet transform [LMM94],[COG95] and more recently, the dual-tree complex wavelet transform [NHBC01], [LON*04] have been used in many applications to fuse images.

Multiresolution analysis turned out to produce suboptimal results in a difficult to tune and timeconsuming process. As we wanted to focus the fusion of the two datasets on edge regions, an adapted version of the weighted arithmetic image fusion is used. It employs a region based encoding of the weights for the high energy (HE) and the low energy (LE) dataset.

3.2.3 Local surface extraction

There are several methods that try to improve the surface extraction from industrial 3DCT data. Based on the ideas of Sethian [Set99], Whitaker and Breen's approach [WB98] considers the zero level-set of a volume as a deformable surface. The surface is then deformed in order to minimize the mean curvature on the surface. More recently, a comprehensive book on level-set models and dynamic implicit surfaces was published by Osher and Fedkiw [OF03]. Level-set evolution is computationally expensive and timeconsuming on commodity hardware, and therefore undesirable for dimensional measurement tasks.

Kindlmann and Durkin [KD98] take the data value as well as the gradient magnitude and the second derivative in order to design and explore a 3D transfer function space. Kniss et al. [KKH01] have designed transfer function widgets that build on Kindlmann and Durkin's method. As Kindlmann and Durkin originally designed their method for volume visualization, the extraction of surface models is not included.

Methods which extract surface models from binary data were proposed by Whitaker [Whi00] and Gibson [Gib98].

Whitaker proposed to change the constrained deformable surface model to a constrained level-set model, in order to create smooth models while bypassing the need for a separate surface representation. Gibson generates feature-preserving surface models by treating the binary input data as a constraining element in an energy-minimizing deformable surface system. In these methods, to a large extent the quality of the output

depends on the prior segmentation, which would introduce another expensive step to the workflow.

Heinzl et al. [HKKG06] proposed a pipeline, which uses 3D image processing filters for preprocessing and segmentation of 3DCT datasets in order to create the surface model. In particular, after an edge preserving prefiltering step, a watershed filter is applied on the gradient magnitude image. The resulting binary segmented data is taken for the construction of a surface model using constrained elastic-surface nets. Due to segmentation of material regions, fine details might get lost and therefore measurement errors are introduced. Further more the pipeline is designed for and applicable on single material components (for details see chapter 2).

As the requested output of the workflow is a surface model, we apply a modified version of Steinbeiss's method [Ste05] using a modified noise reduction scheme. This method locally adapts surface vertices to determine the best local surface position. Using an initial suitable surface model of the specimen, greyvalue profiles are calculated in the direction of each point's surface normal. The vertex location is then adjusted to correspond to the position with maximal gradient magnitude.

In this chapter the DECT workflow for surface extraction from multi-material components is introduced. We further discuss the results of applying the workflow to testparts as well as real world industrial components.

3.3 DECT workflow for surface extraction from multi-material components

The basis of our approach is the dual source / dual exposure technology using a micro-focus and a macro-focus X-ray source. The high energy (HE) macro-focus scan generates nearly artefact-free but blurry, less precise and more noisy data. Usually macro-focus CT is the method of choice when examining large or high density components. Due to the higher energies used in macro-focus X-ray sources, the X-ray spot size (origin of the X-rays) is larger compared to micro-focus X-ray sources. It is approximately 2 mm versus 5 μm to 320 μm depending on the selected energy setting. The ideal case of a near punctiform X-ray source for an optimal projection image on the detector is abandoned in macro-focus CT in order to achieve higher penetration lengths. In contrast, the low-energy (LE) micro-focus measurement generates high precision but artefact-affected data. The smaller X-ray spot size supports the generation of crisp and precise images, but the limited energy restricts penetration lengths.

Most of the approaches mentioned in the previous chapter are focused on a specific problem within the visualization pipeline. Our goal is to combine and extend existing methods according to the requirements of metrology. The workflow shall be applicable in every day use for dimensional
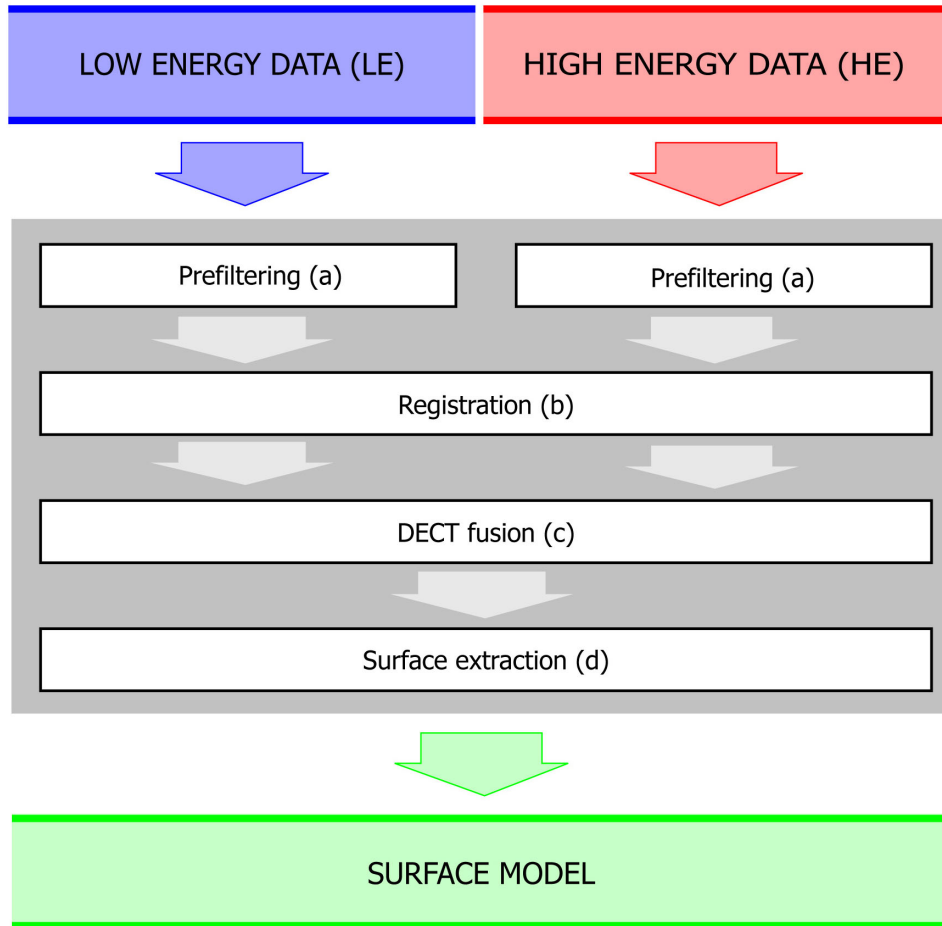
Figure 3.3: *DECT workflow for surface extraction from multi-material components; Input: Volume dataset from a low energy scan, volume dataset from a high energy scan; Output: Improved surface mesh.*

measurements of multi-material components. As we do not have access to the projection images, the reconstructed volumes of the high energy (HE) and the low energy (LE) measurement are used as input. In the following subsections all components of the proposed DECT workflow including DECT fusion and local surface extraction are discussed in detail (see Figure 3.3).

3.3.1 Preprocessing

Due to the different characteristics in each of the two scanned datasets concerning artefacts and signal to noise ratio, a preprocessing step is essential. Both high energy (HE) and low energy (LE) datasets are affected to a certain degree by ambient noise. Especially the HE dataset has to be prepro-
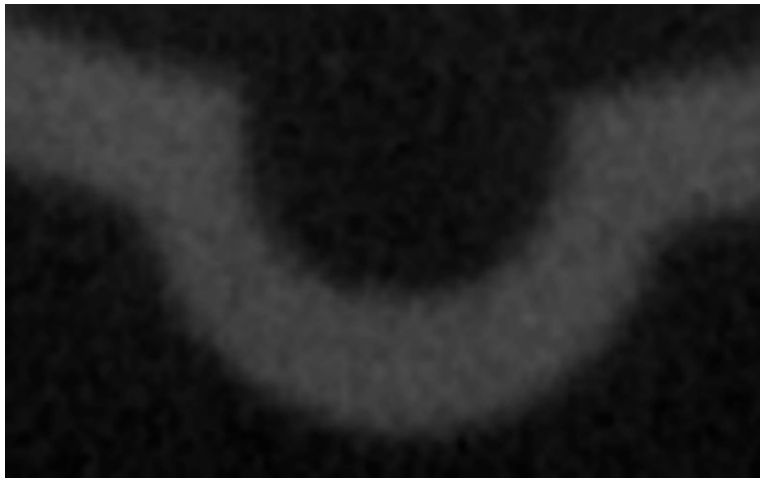
(a)
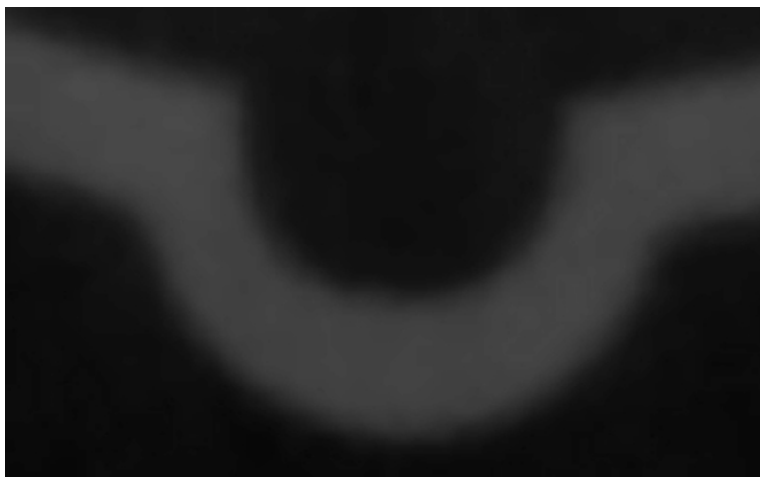
(b)

Figure 3.4: *Anisotropic-diffusion filter, axial cross section through a cutout of a 400V connector, (a) before and (b) after anisotropic diffusion filtering. Smaller artefacts are removed and the dataset's noise is decreased.*

cessed to reduce noise due to a more intense noise level of the detector in the higher energy bands. In case of the LE dataset, the preprocessing step reduces the propagation of artefacts to subsequent steps of the workflow.

The preprocessing is accomplished by applying anisotropic diffusion which was first proposed by Perona and Malik [PM90]. More recently, a comprehensive book on the topic of geometry-driven diffusion was edited by ter Haar Romeny [tHR94]. Compared to isotropic smoothing, the characteristic of anisotropic diffusion filters is to smooth the data without blurring or moving edges. The dataset's noise is reduced but specific image fea-

tures are preserved. As these properties are desirable for dimensional measurement, Perona and Malik's anisotropic diffusion method is used in the DECT workflow. For a detailed description on the principle of anisotropic diffusion see section 2.3.1.

When applying an anisotropic-diffusion filter, the dataset's inherent noise can be significantly reduced without loosing edge information. Scattered radiation effects are removed without blurring edges. This is essential for surface detection (see Figure 3.4).

3.3.2   Registration

When measuring a specimen using different X-ray source setups of the CT scanner, slight changes in the positioning and the orientation of the specimen in the dataset may occur. To avoid the propagation of this error, a registration procedure has to be applied. In the DECT workflow the high energy (HE) dataset is considered as the fixed image, as it is robust to artefacts. The low energy (LE) dataset is considered as the moving image which is registered to the fixed image. In order to improve the performance of the registration algorithm with regard to speed and accuracy, multi-resolution approaches are commonly used. The fixed image and the moving image are decomposed into image pyramids, which downsample the images level by level. Starting at the top level of the pyramids the coarsest images of the two pyramids are registered to each other. The registration is refined with each of the succeeding image levels. This guarantees a high robustness of the registration procedure.

In order to ensure the flexibility of using scans from different 3D imaging modalities, a mutual information approach is used. To compute the mutual information between the fixed (HE) and the moving image (LE) the method of Mattes et al. [MHV*01], [MHV*03] is used. This method evaluates the marginal and joint probability density functions (PDF) at discrete positions (bins), which are uniformly spread within the dynamic range of the images. The entropy values are calculated by summing over the bins. Using this approach the fixed image PDF does not need to be smooth, because it does not contribute to the derivatives. A zero order (box car) B-Spline kernel is used for the fixed image intensity PDF. To ensure smoothness, the moving image intensity PDF is computed with a third order B-Spline kernel.

3.3.3   DECT fusion

Due to the higher energies of the used high energy (HE) macro-focus X-ray source, the main object structures of the considered specimens are depicted best in the HE dataset. However, the larger X-ray spot size of the macro-focus X-ray source generates more blurry edges in the datasets. In con-
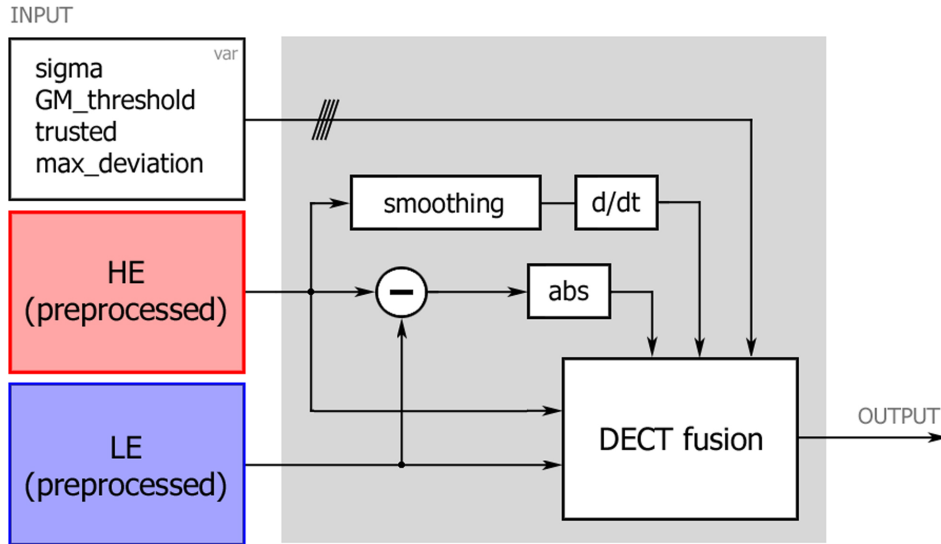
Figure 3.5: *Principle of DECT fusion: The fusion of the LE and the HE input is performed at edge regions of the HE dataset which are defined by the gradient magnitude. The contribution of each dataset is linearly weighted according to the absolute-value difference between the two images. To avoid misclassifications of artefacts the absolute value difference is limited.*

trast, the small X-ray spot size of our micro-focus source supports to create crisp and precise images. However, the limited energy restricts penetration lengths and therefore severe artefacts are induced in the low energy dataset. The severe artefacts in the LE dataset change their characteristics and orientation according to the measurement parameters and the positioning of the specimen in the X-ray beam.

In order to combine the advantages of both measurements, the main object structure from the HE dataset is fused with the crisp edges of the LE dataset. As common image fusion methods as well as multiresolution analysis turned out to be inefficient or suboptimal, we developed a DECT specific approach for image fusion (see Figure 3.5). To determine the edge regions, a gradient magnitude image is extracted by applying a Gaussian filter kernel with a user defined *sigma* followed by a gradient magnitude filter. The thresholding of the smoothed gradient magnitude image allows the specification of edge regions. Only the edge regions above a user defined level (*GM_threshold*) are considered for fusion. To detect artefact-affected regions, an absolute-value difference-image between the HE and the LE measurements is computed. Especially in artefact-affected regions and also in the edge regions, major deviations are depicted in the difference image. Subsequently the datasets are combined by local arithmetic image fusion. In this step the contribution of each dataset is linearly weighted
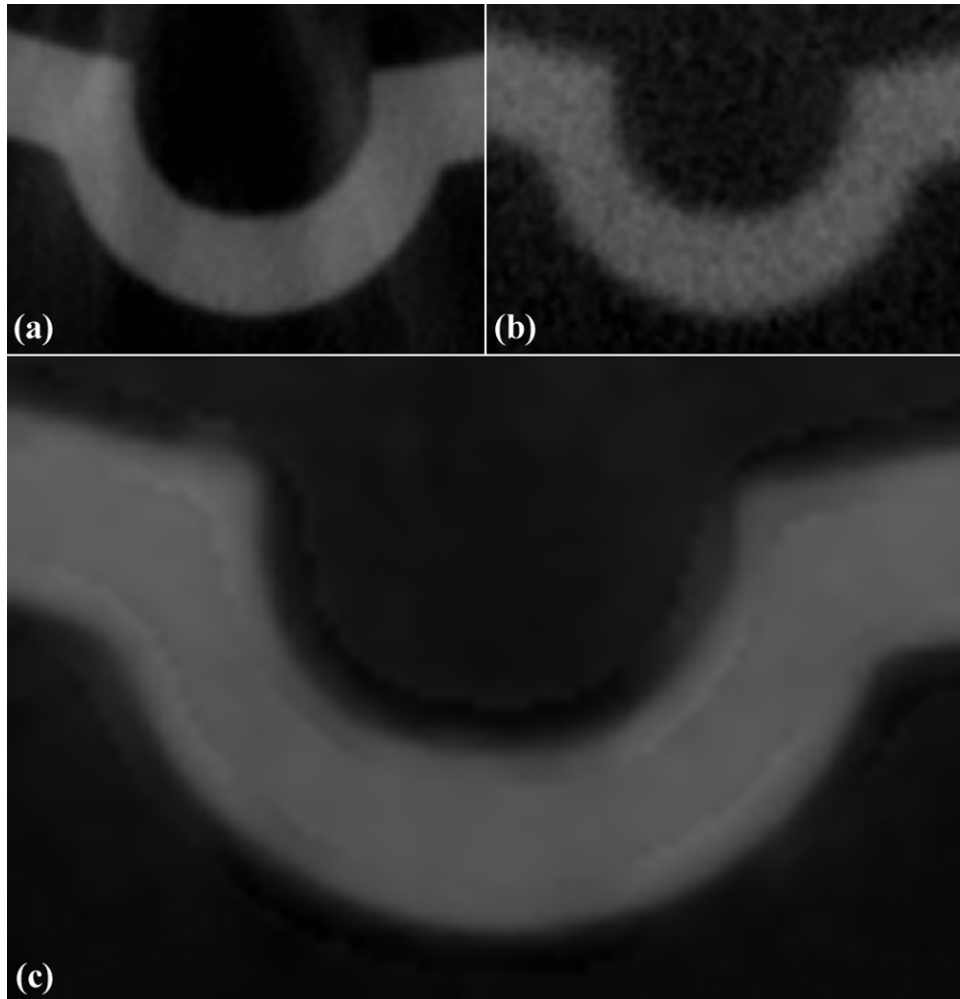
Figure 3.6: *Axial cross section through a cutout of a 400V connector. (a) LE image, (b) HE image and (c) fused image. Using our image fusion approach the edges are significantly enhanced for surface extraction without keeping artefacts from the LE dataset.*

according to the absolute value difference between the two images. To avoid misclassifications of artefacts the absolute-value difference is limited by *max_deviation*. Finally, for trusted regions of low difference in the grey-values of the LE and the HE data, a *trusted* level is defined. Within the trusted level the LE dataset is weighted with 100% (see Figure 3.6).

3.3.4 Local surface extraction

For surface determination we use a local surface extraction approach [Ste05]. First a reliable global isosurface is extracted from the fused dataset. It includes the topology of the underlying data but still contains
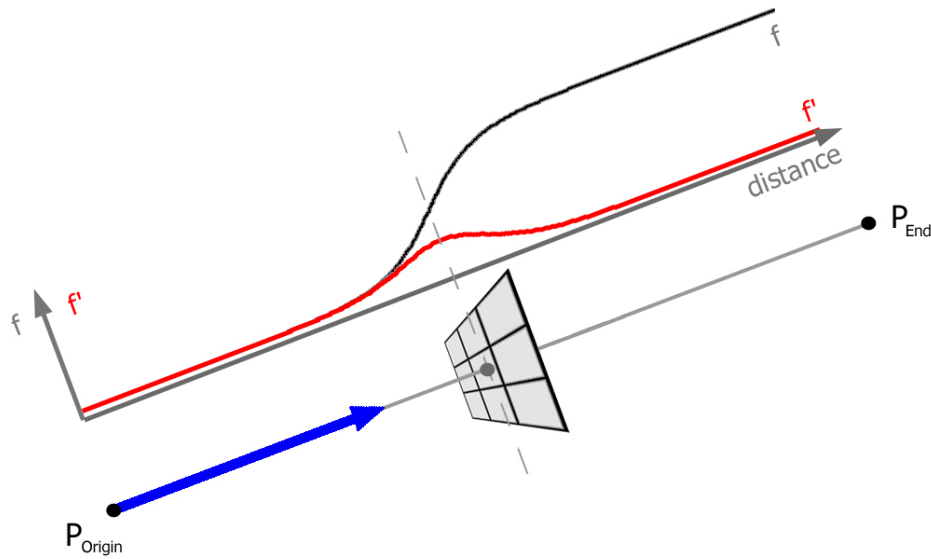
Figure 3.7: *Local surface extraction adapts the surface model by moving surface vertices in the direction of the corresponding point normal to a position with maximum gradient magnitude. The dataset's noise is accommodated by considering the neighborhood of a surface point candidate.*

inhomogeneities and errors due to the locally varying characteristics of the greyvalues. To correct these misclassifications, each surface vertex is moved in the direction of the surface normal. The vertex location is moved along the normal until the gradient magnitude reaches its maximum. This is accomplished by trilinear interpolation of the greyvalues along the surface normal and computing the derivative of the generated greyvalue profile (Figure 3.7). As a constraint, a user-defined maximum distance for the repositioning of a vertex is used (P_{origin}, P_{end}). The local modification of vertices with predefined constraints produces a surface model with improved precision. To reduce repositioning failures due to noise, not only the density profile along the normal is taken into account, but also close-by profiles along directions parallel to the normal. In the tangent plane to the normal direction, a $3 * 3$ neighborhood is used to compute 9 density profiles (see Figure 3.7). The directional derivative along each profile is estimated according to $f'(\mathbf{x}) = f(\mathbf{x}) - f(\mathbf{x} - 1)$, where $\mathbf{x}$ and $\mathbf{x} - 1$ are successive positions along the profile. For each of the nine profiles the position with the maximal gradient magnitude is determined. The improved edge location is calculated by using either a local weighted mean or the median position.
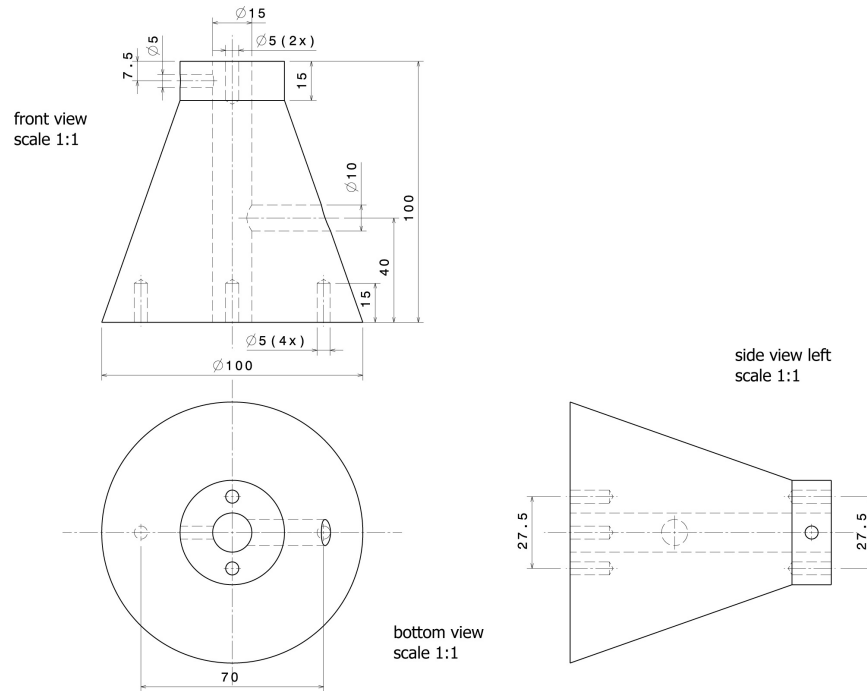
Figure 3.8: _Construction drawing of TP03 including all relevant dimensions._

3.4 Results and discussion

For all specimens high absorbing material is covered by low absorbing material. All CT scans were performed on a HWM RayScan 250E system with a 225 keV micro-focus and a 450 keV macro-focus X-ray source. For the micro-focus setup the best achievable resolution is 5 μm/voxel depending on the maximum dimension of the specimen. For the macro-focus setup the best achievable resolution is 150 μm/voxel. All datasets are stored in 16 bit unsigned short. Reference measurements were performed on a Zeiss SPEC-TRUM 700 (ST3/RDS-RST) Vast XXT coordinate measuring machine with a longitudinal measurement error of 2.2 μm $\cdot\frac{length}{300}$. Our demo application was implemented in Visual C++ using ITK [ISNC03] and VTK [SML04]. For evaluation of deviations the commercial tools Geomagic Qualify [Geo08] and Carl Zeiss Calypso [Car08] are used.

3.4.1 Specimens

TP03

Specimen one (Figure 3.8 and Figure 3.9) is a homogeneous polyethylene testpart (TP03) used for analysis of parameter variations in dimensional measurements. The TP03 is 100 mm in diameter, 100 mm in height and

Table 3.1: *Parameters for specimen one (TP03)*

Parameter	Specimen one HE	Specimen one LE
projections	900	900
voltage (kV)	440	200
current (μA)	1300	450
integration time (ms)	2000	1000
prefiltering	1 mm W + 1.5 mm Cu	1 mm Cu
datasize	$508 * 523 * 611$	$508 * 523 * 611$
voxelsize (μm)	200	200

(a)   (b)
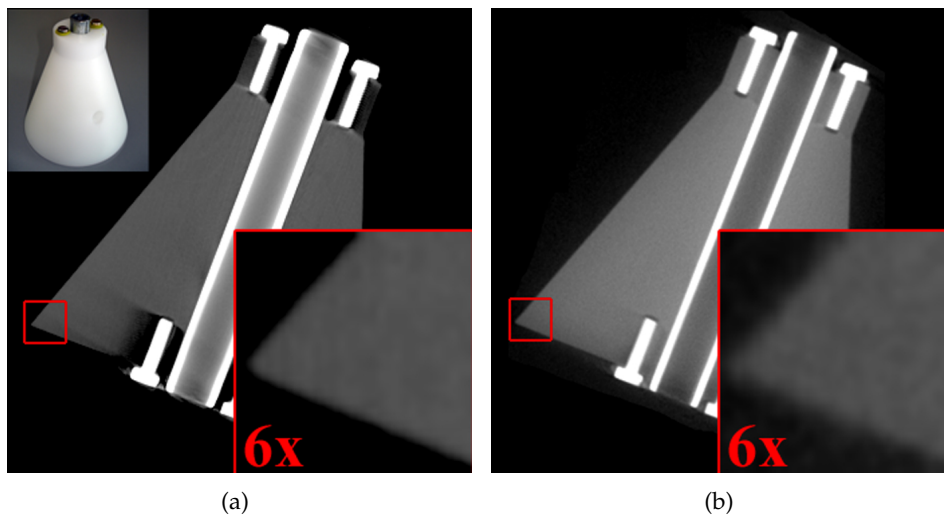
Figure 3.9: *Specimen one: TP03. (a) Axial cross section of micro-CT scan shows severe artefacts in the area of the metallic screws. Artefacts are the dark areas around the screws. (b) shows a cross section of the macro-CT scan. Compared to the LE scan the HE scan is less artefact-affected but less precise and contains more noise. The detail images show a 6x zoom of the edge region marked in red).*

consists of a cone with an attached cylinder. Six smaller vertical drill holes are placed on the bottom and top side, four in the base of the specimen and two on the top. Together with the central drill these features are serving to determine the exactness of a scan by evaluating distances and dimensions of the holes. A round steel bar is positioned in the major central drill and steel screws are placed and fixed in the drill holes, which makes this part a multi-material object. The TP03 was measured twice without moving the specimen but using different X-ray source setups. The first measurement was a high energy (HE) macro-focus scan to generate a dataset with hardly any artefacts, which determines the structure of the specimen. The second measurement was a low energy (LE) high precision micro-focus scan which

Table 3.2: *Parameters for specimen two (400 Volt connector)*

Parameter	Specimen two HE	Specimen two LE
projections	1080	1440
voltage (kV)	440	210
current (μA)	1000	680
integration time (ms)	1000	1000
prefiltering	1 mm W + 1.5 mm Cu	2 mm Cu
datasize	$391 * 552 * 847$	$391 * 552 * 847$
voxelsize (μm)	171	171

(a)   (b)
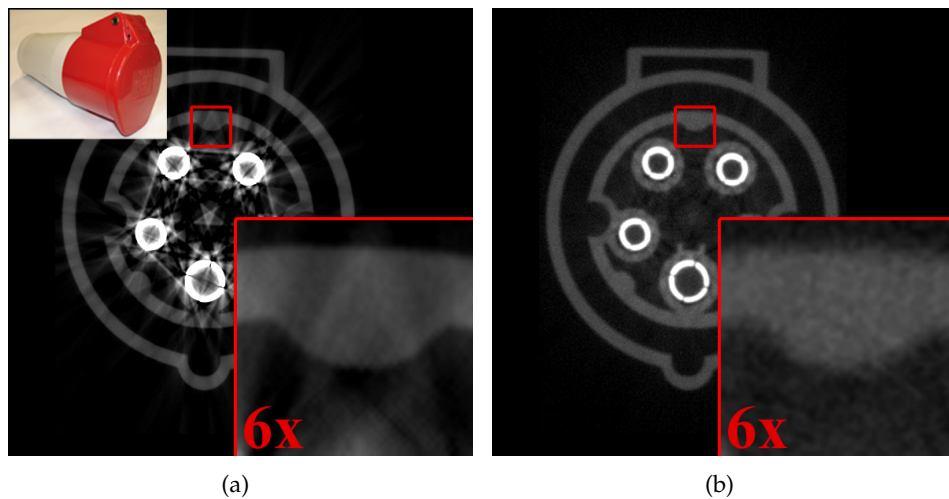
Figure 3.10: *Specimen two: 400 Volt connector. (a) axial cross section of the low energy micro-CT scan shows the typical artefacts within multi-material components due to too low X-ray energies: Starting from the pins severe streaking artefacts exist. (b) Using the high energy macro-CT scan, most of the streaking artefacts can be removed but the edges are more blurry (see detail images).*

generates a highly detailed but artefact-affected dataset. For detailed CT measurement parameters see Table 3.1.

400 Volt connector

Specimen two (Figure 3.10) is a 400 Volt power connector according to the European IEC 60309 system. This component consists of a plastic housing, five power pins, two steel screws to connect the housing parts, two steel-screws for the strain relief of the power cable, a spring and a bearing for the cap mechanism. In Figure 3.2 a 3D rendering of a micro-focus CT scan of specimen two is depicted. This specimen shows severe artefacts around

Table 3.3: *Parameters for specimen three (terminal block)*

Parameter	Specimen three HE	Specimen three LE
projections	1080	1080
voltage (kV)	400	160
current (μA)	2200	660
integration time (ms)	1000	2000
prefiltering	1 mm W + 1.5 mm Cu	2 mm Cu
datasize	$88 * 322 * 324$	$88 * 322 * 324$
voxelsize (μm)	200	200

(a)   (b)
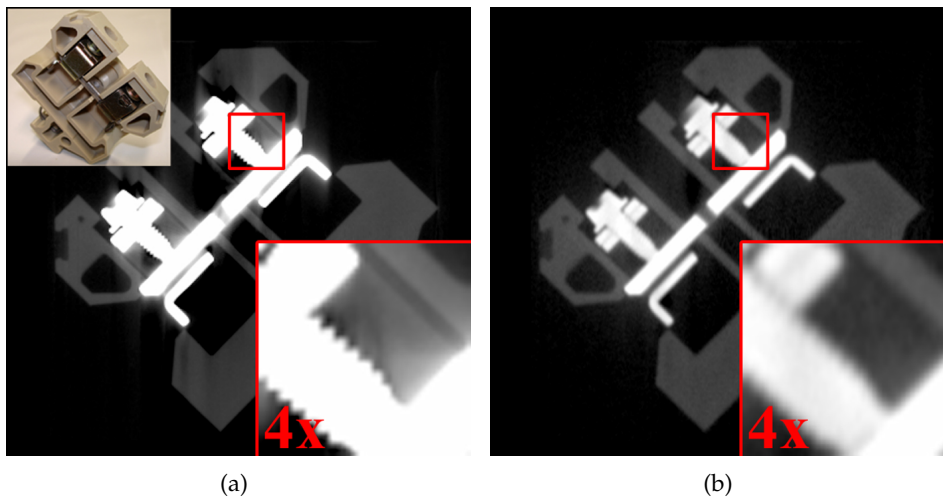
Figure 3.11: *Specimen three: Terminal block. (a) In the cross section of the micro-CT scan streaking artefacts around the metallic clamps are present. (b) shows the cross section of the macro-CT scan. In the area of the screws the disadvantages of the macro-focus CT are revealed: Fine structures disappear (see detail images).*

the power pins. Greyvalue modifications due to scattered radiation of the metal components exceed the plastic's greyvalue. CT measurement parameters are listed in Table 3.2.

Terminal block

Specimen three (see Figure 3.11) is a terminal block from home automation systems and it is 56 * 50 * 11 mm in size. Terminal blocks are widely used, providing a convenient means of connecting electrical wires. This part is built using a plastic body, which acts as a carrier for the metal clamps, a spring, which fixes the terminal on the top hat rail, and finally the two metal clamps holding the wires, which are connected by the power rail.

This representative multi-material component was chosen because of its regular structure and a convenient geometry for coordinate measurement machines (CMM). In total, 16 inspection features of the object were specified to calculate the dimensional deviation to a CMM reference measurement. The CT measurement parameters for the terminal block are listed in Table 3.3.

3.4.2 Tuning the DECT workflow

To generate reliable surface models for dimensional measurement, the parameter settings for each step are essential. As prefiltering step an anisotropic diffusion filter (Figure 3.3(a)) is used, which creates a more homogeneous dataset without modifying edge information. This step is crucial especially for the LE dataset in order to reduce noise and smaller artefacts. The aim of prefiltering is to improve the information to be fused. The noisier a dataset is, the more iterations of the diffusion filter have to be applied. The conductance C (equation 2.3) controls the local degree of smoothing and the areas to be smoothed. The higher the conductance, the more the diffusion filter acts like an isotropic filter, smoothing all regions. The smaller the conductance, the more features are preserved. As we do not want to preserve artefacts, a rather high setting of the conductance is used for the LE dataset and an even higher setting for the HE dataset. For the LE dataset, a parameter setting of at least 5 iterations and a conductance of 10 to 50 turned out to produce reliable results. For the HE measurement we used 10 iterations at a slightly higher conductance of 75 to compute a smoother dataset.

In the registration step (Figure 3.3(b)) the HE dataset is considered as fixed image and the LE dataset as moving image. For the image pyramids a fixed setting of five levels is used.

For the DECT image fusion (Figure 3.3(c)) the gradient image of the Gaussian smoothed HE dataset determines the fusion regions. The wider these edge regions are, the smoother the image fusion will adopt features of the LE dataset. Using a sigma value of at least 0.2, a blurry image of the HE dataset is generated. When applying a gradient magnitude filter on this input image, a smooth gradient image is obtained. Depending on the dataset and the quality of edges, an edge image is produced with a smooth increase and decrease of the gradient magnitudes. The width of a typical edge is supposed to be approximately 5 to 10 voxels wide for a smooth image fusion. The trusted level which weights the LE dataset with 100 % should not exceed the standard deviation of the HE dataset. Otherwise artefacts are transferred to the resulting image.

In the local surface extraction step (Figure 3.3(d)) a reliable surface model is extracted using a global threshold. For the locally improved surface mesh gradient magnitudes along the surface normal have to be eval-

uated. The number of samples and the maximum sample distance have to be specified. The finer the sampling rate, the finer the positioning of the surface vertices. Generally settings of up to 50 samples within voxelsize are a valuable compromise between computation time and accuracy. A more difficult parameter is the maximum sample distance, which serves as a constraint for the repositioning of vertices. Exceeding a maximum sample distance of 5 times the voxelsize may produce erroneous results due to imprecisely oriented surface normals of the isosurface. Usually settings of 2 to 5 times the voxelsize produce a reliable improved surface mesh. Finally the normal orientation (positive, negative or both directions) is also a parameter to be set. Due to the noise in the surface mesh considering the use of both directions produces the most reliable results.

3.4.3 Evaluation of DECT workflow results

To get an overview of deformations throughout the whole specimen compared to reference geometry data, *e.g.,* a CAD model, actual/nominal comparisons are widely used. A common visualization method for actual/nominal comparison is color coding the reference's surface corresponding to the local deviation. To show the different results of generating surface models, actual/nominal comparisons between the CAD model and three surfaces are depicted. The first surface is due to the best global threshold from the LE data. The second surface is due to the best global threshold from the HE data. The third surface is the result of our proposed DECT workflow. Note: the CAD model does not contain the data of the screws and the round bar. The best global thresholds are empirically determined. The metal parts are intended to show the loss in data quality when placing high absorbing components within low absorbing material and to produce deformations in the isosurface due to artefacts. In Figure 3.12(a), high deviations due to streaking artefacts and scattered radiation are depicted in dark red and dark blue. In less artefact-affected areas, a high correspondence between the CAD model and LE measurement can be seen. Figure 3.12(b) shows a more homogeneous distribution of deviations. For the HE measurement, the mean deviation is much higher but hardly any strong artefacts affect the surface. Applying the DECT workflow the advantages of both measurements can be combined. The actual/nominal comparison shows higher accuracy than the HE dataset while reducing artefacts of the LE dataset (see Figure 3.12(c)). In the DECT result not all artefacts could be removed because the trusted level was set to the standard deviation of the HE dataset and therefore these deviations were considered to be real. Using a lower trusted level would introduce noise in parts of the HE datasets.

Specimen two was chosen to demonstrate the DECT workflow's ability to produce reliable surface models without holes. The multi-material characteristics of this specimen produce streaking artefacts and scattered
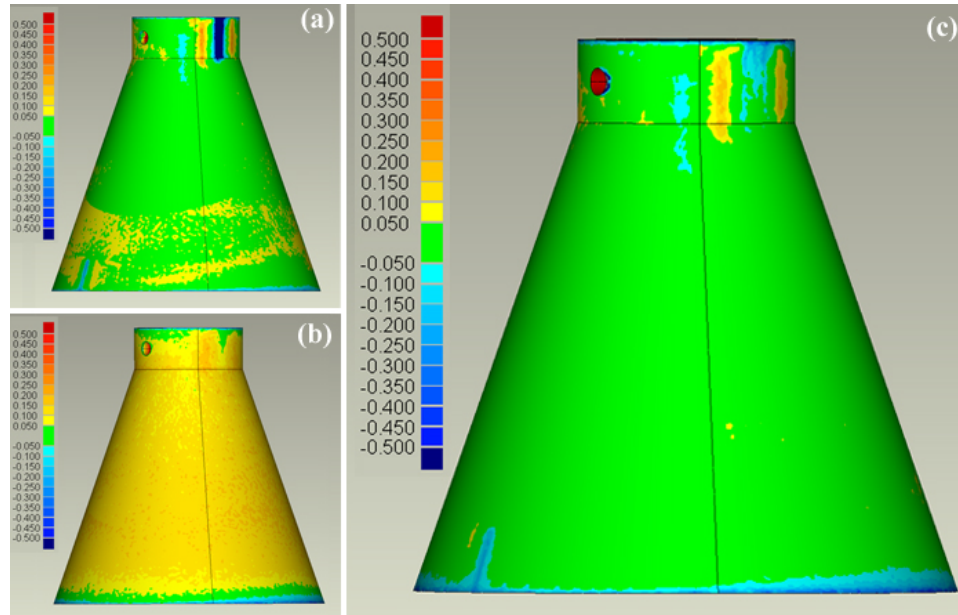
Figure 3.12: *Actual/nominal comparison of specimen one between CAD model and extracted surface models. Deviations in mm are color-coded using the same scale for each actual/nominal comparison. (a) shows the actual/nominal comparison using a global threshold applied to the LE dataset and in (b) to the HE dataset. The result when applying the DECT workflow to specimen one is depicted in (c). Artefacts of the LE measurement can be avoided to a high extent. The smoother characteristic of the DECT surface is indicated by the large low deviation area (green).*

radiation in the reconstructed dataset. These circumstances are depicted in Figure 3.2 and 3.10. When extracting an isosurface from the LE dataset, common methods like Otsu's method [Ots79] turned out to produce unusable results. The best global threshold to create a surface model was determined again empirically. However, a complete and reliable measurement is impossible due to severe artefacts of the derived surface model (Figure 3.13(a)). Using the HE dataset of specimen two, a reliable surface model may be extracted but due to the larger focal spot of the macro-focus source fine details get lost. Furthermore due to the much higher ambient noise level of the HE dataset, the generated surface model has a rather coarse surface structure (see Figure 3.13(b)). When applying the DECT workflow, part of the details are reconstructed by incorporating details from the LE dataset. In the resulting surface model holes were removed, surface deformations through scattered radiation were avoided and fine details were fused into the resulting dataset (see Figure 3.13(c)). For specimen two, slight deformations in the surface can be seen which is again due to a compromise between introduction of the HE dataset's noise and adoption of artefacts from the LE dataset.
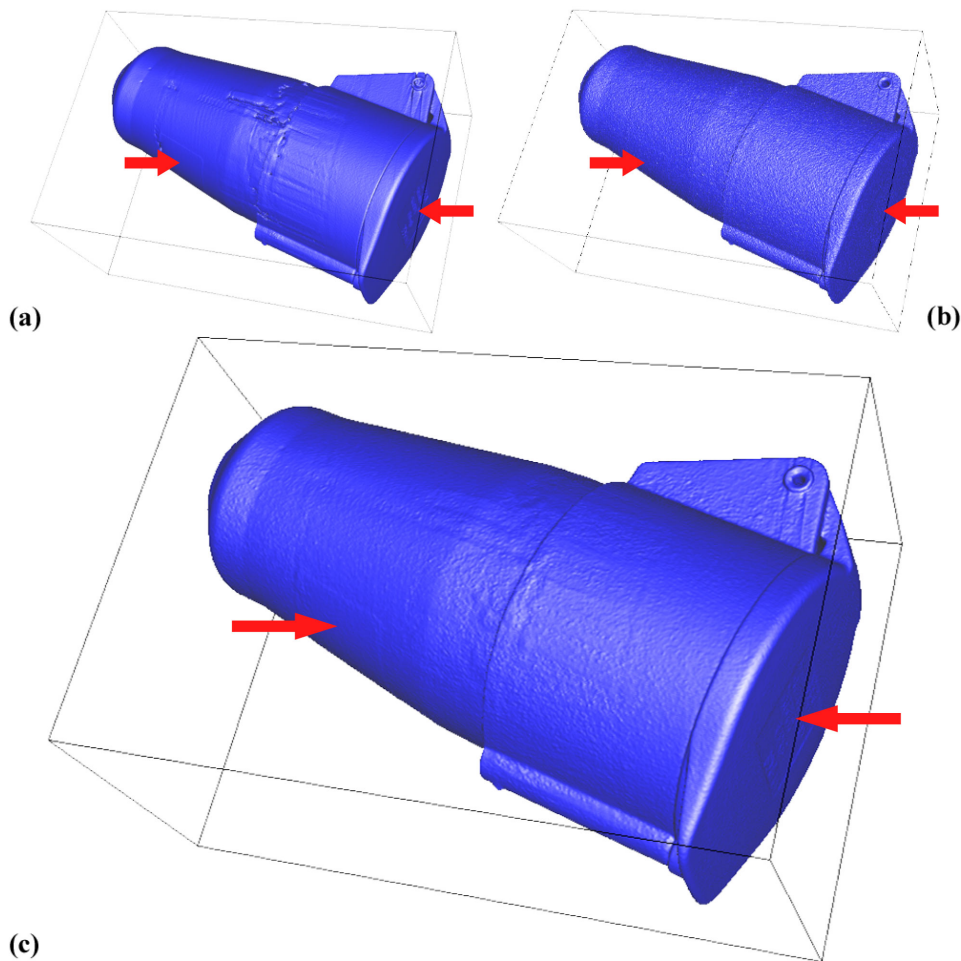
Figure 3.13: *Surface extraction of specimen two using a global threshold applied on (a) the LE dataset and on (b) the HE dataset. (c) depicts the result when applying the DECT workflow on specimen two. Artefacts of the LE measurement can be avoided. The coarse structure and the higher mean deviation of the HE measurement was significantly reduced. DECT fusion even preserves fine details of the LE dataset like the sticker on the jacket of the 400 V connector or the imprint on the cap (see red arrows).*

Specimen three was chosen as another representative multi-material component to demonstrate the performance of the DECT workflow. Dimensional measurement accuracies are verified by specification and evaluation of 16 inspection features (3 diameters of cylinders and 13 distances). As reference, specimen three was measured using a high precision coordinate measuring machine. In order to point out the differences in dimensional measurements, the same features were evaluated in the LE measurement, the HE measurement and the resulting dataset of the DECT workflow using Calypso. As expected, the LE measurement produces a result with higher precision than the HE measurement. In comparison to the LE

Table 3.4: Mean deviations per inspection feature for specimen three

	LE (mm)	(%)	HE (mm)	(%)	DECT (mm)	(%)
overall mean 16	0.0251	0.25	0.0299	0.31	0.0158	0.16
diameters mean 3	0.0309	0.52	0.0402	0.75	0.0206	0.37
lengths mean 13	0.0238	0.19	0.0275	0.21	0.0147	0.11

dataset the HE measurement is less artefact-affected. Applying the DECT workflow, artefacts are reduced, which can be seen in the lower mean deviation per inspection feature. For specimen three the mean deviation per inspection feature can be lowered by more than 1/3 taking the DECT workflow compared to using the LE dataset and nearly 1/2 compared to using the HE dataset (see Table 3.4 for details).

3.5   Summary

A novel workflow for dimensional measurement of multi-material industrial components is presented, allowing reproducible and robust surface extraction. The introduced DECT workflow exploits a dual source / dual exposure approach of dual energy computed tomography. It facilitates dimensional measurement of artefact-affected datasets from multi-material components. The presented DECT workflow combines the advantages of dual X-ray exposure technology by taking two X-ray CT datasets with complementary strengths and weaknesses into account. The workflow integrates image fusion and local surface extraction techniques: After prefiltering both datasets are registered to each other. In the fusion step, the two scans are combined by integrating the low energy (LE) dataset's accuracy with the high energy (HE) dataset's robustness. Finally, a reliable surface model is extracted using a local, adaptive technique.

The accuracy and the applicability of the DECT workflow has been discussed using a testpart as well as two industrial components. Results are depicted in actual/nominal comparisons, reliable surface models, and quantitative measurement errors. For the terminal block, the mean deviation per inspection feature could be decreased by a third compared to using the LE dataset and nearly a half compared to using the HE dataset.

It is not certain that everything is uncertain.

Blaise Pascal

4

Statistical Analysis of
# Multi-Material Components using Dual Energy CT
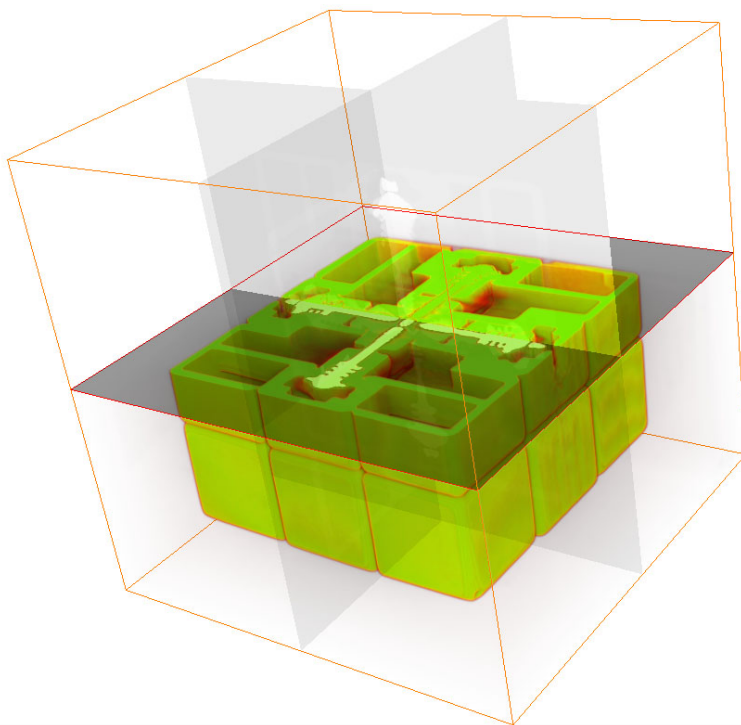
Figure 4.1: *Direct volume rendering of the underlying probability data maps the spatial uncertainty using opacity and color transfer functions. Semitransparent axial, sagittal and frontal cross-sections are used as cutting planes.*

U NCERTAINTY of extracted surface models and consequently of extracted dimensions is a critical issue, which is usually neglected in industrial 3DCT. As each extracted surface only contains sharp borders, which are supposed to characterize the "real" boundary of materials, the entire information on the quality of the interface and in consequence on the uncertainty of extracted dimensions is lost. However especially in the area of metrology of plastics-metal components severe artefacts influence the position of the extracted surface model and therefore the quality of the extracted dimensions.

This chapter describes a novel method for a statistical analysis of multi-material components. The presented work makes use of dual energy CT data acquisition for artefact reduction, in order to optimize CT scans of multi-material components. Using statistical analysis, information on uncertainty is introduced, which allows detailed characterizations of single materials as well as material interfaces.

The major contribution is the development of a specific pipeline based on the dual exposure technique of dual energy CT. After prefiltering and multi-scan fusion, the statistical analysis step computes probability volumes of the fused data using a local histogram analysis technique.

4.1   Introduction

One of the most critical issues in the area of metrology using industrial 3DCT is the problem of artefacts. The characteristics and strength of an artefact is mainly determined by the specimen's geometry, the penetration lengths, the position and orientation in the cone beam, the measurement parameters, and the specimen's material combination. Some of the most common artefact types are noise induced streaks, beam hardening, partial volume effects, aliasing, and scattered radiation [Hsi03]. In the area of metrology artefacts may seriously affect or even prevent reliable measurements. Especially when scanning multi-material components severe streaking artefacts are introduced due to major changes in attenuation from one projection to the next. We addressed this problem in our previous work in chapter 3 [HKG07] reducing artefacts by data fusion of DECT scans.

A further critical problem is the lack of information on the uncertainty of an extracted surface, and in consequence, on the quality of the extracted dimensions. For surface extraction in industrial applications, usually a single isovalue is specified to distinguish between material and air. More recently, research activities concentrate on local surface extraction and en-

hancement, *e.g.*, see Bischoff and Kobbelt [BK02], Gibson [Gib98] and Whitaker and Breen [WB98]. Both local and global surface extractions consider the surface as ground truth for subsequent measurements. As each extracted surface only contains sharp borders characterizing the supposed boundary between materials, the entire information on the quality of the interface is lost.

This chapter introduces a novel approach which addresses both the problem of artefacts and the problem of uncertainty [HKMG08]. For artefact reduction of multi-material components, dual energy CT (DECT) is used. After prefiltering, a gradient magnitude based fusion step combines the two complementary DECT datasets, featuring the strength of each dataset. Using Bayesian classification, a probability volume is extracted containing the probabilities of each single material. Subsequent evaluations are based on the probability dataset.

4.2 Related Work

4.2.1 Dual Energy CT

Dual energy CT (DECT) was originally used for characterization of organic and inorganic materials in baggage control systems for airport security and for examination of drilling cores concerning material properties [IDO*06]. More recently the application area of DECT was expanded to medical and finally industrial CT. The main idea of DECT is to utilize different X-ray spectra in order to optimally characterize multi-material probes. DECT is facilitated by two different techniques: the dual exposure / dual source and the dual detector technique [RD06]. The dual detector technique generates two datasets in one scan by using multi-layer-detectors, sensitive to different energy bands. 3DCTs with a single layer detector are limited to the dual exposure technique. The used 3DCT device is equipped with a single layer detector, featuring a high precision micro-focus and a high power macro-focus X-ray source. Therefore the dual exposure technique is used in this approach.

4.2.2 Multi Scan Fusion

In multi-scan fusion (MSF) recent advances either focus on enhancing projection images, respectively sinograms or on enhancing the reconstructed volumetric datasets. Sinograms are used by Oehler and Buzug [OB07] for artefact correction and are currently a topic of research for multi-scan fusion. As we do not have access to projection images respectively sinograms, these methods are out of scope of our work.

A straight forward approach of MSF is dual viewing: Specimens are scanned twice at different positions and orientations [SHP08] in the cone

beam. Local data fusion allows to identify and reduce artefacts by considering the differences in gradient magnitude and greyvalue. However, orientation-invariant artefacts or artefacts affecting the same region can not be eliminated. More sophisticated approaches exploit DECT to combine multiple, corresponding slice images [SHP08] or multiple volumetric datasets [HKG07]. We apply a fusion scheme similar to Heinzl et al. [HKG07]. Instead of only fusing edge regions and neglecting solid material regions, we propose a multi-scan fusion scheme, which locally fuses the complete datasets. Combining the complete dataset allows to avoid irregularities in the histogram due to only considering edge regions. The presented fusion scheme emphasizes the complementary strengths of each CT modality. The main object structure, which is depicted best in the macro-focus scan, is fused with the sharp edges of the micro-focus scan.

4.2.3 Statistical Analysis

A large variety of application areas document the importance of statistics and uncertainty in visualization. Li et al. [LFLH07] address visualizing uncertainty in large-scale virtual astrophysical environments. Rheingans and Joshi [RJ99] study positional uncertainty in molecule models. Lundström et al. [LLY06] present an automatic tissue detection scheme for medical visualization.

Recent advances in the area of statistical analysis focus on uncertainty visualization, fuzzy segmentation, and transfer function design. An overview of uncertainty visualization is outlined by the following techniques: Wittenbrink et al. [WPL96] are using geometric glyphs visualizing uncertainty in vector field data. Kniss et al. [KUS*05] proposed a method to explore uncertainty, risk, and probabilistic decision of surface boundaries in direct volume rendering (DVR). Rheingans and Joshi [RJ99] proposed the rendering of the likelihood domain itself. Rhodes et al. [RLBS03] are mapping the confidence of isosurfaces to hue or texture. In our approach, we color-code uncertainty on isosurfaces and show a color-coded DVR of probability datasets.

In fuzzy segmentation, each voxel has a certain degree of belonging to a region, facilitating segmentation at subvoxel accuracy. The importance of fuzzy classification with respect to material boundaries is discussed by Tzeng and Ma [TM04]. Grigoryan and Rheingans [GR04] employ a point cloud approach representing the spatial uncertainty in segmented data. Stalling et al. [SZH98] use additional probability information in order to supplement region labels. In our work, we are using the spatial probabilities of each material to fuzzy segment a real world component.

In the area of transfer function design, Bajaj et al. [BPS97] introduced the contour spectrum, which performs statistical analysis to create transfer function lookup tables. Multi-dimensional transfer functions, introduced
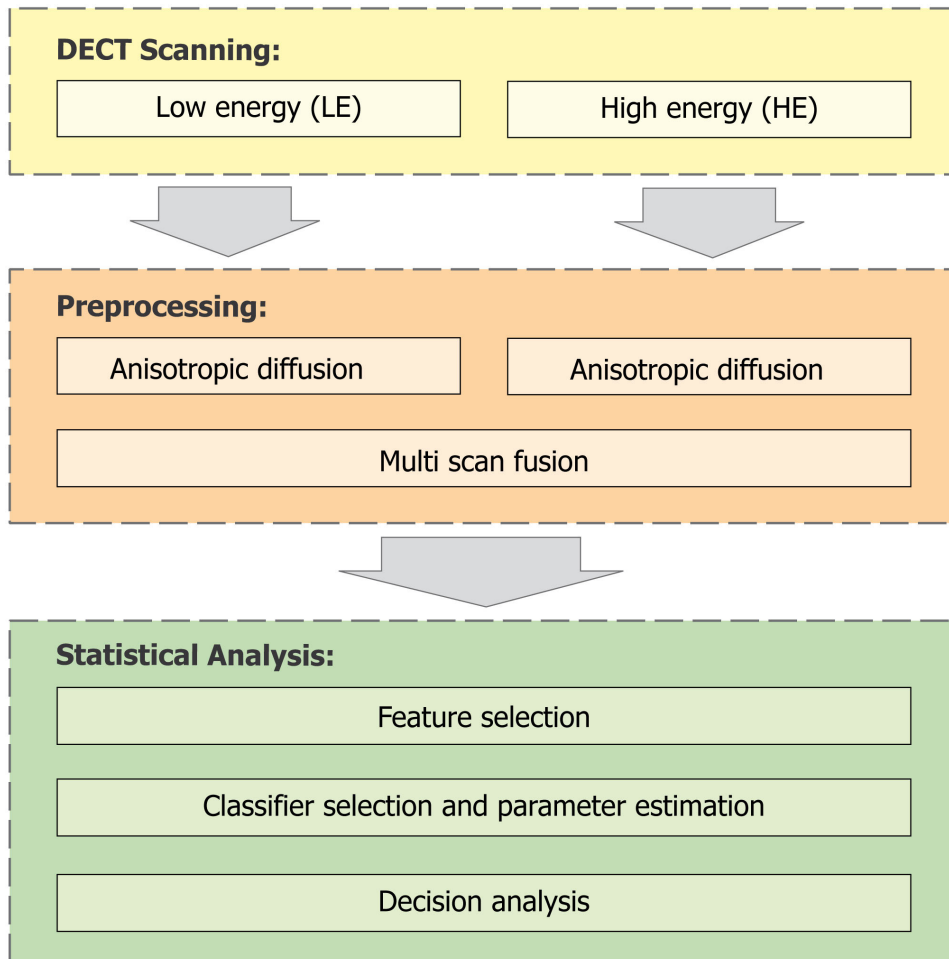
Figure 4.2: *Principle scheme of the pipeline for statistical analysis of multi-material components. Input: HE and LE dataset, Output: probability volume.*

by Levoy [Lev88], enhance the transfer function domain using additional dimensions. While Levoy suggested the use of the gradient magnitude, Kindlmann and Durkin [KD98] even included the second derivative. Due to artefacts and overlapping regions, multi-dimensional transfer functions turned out to be unusable in our situation.

In the presented approach, we follow the idea of Kniss et al. [KUS*05] to use statistical classification for generating information on uncertainty of CT datasets. We introduce a pipeline model (see Figure 4.2), which automatically classifies individual materials in an easy to use process. In particular, our approach is based on local histogram analysis using partial range histograms, which were originally introduced by Lundström et al. [LLY06].

(a) LE

(b) HE
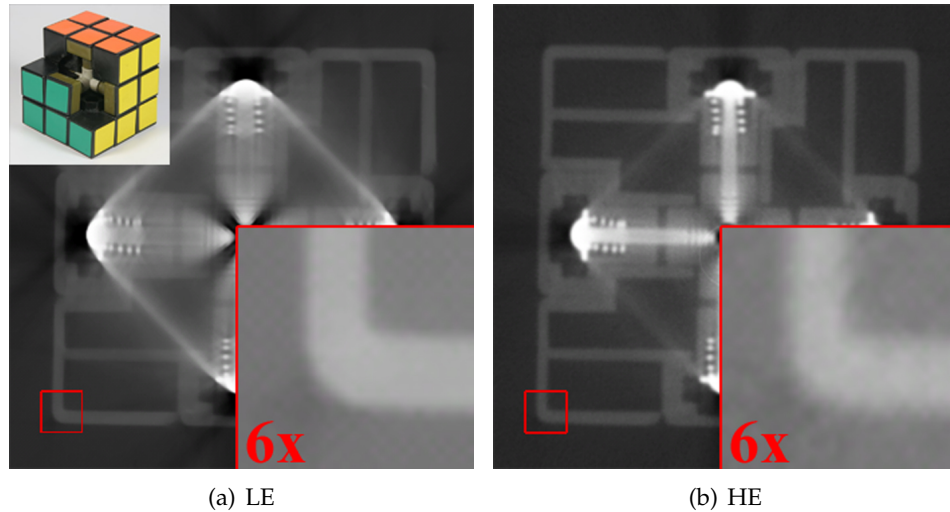
Figure 4.3: *Axial cross sections through the Rubik's cube datasets. (a) Severe artefacts modify greyvalues in the LE scan near high absorbing components. (b) Less artefact-affected but more blurry HE scan. For a better visualization of the inherent noise, a contrast windowing was applied on the detail images (photograph courtesy of R. Frisch).*

4.3 Pipeline for Statistical Analysis of Multi-Material Components

To facilitate statistical analysis of artefact-affected industrial CT data, a customized pipeline was developed. The pipeline for statistical analysis of multi-material components is based on dual energy CT and combines pre-filtering, multi-scan fusion and statistical analysis (Figure 4.2). The pipeline is demonstrated step by step on a real world object, the Rubik's Cube (for a detailed description of this specimen see section 4.4.1).

4.3.1 Dual Energy CT Scanning

DECT scans are facilitated by two subsequent scans without moving the specimen: A low energy (LE) micro-focus scan yields a highly detailed but artefact-affected scan. It generates better scanning results for low absorbing materials. However, severe artefacts are introduced in the presence of high absorbing components (see bright and dark streaks in Figure 4.3(a)). The subsequent high energy (HE) macro-focus scan yields maximal penetration lengths. HE scans generate almost artefact free results, but the bigger focal spot of the X-ray source introduces additional blur (Figure 4.3(b)).

(a) unfiltered (HE scan)   (b) filtered (HE scan)
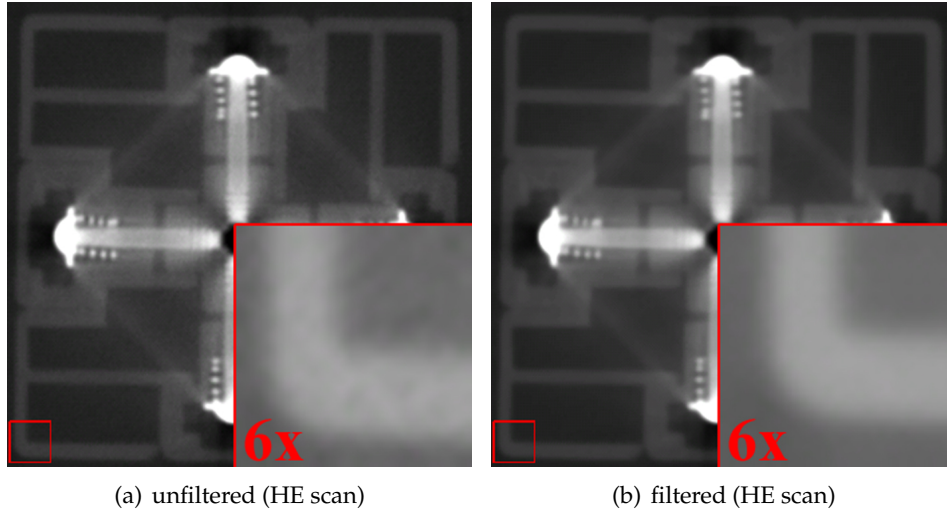
Figure 4.4: *Axial cross sections through HE scan of the Rubik's cube dataset (a) before and (b) after anisotropic diffusion filtering. The dataset's inherent noise is significantly reduced without moving or degrading edges. A contrast windowing was applied on the detail images for a better visualization.*

4.3.2 Preprocessing

Anisotropic Diffusion

A preprocessing step is used to reduce the propagation of noise and smaller artefacts through the pipeline. For prefiltering without moving or degrading edges, the anisotropic diffusion filtering of HE and LE data is used similarly to our previous work [HKKG06] (see chapter 2.3.1 for details). Applying the anisotropic-diffusion filter on the Rubik's Cube dataset, the dataset's inherent noise is significantly reduced without moving or degrading edges (see section 2.3.1 and Figure 4.4).

Multi-Scan Fusion

To reduce artefacts, which especially emerge when scanning multi-material components, a custom fusion scheme was developed. The aim of this step is to extract details of the LE scan, without introducing artefacts. Compared to our previous work in chapter 3 [HKG07], a smooth fusion throughout the whole dataset has to be ensured to prevent modifications of the statistical greyvalue distribution, which is undesirable in statistical analysis. In the first step the region type (RT) of each voxel is determined using spatial greyvalues and gradient magnitudes. Three different region types are distinguished: homogeneous, transition, and artefact-affected region. At each spatial position the weights for the LE and the HE dataset are computed ac-

---

Algorithm 1 Multi-Scan Fusion (MSF)

Δ_{GV} (greyvalue (GV) difference HE-LE dataset); Δ_{GM} (gradient magnitude (GM) difference HE-LE); ϵ_{GV} (max GV difference); ϵ_{GM} (max GM difference); c_{min} (min GM); c_{GM} (GM transition)

---

procedure MSF($\epsilon_{GV}, \epsilon_{GM}, c_{min}, c_{GM}$)
    for all $correspondingvoxels \in LE, HE$ **do**
        $RT \leftarrow RegionType(\epsilon_{GV}, \epsilon_{GM}, c_{min}, c_{GM})$
        if $RT == ArtefactAffected$ **then**
            $w_{LE} \leftarrow 0; w_{HE} \leftarrow 1$
        else if $RT == Transition$ **then**
            $w_{LE} \leftarrow Sigmoid(GM_{HE} - c_{GM})$
            $w_{HE} \leftarrow (1 - w_{LE})$
        else
            $w_{LE} \leftarrow 0.5; w_{HE} \leftarrow 0.5$
        end if
        $Fused \leftarrow (w_{LE} * GV_{LE} + w_{HE} * GV_{HE})$
    end for
end procedure

procedure REGIONTYPE($\epsilon_{GV}, \epsilon_{GM}, c_{min}, c_{GM}$)
    if ($|\Delta_{GV}| > \epsilon_{GV}$ or $|\Delta_{GM}| > \epsilon_{GM}$) **then**
        $RT \leftarrow ArtefactAffected$
    else
        if ($\Delta_{GM} > c_{min}$ & $GM_{HE} > c_{GM}$ & $GM_{LE} > c_{GM}$) **then**
            $RT \leftarrow Transition$
        else
            $RT \leftarrow Homogeneous$
        end if
    end if
    return RT
end procedure

---

cording to the region type. In artefact-affected regions, only the HE dataset is considered and weighted with 1. Homogeneous regions are equally weighted for noise reduction. For transition regions a Sigmoid function is used in the range of 0.5 to 1.0, weighting the greyvalues of each dataset according to the local gradient magnitude of the preprocessed HE scan. Compared to a linear weighting, the Sigmoid function allows a stronger consideration of the detailed LE scan to achieve sharper boundaries (see Algorithm 1 and Figure 4.5).
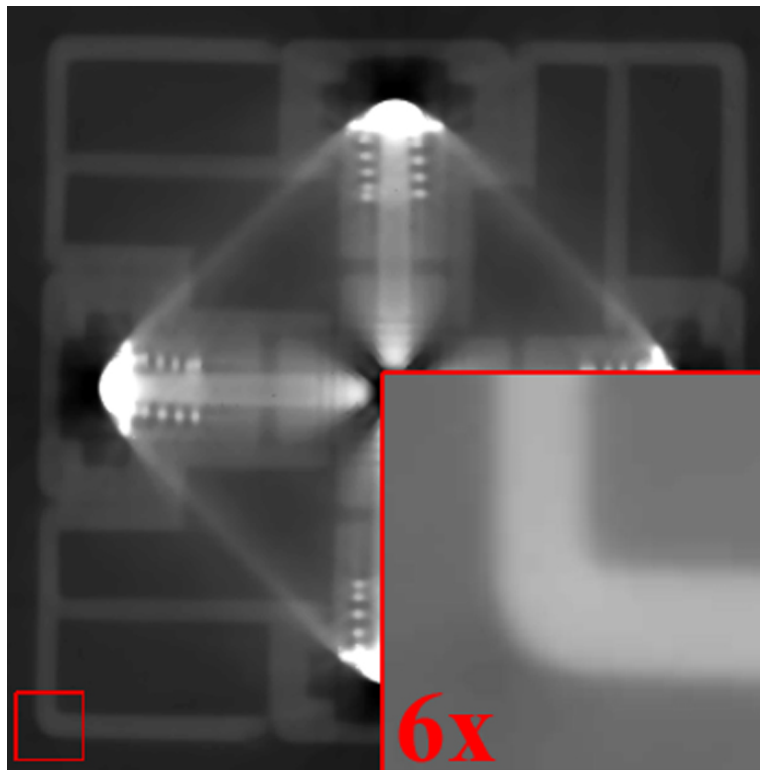
Figure 4.5: *Axial cross section through the fused dataset of the Rubik's cube dataset. Compared to the LE scan, artefacts are significantly reduced. The detail image shows a smooth characteristic of the greyvalues with sharp edges (contrast windowing was applied on the detail image).*

4.3.3 Statistical Analysis

For statistical analysis, Bayes' decision theorem is applied. The basis of Bayesian decision theory is the idea of quantifying trade-offs and costs in classification decisions. Classifications using Bayesian decision theory consists of 3 major steps: 1) feature selection, 2) selection and estimation of the classifier, and 3) estimation of the class conditional PDF and decision analysis. Bayes' decision theorem provides the relationship between class conditional and posterior probability. The class conditional probability is defined as the probability of an event A, given the occurrence of another event B. The posterior probability of a random event is the conditional probability that is assigned after the relevant evidence is taken into account.

Feature Selection

In the case of statistical analysis of multi-material components the task of the classifier is to distinguish between the different materials. Firstly,

each material is assigned to a class ω_j, *e.g.*, for plastic-metal components: $\omega_0 \leftarrow air$, $\omega_1 \leftarrow plastics$ and $\omega_2 \leftarrow metal$. The second task is to select "good" features to distinguish the different classes. A "good" feature is discriminating, easy to extract and should be position, orientation and scale invariant.

For decomposing CT datasets into individual materials, the spatial greyvalues are used as feature. Including more dimensions to the feature vector, *e.g.*, gradient magnitude or the 2nd derivative, does not necessarily result in a better classifier. Due to artefacts and performance issues of the classification, the feature vector was not extended beyond using the greyvalues.

Classifier Selection and Parameter Estimation

The selection of a reliable classifier is the most critical step. To construct the classifier, the following assumptions are taken for 3DCT: Homogeneous materials should generate constant greyvalues. Due to partial volume effects, greyvalues are modified in the edge regions of a material. Furthermore, irregularities are introduced due to the characteristics of detector and X-ray source as well as the 3D reconstruction. As the greyvalues of a homogeneous material tend to be continuously distributed, the classifier is modelled by a probablistic distribution (probability density function $p(\mathbf{x}|\omega_j)$, $\mathbf{x}$ denotes a sample feature vector). Based on these assumptions we consider the classifier to be Gaussian-distributed for the subsequent steps.

Gaussian curve fitting is used to setup the probability density function (PDF) $p(\mathbf{x}|\omega_j)$ of a class ω_j. An expectation maximization scheme based on Gaussian mixture models, which was applied to the global histogram, turned out to produce suboptimal PDFs. Due to the overlapping characteristic of the material distributions in the histogram, especially of the low absorbing material and air, the Gaussian parameters degenerated.

In contrast, local histogram analysis allows to reconstruct each material's histogram H_{ω_j}. We apply a method for histogram decomposition, which is based on Lundström et al. [LLY06]. Initially, the histogram of a dataset is divided into partial range histograms (PRH). A PRH is defined as the histogram for a set of typically cube sized neighborhoods which are within a given intensity range. To select the blocks, which are added to the PRH, the range weight criterion is used. The range weight defines the percentage of voxels within a predefined range around a local maximum: $\mu \pm \alpha * \sigma$ (α denotes the range of considered standard deviations). So a cube sized block is added to a PRH if the range weight is high enough.

In order to reconstruct each material's histogram H_{ω_j} by recombination of PRHs, Lundström et al. rely on a custom heuristic for medical datasets. This heuristic employs the criteria $\sigma_{max}/\sigma_{min} <= 4$ and $\mu_{max} - \mu_{min} <= \sigma_{min} * max(1, 2 - \sigma_{min}/40)$, which performed well on their

datasets. Unfortunately this heuristic turned out to be unusable on uncalibrated industrial CT data. Therefore we developed a new recombination method based on weighted multi-dimensional KMeans, which is applicable on datasets of any domain: For each extracted PRH a feature vector is defined, which consists of μ and σ. While μ corresponds to the highest peak in the PRH, σ is estimated by Gaussian curve fitting, minimizing the accumulated height difference. The wider the partial ranges $\mu \pm \alpha * \sigma$, the more data of the PRH is considered for the fit. As in each PRH only one feature is dominant, α of 2 covers the range of about 95% of the Gaussian distribution for the fit. For recombination of the PRHs to a material's histogram H_{ω_j}, weighted KMeans [DHS00] is used. The extracted feature vector of each PRH is weighted with the sum of frequencies in the PRH. This allows preferring larger PRHs over smaller ones. KMeans clustering requires the number of clusters to be separated, which corresponds to the number of defined classes ω_j. So for each cluster a random initial cluster center is set up. The feature vectors of each PRH are assigned to the nearest cluster center. After all feature vectors are classified, a new cluster center is calculated and the algorithm restarts. The algorithm stops as soon as the cluster centers are not changing anymore and the final cluster centers are found. Finally the PRHs of each cluster are combined to generate each material's histogram H_{ω_j}.

To estimate the classifier for a class ω_j, the parameters of the PDF $p(\mathbf{x}|\omega_j)$ of each material's histogram H_{ω_j} have to be estimated. μ_{ω_j} is considered to coincide with the highest peak in the histogram. To reduce errors of irregularities and smaller spikes in the histogram, σ_{ω_j} is calculated as the mean of two estimations: Firstly, $\sigma_{\omega_j,1}$ is estimated by a Gaussian curve fitted to the peak of the material's sub-histogram with a partial range using $\alpha = 2$ since the entire peak is exposed. Secondly, the overall standard deviation $\sigma_{\omega_j,2}$ of the histogram H_{ω_j} is calculated. The mean of $\sigma_{\omega_j,1}$ and $\sigma_{\omega_j,2}$ is used to specify σ_{ω_j}. The resulting material histograms for each class ω_j of the Rubik's cube dataset and the corresponding PDFs $p(\mathbf{x}|\omega_j)$ are depicted in Figure 4.6.

Estimation of Class Conditional PDF and Decision Analysis

For decision analysis a probability dataset is calculated from the prefiltered and fused LE and HE datasets. The probability dataset contains a probability vector at each spatial position. The components of a probability vector contain the posterior probabilities of the corresponding spatial greyvalue of belonging to a considered class ω_j.

The probability vector is calculated using Bayes' theorem:

$$p(\omega_j|\mathbf{x}) = \frac{p(\mathbf{x}|\omega_j)P(\omega_j)}{p(\mathbf{x})}, \tag{4.1}$$

(a) ω_0 (air)

(b) ω_1 (plastics)
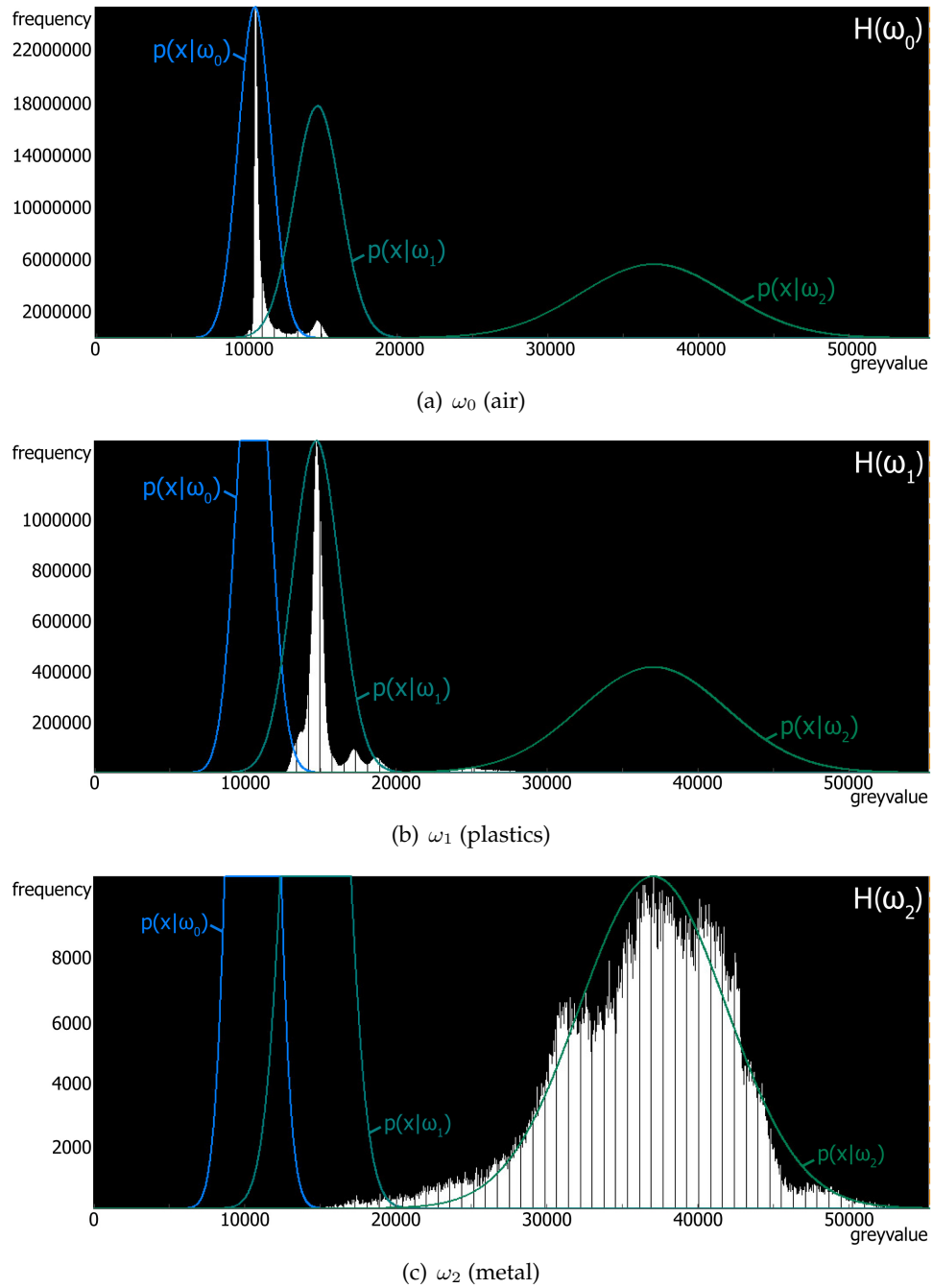
(c) ω_2 (metal)

Figure 4.6: *Resulting sub-histograms of the Rubik's cube dataset are depicted (a) for class ω_0 (air), (b) for class ω_1 (plastics) and (c) for class ω_2 (metal). The blue to green graphs depict the extracted probability density functions $p(x|\omega_j)$ for each class scaled to the maximum of the peak of the corresponding histogram H_{ω_j}.*

The posterior $p(\omega_j|\mathbf{x})$ of a random event weights the class conditional PDF $p(\mathbf{x}|\omega_j)$ against the observed evidence $p(\mathbf{x})$ and the prior information $P(\omega_j)$. The class conditional PDFs $p(\mathbf{x}|\omega_j)$ describe the probabilities of a greyvalue belonging to a certain class ω_j. The evidence is defined as

$$p(\mathbf{x}) = \sum_{j=0}^{c-1} p(\mathbf{x}|\omega_j)P(\omega_j), \tag{4.2}$$

which is the sum of all class conditional PDFs $p(\mathbf{x}|\omega_j)$. The evidence serves as a scaling factor, which guarantees the posterior probabilities $p(\omega_j|\mathbf{x})$ to sum to 1. The prior probability value $P(\omega_j)$ is a marginal probability, which describes the statistical probability of a material ω_j when picking a random position in the dataset.

In order to calculate the probability volume of a fused DECT dataset, first of all the prior probability $P(\omega_j)$ of each material has to be determined. As the volumetric ratios of a material should not influence local boundaries, the priors $P(\omega_j)$ for each material ω_j are evenly set to $1/c$. The class conditional PDFs $p(\mathbf{x}|\omega_j)$ are estimated using the local histogram approach introduced in subsection 4.3.3. The evidence $p(\mathbf{x})$ is calculated using equation 4.2 and the posterior $p(\omega_j|\mathbf{x})$ using equation 4.1.

In Figure 4.7 the resulting posterior probability volume of the Rubik's cube dataset is depicted. Figure 4.7(a) shows an axial cross section which depicts the posterior probability $p(\omega_0|\mathbf{x})$ of class ω_0 (air), Figure 4.7(b) the posterior probability $p(\omega_1|\mathbf{x})$ of class ω_1 (plastics) and Figure 4.7(c) the posterior probability $p(\omega_2|\mathbf{x})$ of class ω_2 (metal). Bright areas depict regions with high probabilities near 1 and dark regions vice versa low probabilities near 0. In this context probability volumes allow robust and reproducible fuzzy segmentations of each material.

4.4 Results and discussion

All evaluated specimens are multi-material components consisting of low absorbing material (plastics) and high absorbing material (metal). The CT scans were performed on a HWM RayScan 250E system with a 225 kV micro-focus and a 450 kV macro-focus X-ray source. As reference, CAD models are used. The demo application was implemented in Visual C++ using ITK [ISNC03] and VTK [SML04].

4.4.1 Specimens

Rubik's Cube

Specimen one (Figure 4.3) is a mechanical puzzle. The original Rubik's cube consists of three intermediate levels in height, width and depth. Each

(a) ω_0 (air)

(b) ω_1 (plastics)

(c) ω_2 (metal)
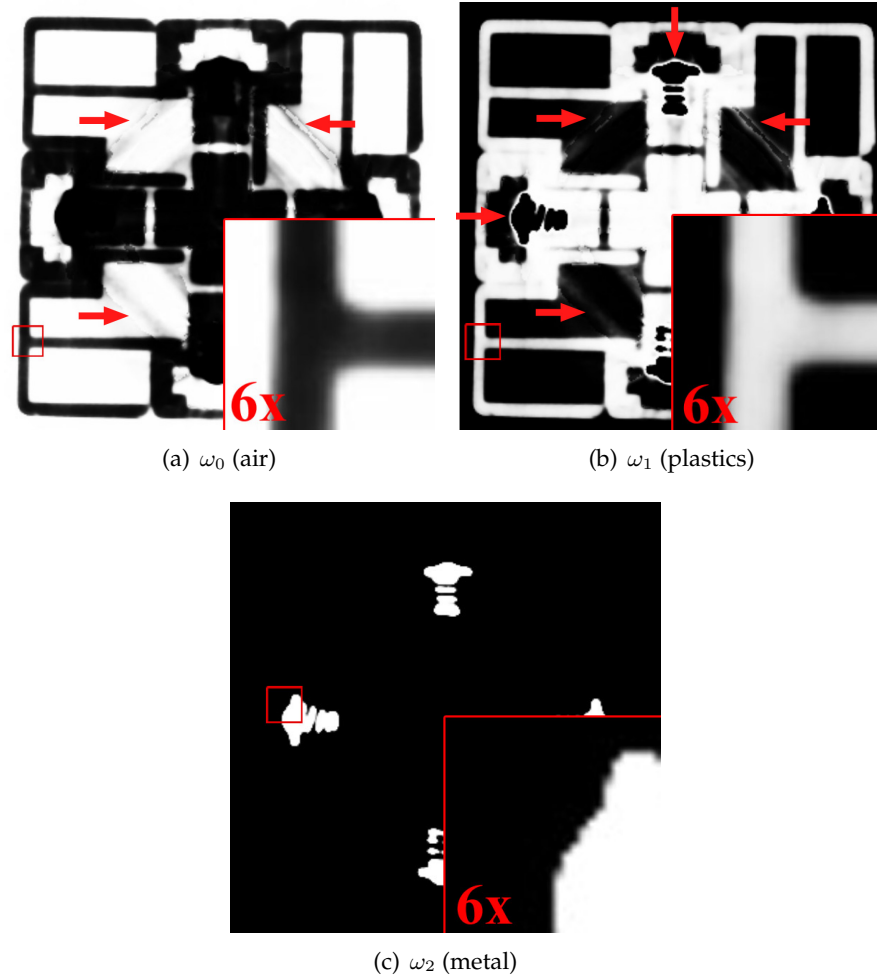
Figure 4.7: *Axial cross section through the resulting probability volume of the Rubik's cube dataset depicting the probabilities of (a) air, (b) plastics and (c) metal and the implicit fuzzy segmentation of each material. Bright regions refer to high probabilities near 1, dark regions to low ones near 0. Minor modifications due to the HE dataset are still visible in the probability volume (see red arrows).*

face is covered by nine stickers of one of six solid colors. Disassembling the cube gives 21 pieces: a core piece consisting of three intersecting axes, which hold the six center squares, and twenty smaller plastic pieces for the subsections. The six squares of the core piece are mounted to the axis cross using six steel screws. Springs pushing the squares of the core piece allow flexible movement of the axes. The CT measurement parameters for the Rubik's cube are listed in Table 4.1.

Table 4.1: *Parameters for specimen one (Rubik's cube)*

Parameter	Specimen one HE	Specimen one LE
projections	810	810
voltage (kV)	420	150
current (μA)	1200	400
integration time (ms)	285	500
prefiltering	1 mm W + 1.5 mm Cu	1 mm Cu
datasize	$401 * 401 * 401$	$401 * 401 * 401$
voxelsize (μm)	200	200

TP03

Specimen two (Figure 3.9) is a polyethylene testpart consisting of a cone
with an attached cylinder. Six smaller vertical drill holes are placed on the
bottom and top side, four in the base of the specimen and two on the top.
The central drill and the six smaller drill holes are equipped with screws
and a steel bar, in order to artificially create a multi-material component.
For detailed CT measurement parameters see Table 3.1.

4.4.2 Tuning the pipeline

The differentiation between the different region types in the fusion step is
controlled by greyvalue and gradient magnitude based parameters. The
parameters ϵ_{GM}, ϵ_{GV} and c_{GM} are individually determined by a histogram
analysis of the spatial differences in greyvalue respectively gradient mag-
nitude. ϵ_{GM} and ϵ_{GV} are used to specify the main peak range of the cor-
responding histogram, while c_{GM} sets the minimum for a valid transition
between the classes. c_{min} is a negative value depicting the minimal thresh-
old of ΔGM, which helps to avoid streaking artefacts in the fused result.
It is supposed to be lower than ϵ_{GM} and set in the range of $0.5 * \epsilon_{GM}$ to
ϵ_{GM}. The extraction of partial range histograms requires two parameters to
control the extraction process of each material's histogram. ϵ_{PRH} controls
the generation of PRHs. A cube sized neighborhood block is added to the
PRH if the range weight is high enough. The higher ϵ_{PRH}, the more ho-
mogeneous is the corresponding region of a PRH, but also the more PRHs
are extracted. Values between 0.8 and 0.9 proved to be a good trade-off
between the number of extracted PRHs and homogeneity. Furthermore,
the precision of a PRH is controlled by the neighborhood size. 8^3 is a typ-
ical setting for our datasets. To capture smaller structures lowering the
neighborhood size is suggested. Due to the weighted multi-dimensional
KMeans PRH recombination, the specification of further parameters is not
necessary.
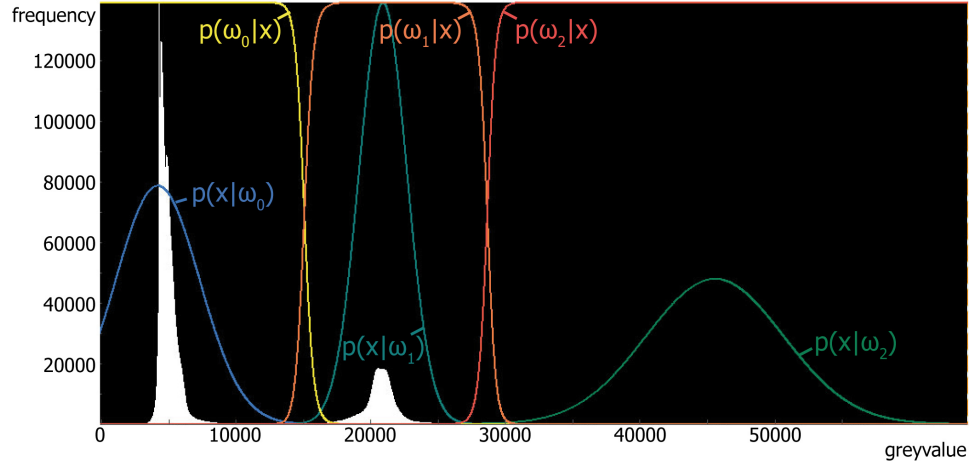
Figure 4.8: *Histogram of specimen two. Blue to green graphs depict the extracted class conditional PDFs $p(\mathbf{x}|\omega_j)$ of each material. Yellow to orange graphs plot smooth and overlapping posteriors $p(\omega_j|\mathbf{x})$ for calculating the probability volume.*

4.4.3 Evaluation of results

Extraction of PDFs

The extraction of class conditional PDFs and the corresponding posteriors is demonstrated using specimen two. Narrow PDFs $p(\mathbf{x}|\omega_j)$ result in sharp transitions of the posterior $p(\omega_j|\mathbf{x})$. However, sharp transitions generate segmentation-like probability volumes, which degenerate the extracted probability surfaces to jagged representations.

Wide and overlapping probability density functions $p(\mathbf{x}|\omega_j)$ allow the calculation of posteriors with smooth transitions, which serve for calculating probability volumes with fuzzy transitions. Figure 4.8 depicts the extracted class conditional PDFs $p(\mathbf{x}|\omega_j)$ (blue to green graphs) and the resulting posteriors $p(\omega_j|\mathbf{x})$ (yellow to orange graphs) in the corresponding histogram.

Fuzzy segmentation

Another application area realized by probability volumes is fuzzy segmentation. Common segmentation methods based on binary encoding are lacking information on uncertainty. Probability volumes contain spatial probability values and therefore an implicit fuzzy segmentation. Using fuzzy segmentation, transition and artefact-affected regions are considered with decreased probability values and do not generate jagged structures due to binary segmentation. Figure 4.7 depicts axial cross sections of each material of specimen one. Figure 4.9 shows volume renderings of a (a) threshold based binary segmentation and (b) the resulting fuzzy segmentation of the

(a)   (b)
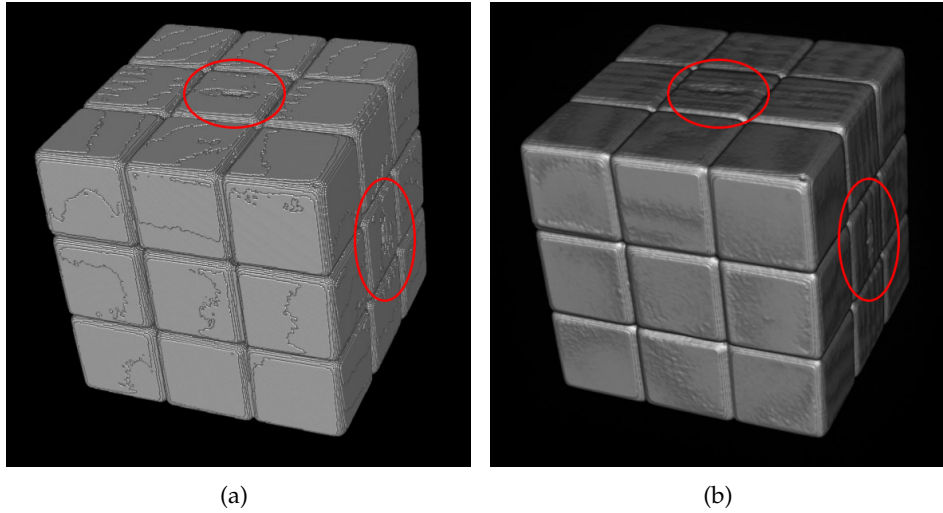
Figure 4.9: *Volume rendering of (a) threshold-based binary segmentation and (b) fuzzy segmentation of plastics of specimen one using a probability threshold of 0.9. Fuzzy segmentation generates a detailed representation of the segmented material (see red circles).*

plastics class of the Rubik's cube dataset using a probability threshold of 0.9.

Metrology

To get an overview of a surface model's deviations compared to reference geometry data, actual/nominal comparisons are widely used. Actual/nominal comparisons color-code deviations between the surfaces of the test model and the reference model on the surface of the reference model. Figure 4.10 depicts 4 actual/nominal comparisons (reference: CAD model). The upper two images depict 3D actual/nominal comparisons of the best global isosurface (Figure 4.10(a)) respectively isoprobability surface (Figure 4.10(b)). Compared to the isosurface, the actual/nominal comparison of the isoprobability surface shows similar or marginally lower deviations on the outer surface. To reveal internal deviations, a 2D comparison is carried out on the best global isosurface (Figure 4.10(c)) respectively isoprobability surface (Figure 4.10(d)). The 2D actual/nominal comparison shows the deviations of reference and test model on the contour of the reference's surface at a predefined cutting plane. 2D actual/nominal comparisons reveal the major advantage when using probability volumes on internal structures. The global isosurface is not able to capture transitions to a neighboring higher absorbing material and a lower absorbing material using one single threshold (Figure 4.10(c)). Erroneous results are generated due to incomplete data (red circles and arrows). In contrast, using the iso-

(a) Isosurface

(b) Probability surface

(c) Isosurface

(d) Probability surface
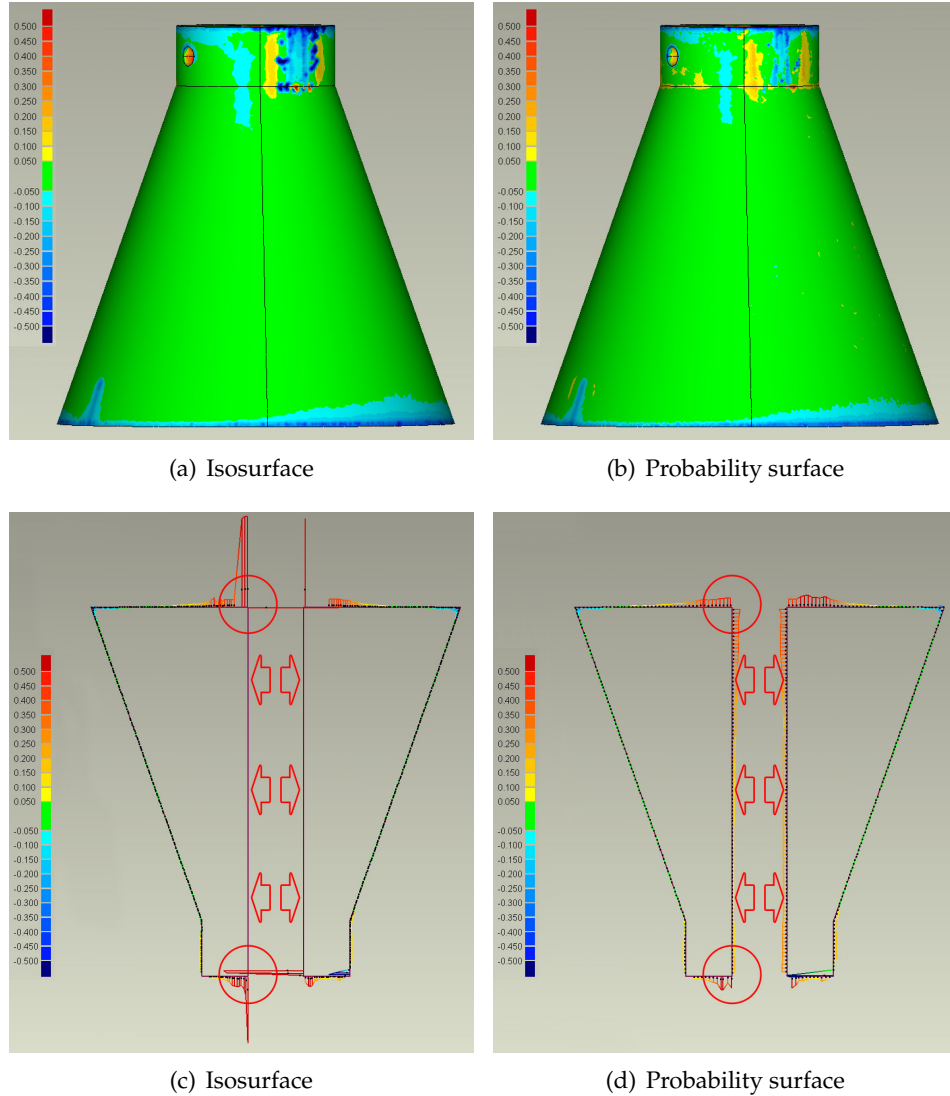
Figure 4.10: *Actual/nominal comparisons of probability surface and isosurface of specimen two. The colorscale denominates the deviations from the reference to test model in mm. The outer surface shows similar deviations in the actual/nominal comparisons of (a) isosurface and (b) probability surface. 2D cross sections reveal that only the probability approach captures internal transitions (red circles and arrows) in images (c) and (d).*

probability surface the complete contour is evaluated. The isoprobability surface facilitates an individual evaluation of each material in the dataset concerning all transitions to all neighboring materials (see Figure 4.10(d)).
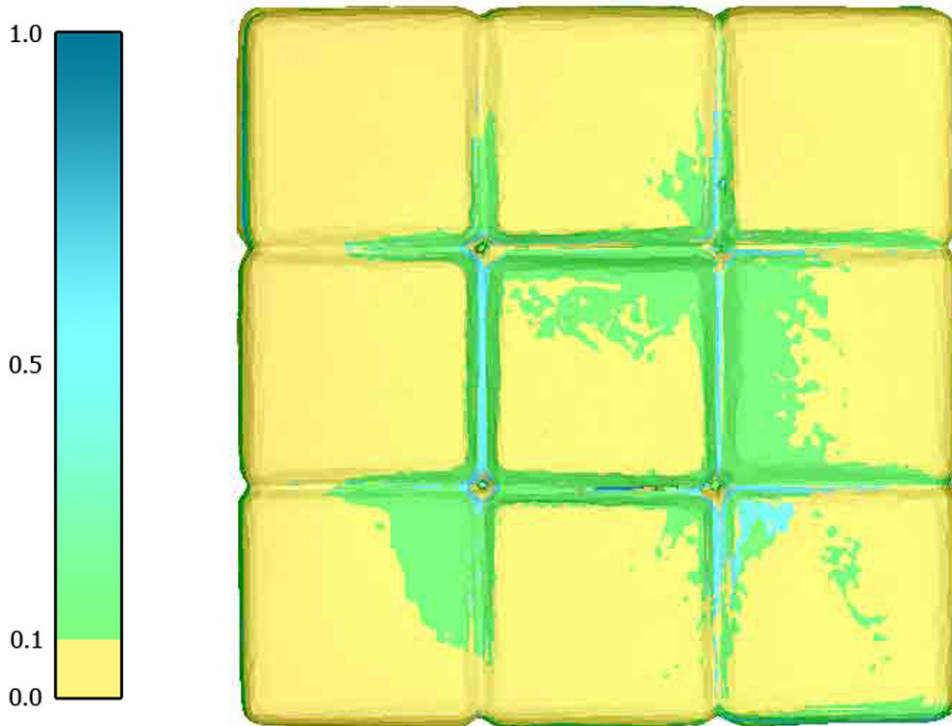
Figure 4.11: *Uncertainty mapping. Color coding of an isosurface of specimen one by mapping interpolated uncertainty on the surface. Blue regions depict high uncertainty, yellow regions low uncertainty. Green areas depict elevated uncertainty.*

Uncertainty Visualization

Visualizing uncertainty allows an overall estimation on the quality of a scan. We present two different approaches, uncertainty mapping and direct volume rendering (DVR) of probability data demonstrated on the Rubik's cube. Using uncertainty mapping (Figure 4.11), the interpolated spatial uncertainty values of a considered class are color-coded on the evaluated surface. Blue regions depict high uncertainty, while yellow indicates low uncertainty. The green areas depict elevated uncertainty due to minor deformations and smaller artefacts (scattered radiation between the subsections of each level in the cube).

Figure 4.12 shows a direct volume rendering (DVR), color-coding the probabilities using a color and opacity transfer function. Green depicts high probabilities of 95 - 100%, while red depicts probabilities down to 50%. Elevated uncertainty is clearly visible in the bottom section due to greyvalue modifications caused by the specimen holder. In Figure 4.1 semitransparent axial, sagittal and frontal cross-sections are used as cutting planes on the probability volume in order to evaluate uncertainties in the internal structure.
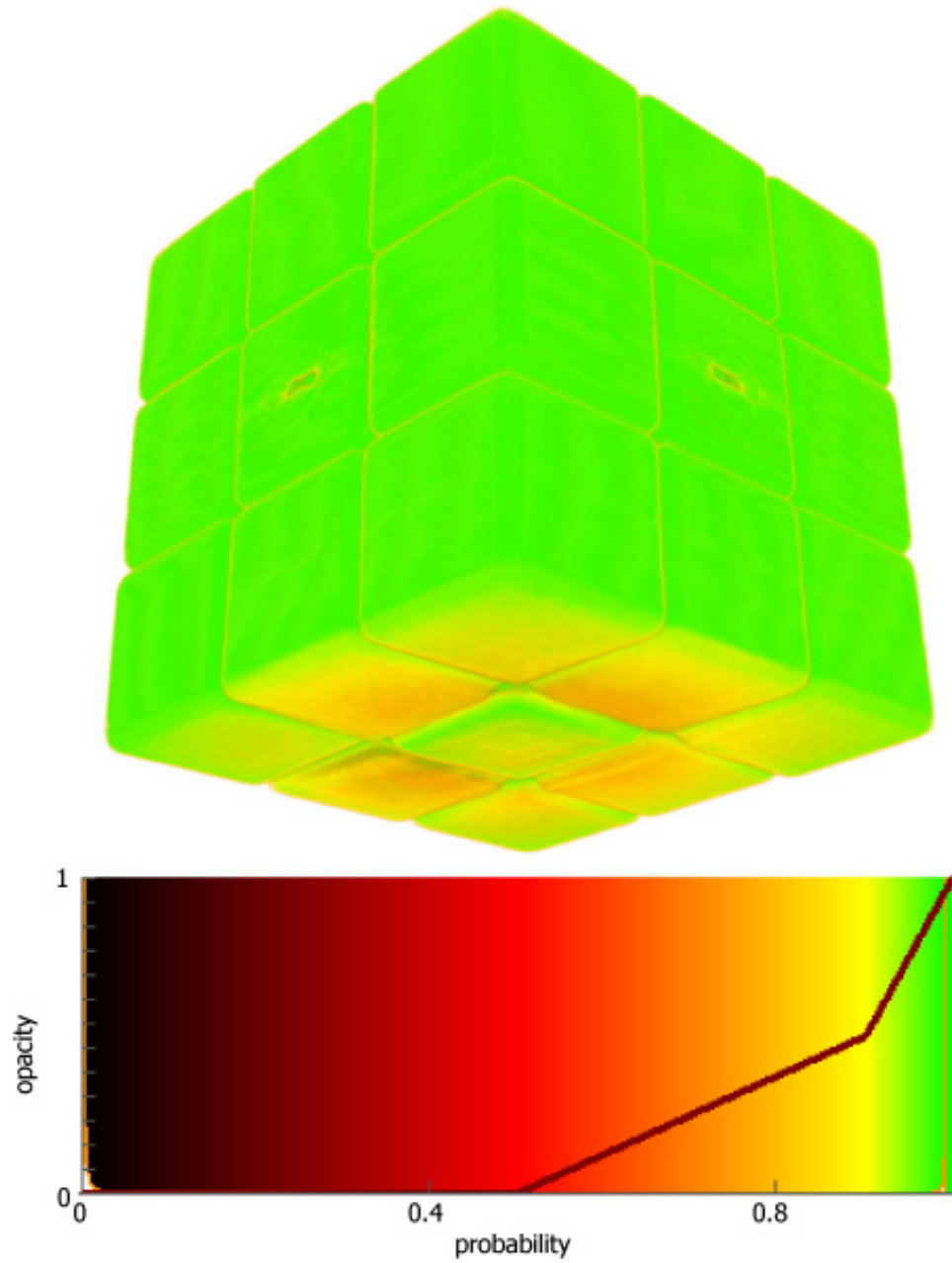
Figure 4.12: *Direct volume rendering (DVR) of the probability dataset of specimen one using color and opacity transfer functions. The bottom area with elevated uncertainty is due to greyvalue modifications caused by the specimen holder.*

4.5 Summary

A novel pipeline for statistical analysis of multi-material components is presented applying dual source / dual exposure approach of dual energy computed tomography for artefact reduction. After prefiltering and multi-scan fusion, the statistical analysis is carried out by computing probability volumes using a local histogram analysis technique.

The accuracy and the applicability of the pipeline has been discussed using a testpart and a real world component. Results of the extracted PDFs, posteriors, and the corresponding probability volumes are depicted by means of 2D and 3D actual/nominal comparisons, a comparison between binary and fuzzy segmentation, and two different methods of uncertainty visualization. The approach is applicable in the area of fuzzy segmentations, metrology applications, and uncertainty visualization.

*Ideas are like rabbits. You get a couple and learn how to
handle them, and pretty soon you have a dozen.*

John Steinbeck

5

Summary and Conclusions

INDUSTRIAL 3DCT is currently on the edge of advancing from a non destructive testing method, providing uncalibrated subjective characterizations for visual inspection, to a fully standardized means of dimensional measurement for industrial use. Partially industrial 3DCT is already used for dimensionally measuring complex components. Especially in the area of first part inspections of new components, an increasing number of companies is benefitting from industrial 3DCT. Sporadically the first pioneers start using 3DCT for quality control in the production process.

However, 3DCT faces limitations in the measurement precision, the disadvantages of artefacts especially of multi-material components, and the fact that there are no applicable standards available. These disadvantages prevent 3DCT from being considered as substitute or extension for conventional means of dimensional measurement, *e.g.*, optical or tactile coordinate measurement. Currently, there is a lot of research activity to overcome the drawbacks of 3DCT in the area of dimensional measurement. A standard draft for computed tomography in industrial metrology is developed in the VDI/VDE-GMA Fachausschuss 3.33 "Computertomographie in der industriellen Messtechnik" of the association of german engineers (VDI) by a board of manufacturers, research institutes, and users. As long as this standard is not available companies hesitate to integrate 3DCT into quality control.

Considering the equipment technology of industrial 3DCT, flat panel detectors with lower pixel pitch, increased resolution and improved X-ray detection layers are in development. 2000 by 2000 pixel detectors are finally becoming popular and applicable in terms of computational effort for every day use. Furthermore, novel X-ray sources with high power targets are in development, which allow a reduction of the focal spot size while keeping or even increasing the used X-ray power. Also the precision of linear bearings and rotary tables is continuously enhanced.

In the area of software development, several groups are working on novel high speed reconstruction algorithms with enhanced precision. Artefact reduction for multi-material specimens is a topic, which many research groups are currently working on. Also data evaluation is a field of research, where a whole body of work is in progress.

This thesis presents different methodologies in the area of data evaluation of industrial 3DCT scans. The main focus lies in the development of novel pipelines or workflows for specific industrial problems including comparisons to common methods. In order to provide insight into the extracted results, convenient and easy to understand means of visualization are used and evaluated. In the presented methods four main aspects concerning metrology using industrial 3DCT are emphasized:

Robust surface extraction of homogeneous industrial workpieces is of great importance for actual/nominal comparison and dimensional measurement tasks. It is one of the major aims in the area of metrology using industrial 3DCT. Concerning this topic a novel pipeline for industrial workpiece segmentation is presented, allowing automated and effective actual/nominal comparisons. The introduced method offers the possibility to extract reproducible surface models from artefact-distorted volumes.

Artefact reduction via dual energy CT. Dual energy CT (DECT) is a new method to reduce artefacts, especially in the case of multi-material components by taking two 3DCT datasets with complementary strengths and weaknesses into account. In this context the dual source / dual exposure technique of DECT is exploited to combine the benefits and advantages of a low and a high energy scan of a specimen. Using DECT, it is possible to integrate the low energy (LE) dataset's accuracy with the high energy (HE) dataset's robustness. Therefore DECT facilitates dimensional measurement of artefact-affected datasets from multi-material components.

Surface extraction of multi-material components is an upcoming research area. A major part of new industrial components consist of multiple materials, at least after assembly. When scanning multi-material components, severe artefacts distort datasets and prevent from reliable dimensional measurements. In this work this problem is addressed by a novel workflow for dimensional measurements of multi-material industrial components, allowing a reproducible and robust surface extraction.

Statistical analysis of multi-material components A novel pipeline for statistical analysis of multi-material components is presented applying DECT for artefact reduction. After prefiltering and multi-scan fusion,

the statistical analysis is carried out by computing probability volumes using a local histogram analysis technique. The accuracy and the applicability of the pipeline has been discussed using a testpart and a real world component. Application areas can be found in fuzzy segmentations, metrology applications and uncertainty visualization.

In all of the above mentioned aspects, this thesis presents novel contributions. While in the area of robust surface extraction for homogeneous materials in the meantime commercial tools are already available, artefact reduction as well as surface extraction of multi-material components is not yet in industrial use. Especially these areas require further research in order to refine and optimize the generated results. The statistical analysis of multi-material components in the field of industrial 3DCT is an interesting approach of calculating and visualizing uncertainty of 3DCT datasets. Using this approach, the expected uncertainty of dimensional measurement features or surface models is extracted directly from the underlying datasets. If companies get an impression of the quality of their datasets and in which areas they have to expect an elevated uncertainty, their awareness of the advantages but also of the pitfalls of 3DCT will increase.

What is still missing for the integration of metrology using 3DCT into quality control are the following open issues. The 3DCT data evaluation methods are typically strongly related to the used parameter settings in the underlying algorithms. Therefore, a reproducible and fully automated evaluation of dimensional measurement features without user interaction would increase the acceptance of 3DCT in this particular field. Furthermore the achieved precision of dimensional measurements using 3DCT is usually lower and and in several cases insufficient compared to the precision achieved using common tools. Finally a standard is needed for metrology using 3DCT, which will open the doors to a fully integration into industrial quality control.

A classic is something that everybody wants to have read and nobody wants to read.

Marc Twain

Bibliography

[Bar07]   BARTSCHER M. (Ed.):.   *Geometriebestimmung mit industrieller Computertomographie - Aktueller Stand und Entwicklungen* (Braunschweig, Germany, 2007), no. PTB-Bericht PTB-F-54, Physikalisch Technische Bundesanstalt Braunschweig und Berlin, Wirtschaftsverlag NW.

[BK02]   BISCHOFF S., KOBBELT L.:   Isosurface reconstruction with topology control.   In *Pacific Conference on Computer Graphics and Applications* (2002), pp. 246–255.

[BPS97]   BAJAJ C. L., PASCUCCI V., SCHIKORE D. R.:   The contour spectrum.   In *IEEE Visualization 1997* (1997), pp. 167–173.

[Bur84]   BURT P. J.:   The pyramid as a structure for efficient computation.   In *Multiresolution Image Processing and Analysis* (1984), Rosenfeld A., (Ed.), Springer-Verlag, pp. 6–35.

[Car08]   CARL ZEISS INDUSTRIELLE MESSTECHNIK GMBH: Calypso - visual metrology. `http://www.zeiss.de/calypso`, December 16th 2008.

[COG95]   CHIPMAN L., ORR Y., GRAHAM L.: Wavelets and image fusion. In *Proceedings of the International Conference on Image Processing* (1995), vol. 3, pp. 248–251.

[DHS00]   DUDA R. O., HART P. E., STORK D. G.: *Pattern Classification (2nd Edition)*. Wiley-Interscience, 2000.

[Fuc98]   FUCHS T.:   *Strahlaufhärtungskorrekturen in der Computer-Tomographie*. PhD thesis, Friedrich Alexander Universität Erlangen Nürnberg, 1998.

[Geo08]   GEOMAGIC, INC.: Geomagic: The magic of making it simple.
            `http://www.geomagic.com`, December 16th 2008.

[Gib98]   GIBSON S. F. F.: Constrained elastic surface nets: generating
            smooth surfaces from binary segmented data. In *MICCAI '98:
            Proceedings of the First International Conference on Medical Image
            Computing and Computer-Assisted Intervention* (1998), pp. 888–
            898.

[GR04]   GRIGORYAN G., RHEINGANS P.: Point-based probabilistic
            surfaces to show surface uncertainty. In *IEEE Transactions
            on Visualization and Computer Graphics* (2004), vol. 10, Issue 5,
            pp. 564–573.

[HDL*04]   HOPKINS F., DU Y., LASIUK B., ABRAHAM A., BASU S.: An-
            alytical correcions for beam-hardening and object scatter in
            volumetric computed tomography systems. In *Proceedings of
            WCNDT* (2004), pp. 462–468.

[Her79]   HERMAN G. T.: Correction for beam hardening in computed
            tomography. In *Physics in Medicine and Biology* (1979), vol. 24,
            pp. 81–106.

[HKG07]   HEINZL C., KASTNER J., GRÖLLER E.: Surface extraction
            from multi-material components for metrology using dual en-
            ergy CT. In *IEEE TVCG (Proceedings of IEEE Visualization 2007)*
            (2007), vol. 13, Issue 6, pp. 1520–1527.

[HKKG06]   HEINZL C., KLINGESBERGER R., KASTNER J., GRÖLLER E.:
            Robust surface detection for variance comparison. In *Pro-
            ceedings of Eurographics/IEEE-VGTC Symposium on Visualisa-
            tion* (2006), pp. 75–82.

[HKMG08]   HEINZL C., KASTNER J., MÖLLER T., GRÖLLER E.: Statisti-
            cal analysis of multi-material components using dual energy
            CT. In *Proceedings of the 13th International Fall Workshop Vision,
            Modeling, and Visualization 2008* (2008), pp. 179–188.

[HMMW03]   HUANG R., MA K.-L., MCCORMICK P., WARD W.: Visualiz-
            ing industrial CT volume data for nondestructive testing ap-
            plications. In *VIS '03: Proceedings of the 14th IEEE Visualization
            2003 (VIS'03)* (2003), pp. 547–554.

[Hsi03]   HSIEH J.: *Computed Tomography: Principles, Design, Artifacts
            and Recent Advances*. SPIE-The International Society for Opti-
            cal Engineering, 2003.

[IDO*06]   IOVEA M., DULIU O., OAIE G., RICMAN C., MATEIASI G.: Dual-energy computer tomography and digital radiography investigation of organic and inorganic materials. In *Proceedings of European Conference on Non Destructive Testing (CD-ROM)* (2006).

[IOR*05]   IOVEA M., OAIE G., RICMAN C., MATEIASI G., NEAGU M., SZOBOTKA S., DULIU O.: Dual energy x-ray computer axial tomography and digital radiography investigation of cores and other objects of geological interest. In *32nd International Geological Congress* (2005).

[ISNC03]   IBANEZ L., SCHROEDER W., NG L., CATES J.: *The ITK Software Guide*, first ed. Kitware, Inc., `http://www.itk.org`, 2003.

[Kas05]   KASPERL S.: *Qualitätsverbesserungen durch referenzfreie Artefaktreduzierung und Oberflächennormierung in der industriellen 3D-Computertomographie*. PhD thesis, Technische Fakultät der Universität Erlangen Nürnberg, 2005.

[Kas08]   KASTNER J. (Ed.):. *Industrielle Computertomograpie - Zerstörungsfreie Werkstoffprüfung, 3D-Materialcharakterisierung und Geometriebestimmung* (Wels, Austria, 2008), Upper Austrian University of Applied Sciences - Wels Campus, Shaker Verlag.

[KD98]   KINDLMANN G., DURKIN J. W.: Semi-automatic generation of transfer functions for direct volume rendering. In *IEEE Symposium on Volume Visualization (VV '98)* (1998), pp. 79–86.

[KKH01]   KNISS J., KINDLMANN G., HANSEN C.: Interactive volume rendering using multi-dimensional transfer functions and direct manipulation widgets. In *VIS '01: Proceedings of the conference on Visualization '01* (Washington, DC, USA, 2001), IEEE Computer Society, pp. 255–262.

[KSBS04]   KASTNER J., SCHLOTTHAUER E., BURGHOLZER P., STIFTER D.: Comparison of x-ray computed tomography and optical coherence tomography for characterisation of glass-fibre polymer matrix composites. In *Proceedings of World Conference on Non Destructive Testing* (2004), pp. 71–79.

[KUS*05]   KNISS J., UITERT R. V., STEPHENS A., LI G., TASDIZEN T.: Statistically quantitative volume visualization. In *IEEE Visualization 2005* (2005), pp. 287–294.

[LC87]   LORENSEN W., CLINE H.: Marching cubes: a high resolution 3D surface construction algorithm. In *ACM SIGGRAPH Computer Graphics* (1987), vol. 21, pp. 163–169.

[Lev88]   LEVOY M.: Display of surfaces from volume data. In *IEEE Computer Graphics and Applications* (1988), vol. 8, Issue 3, pp. 29–37.

[LFLH07] LI H., FU C.-W., LI Y., HANSON A.: Visualizing large-scale uncertainty in astrophysical data. In *IEEE TVCG (Proceedings of IEEE Visualization 2007)* (2007), vol. 13, Issue 6, pp. 1640–1647.

[LLY06]   LUNDSTRÖM C., LJUNG P., YNNERMAN A.: Local histograms for design of transfer functions in direct volume rendering. In *IEEE TVCG (Proceedings of IEEE Visualization 2006)* (2006), vol. 12, Issue 6, pp. 1570–1579.

[LMM94]   LI H., MANJUNATH B., MITRA S.: Multisensor image fusion using the wavelet transform. In *Image Processing, 1994. Proceedings. ICIP-94., IEEE International Conference* (1994), vol. 1, pp. 51–55.

[LON*04] LEWIS J. J., O'CALLAGHAN R. J., NIKOLOV S. G., BULL D. R., CANAGARAJAH C. N.: Region-based image fusion using complex wavelets. In *Proceedings of the Seventh International Conference on Information Fusion* (2004), vol. I, pp. 555–562.

[MHV*01] MATTES D., HAYNOR D. R., VESSELLE H., LEWELLEN T., EUBANK W.: Nonrigid multimodality image registration. In *Medical Imaging 2001: Image Processing* (2001), pp. 1609–1620.

[MHV*03] MATTES D., HAYNOR D. R., VESSELLE H., LEWELLEN T., EUBANK W.: PET-CT image registration in the chest using free-form deformations. In *IEEE Transactions in Medical Imaging* (2003), vol. 22, pp. 120–128.

[NHBC01] NIKOLOV S., HILL P., BULL D., CANAGARAJAH C.: *Wavelets in Signal and Image Analysis*, vol. 19. Kluwer Academic Publishers, 2001, ch. Wavelets for image fusion, pp. 213–244.

[OB07]   OEHLER M., BUZUG T. M.: A sinogram-based metal artifact suppression strategy for transmission computed tomography. In *Geometriebestimmung mit industrieller Computertomographie, PTB-Bericht PTB-F-54* (Braunschweig, 2007), pp. 255–262.

[OF03]   OSHER S., FEDKIW R.: *Level Set Methods and Dynamik Implicit Surfaces*. Springer-Verlag, 2003.

[OHP81]   OLSON E. A., HAN K. S., PISANO D. J.: CT reprojection polychromaticity correction for three attenuators. In *IEEE Transactions on Nuclear Science* (1981), vol. 28, pp. 3628–3640.

[Ots79]   OTSU N.: A threshold selection method from grey level histograms. In *IEEE Transactions on Systems, Man, and Cybernetics* (1979), vol. 9, pp. 62–66.

[PM90]   PERONA P., MALIK J.: Scale-space and edge detection using anisotropic diffusion. In *IEEE Transactions on Pattern Analysis and Machine Intelligence* (1990), vol. 12, pp. 629–639.

[PX04]   PETROVIC V., XYDEAS C.: Gradient-based multiresolution image fusion. In *IEEE Transactions on Image Processing* (2004), vol. 13, pp. 228–237.

[RD06]   REBUFFEL V., DINTEN J.-M.: Dual-energy x-ray imaging: benefits and limits. In *Proceedings of European Conference on Non Destructive Testing (CD-ROM)* (2006).

[RJ99]   RHEINGANS P., JOSHI S.: Visualization of molecules with positional uncertainty. In *Data Visualization '99* (1999), E.Gröller, H.Löffelmann,, W.Ribarsky, (Eds.), Springer-Verlag Wien, pp. 299–306.

[RLBS03]   RHODES P. J., LARAMEE R. S., BERGERON R. D., SPARR T. M.: Uncertainty visualization methods in isosurface rendering. In *Eurographics 2003* (2003), Chover M., Hagen H.,, Tost D., (Eds.), pp. 83–88.

[ŠD02]   ŠRÁMEK M., DIMITROV L. I.: Segmentation of tomographic data by hierarchical watershed transform. *Journal of Medical Informatics and Technologies*, 3 (2002), 161–169.

[Set99]   SETHIAN J.: *Level Set Methods and Fast Marching Methods: Evolving Interfaces in Computational Geometry, Fluid Mechanics, Computer Vision and Materials Sciences*, second ed. Cambridge University Press, 1999.

[SHP08]   SCHMITT R., HAFNER P., POLLMANNS S.: Kompensation von Metallartefakten in tomographischen Aufnahmen mittels Bilddatenfusion. In *Proceedings of Industrielle Computertomographie, Fachtagung 2008* (2008), pp. 117–122.

[Sie08]   SIEMENS: Home > healthcare > products & solutions > detection and diagnosis > computed tomography > dual source CT > somatom definition. `http://www.medical.siemens.com`, December 16th 2008.

[SML04]   SCHROEDER W., MARTIN K., LORENSEN B.: *The Visualization Toolkit - An Object-Oriented Approach To 3D Graphics*, third ed. Kitware, Inc., `http://www.vtk.org`, 2004.

[SS00]   SIMON M., SAUERWEIN C.: Cone beam tomography for quality control and rapid product development. In *Insight* (2000), vol. 42, Number 10, pp. 651–655.

[Ste05]   STEINBEISS H.:   *Dimensionelles Messen mit Mikro-Computertomographie*.   PhD thesis, Technische Universität München, 2005.

[SZH98]   STALLING D., ZÖKLER M., HEGE H.: Interactive segmentation of 3D medical images with subvoxel accuracy. In *Computer Assisted Radiology and Surgery* (1998), Lemke H., Inamura K., Vannier M.,, Farman A., (Eds.), pp. 137–142.

[tHR94]   TER HAAR ROMENY B. M.: *Geometry Driven Diffusion in Computer Vision. Series on Computational Imaging and Vision*. Kluwer Academic Publishers, Dordrecht, the Netherlands, 1994.

[TM04]   TZENG F.-Y., MA K.-L.:   A cluster-space visual interface for arbitrary dimensional classification of volume data. In *IEEE/EG Symposium on Visualization* (2004), pp. 17–24.

[Vol04]   VOLUME GRAPHICS GMBH: *VG Studio Max 1.2 - User's Manual*. Volume Graphics GmbH, Heidelberg, Germany, 2004.

[VS91]   VINCENT L., SOILLE P.: Watersheds in digital spaces: An efficient algorithm based on immersion simulations. In *IEEE Transactions on Pattern Analysis and Machine Intelligence* (1991), vol. 13, Issue 6, pp. 583–598.

[WB98]   WHITAKER R. T., BREEN D. E.: Level-set models for the deformation of solid objects. In *The third international workshop on implicit surfaces* (1998), pp. 19–35.

[Whi00]   WHITAKER R. T.: Reducing aliasing artifacts in iso-surfaces of binary volumes. In *VVS '00: Proceedings of the 2000 IEEE Symposium on Volume Visualization* (2000), pp. 23–32.

[Wik08a]   WIKIPEDIA: Metrology.   `http://en.wikipedia.org/wiki/Metrology`, December 16th 2008.

[Wik08b]   WIKIPEDIA: Quality. `http://en.wikipedia.org/wiki/Quality`, December 16th 2008.

[WPL96]   WITTENBRINK C. M., PANG A. T., LODHA S. K.: Glyphs for visualizing uncertainty in vector fields. In *IEEE Transactions on Visualization and Computer Graphics* (1996), vol. 2, Issue 3, pp. 266–279.

[WWH99]   WILLIAMS M. L., WILSON R. C., HANCOCK E. R.: Deterministic search for relational graph matching. *Pattern Recognition 32*, 7 (1999), 1255–1271.

When I examine myself and my methods of thought, I come to the conclusion that the gift of fantasy has meant more to me than any talent for abstract, positive thinking.

Albert Einstein

Curriculum Vitae

Personal data

Christoph Heinzl
born on August 16th, 1978
in Schärding, Austria.

Altschwendt 84/6
4721 Altschwendt, Austria
Phone: +43 (0) 699 11050166
eMail: c.heinzl@gmail.com

Education

2004 -	Institute of Computer Graphics and Algorithms, Vienna University of Technology, Austria
	Doctoral studies (computer science).
	Dissertation in the area of "Analysis and Visualization of Industrial CT Data"
	Supervisor: Prof. Eduard Gröller.
21.07.2000	Graduation with merit
	Diplom Ingenieur für Automatisierte Anlagen und Prozesstechnik (FH)
	Thesis: "Implementation of a Windows NT - based Visualization System for Plasma Nitriding Plants"
	Advisor: Prof.(FH) Daniel Heim
1996–2000	Upper Austrian University of Applied Sciences - Wels Campus, Austria
	Master's studies (Automation Engineering).
1988–1996	Grammar School
	Schärding, Austria
1984–1988	Elementary school
	Raab, Austria

Work experience

03/2005–	Research Associate in the area of Analysis and Visualization of Industrial CT Data
	Project acquisition and management of the SimCT and the SmartCT project
	University of Applied Sciences, Wels Campus, Wels, Austria
11/2002–09/2004	Software design engineer
	Project planning, development, implementation and startup of control and visualization systems for silicon-on-insulator (SOI), temporary and plasma bonders
	EVG EV Group E. Thallner GmbH, Austria
02/2000–02/2002	Automation Engineer
	Project planning, supervision and implementation of customer-specific software projects in the area of plasma nitriding plants, central building control systems and small power stations
	RÜBIG Gmbh & Co KG, Austria

Professional Activities

» Project management:
  › SimCT - Simulation eines industriellen 3D Computertomografen (360k€)
  › SmartCT - Genaue Geometriebestimmung und Interfacecharakterisierung von Multimaterialbauteilen mittels Kegelstrahl - CT (388k€)

» Organizing Committee Member:
  › Industrielle Computertomografie Fachtagung, Zerstörungsfreie Werkstoffprüfung, 3D-Materialcharakterisierung und Geometriebestimmung, 27-28th February 2008, Wels, Austria, 2008
  › CT Day, Computed Tomography and 3D-Analysis for Science and Industry, 19th September 2008, Wels, Austria, 2006

» Reviewing:
  › Eurographics 2008, 29th annual conference of the European Association for Computer Graphics
  › Elsevier Nondestructive Testing and Evaluation (NDT & E)

Publications

2008:

» **C. Heinzl**, J. Kastner, T. Möller, E. Gröller, Statistical Analysis of Multi-Material Components using Dual Energy CT, In *Proceedings of Vision, Modeling, and Visualization, Konstanz, Germany, 2008*, pp. 179–188

» **C. Heinzl**, J. Kastner, E. Gröller, High Dynamic Range Imaging for Contrast Enhancement of X-ray images, In *Proceedings of IEEE Workshop on X-Ray Micro Imaging of Materials, Devices, and Organisms, Dresden, Germany, 2008*

» J. Kastner, F. Pfeifer, **C. Heinzl**, R. Freytag, Pipeline for Evaluation of CT-data of Glass-fibre Reinforced Plastics, In *Proceedings of DGZFP DACH Conference, St. Gallen, Switzerland, 2008*

» **C. Heinzl**, J. Kastner, E. Gröller, Geometriebestimmung von Multimaterialbauteilen und reproduzierbare Oberflächenextraktion, In *Proceedings of Industrielle Computertomografie Fachtagung 2008, Wels, Austria*, pp. 151–156

2007:

» **C. Heinzl**, J. Kastner, E. Gröller, Surface Extraction from Multi-Material Components for Metrology using Dual Energy CT, In *IEEE Transactions on Visualization and Computer Graphics (Proceedings of IEEE Visualization 2007), Vol. 13, No. 6, 2007*, pp. 1520–1528

» **C. Heinzl**, J. Kastner, B. Georgi, H. Lettenbauer, Comparison of surface detection methods to evaluate cone-beam computed tomography data for three dimensional metrology, In *International Symposium on Digital industrial Radiology and Computed Tomography, Lyon, France, 2007*

» J. Kastner, D. Salaberger, **C. Heinzl**, Measurement of microparts and reproducible surface extraction, In *PTB-Report Geometriebestimmung mit industrieller Computertomographie - Aktueller Stand u. Entwicklungen, Braunschweig, Germany, 2007*, pp. 181–192

2006:

» **C. Heinzl**, J. Kastner, E. Gröller, Reproducible Surface Extraction for Variance Comparison in 3D Computed Tomography, In *European Conference on Non-Destructive Testing, Berlin, Germany, 2006*

» **C. Heinzl**, R. Klingesberger, E. Gröller, J. Kastner, Robust Surface Detection for Variance Comparison and Dimensional Measurement, In *Proceedings of Eurographics/IEEE VGTC Symposium on Visualization, Lissabon, Portugal, 2006*, pp. 75–83

2000:

» **C. Heinzl**, Implementierung eines Windows NT - basierenden Visualisierungssystems für Plasmanitrieranlagen, *Diploma Thesis, Upper Austrian University of Applied Sciences, Wels Campus, 2000*

Awards and Honors

| November 2007 | Nominee Best Application Paper Award at IEEE Visualization 2007, Sacramento USA |

Programming skills

» Visual C++, Visual C#, Visual Basic, Java, MATLAB
» MFC, QT, .NET
» ITK, VTK, CUDA, OpenGL
» HTML, SQL
» Industrial robot programming (GencoBot), Siemens S5/S7, FPGA/PAL programming

Additional skills / attended courses and seminars

» Wie konzipiert man gute F&E Förderanträge
» Nationale und europäische Förderungen im F&E Bereich
» Wirkungsvoll Kommunizieren: Ein persönlichkeitsorientiertes Gesprächstraining
» Windows XP und .Net Technologien im Bereich der Automatisierungstechnik
» Cimplicity HMI Human Machine Interface
» Qualitätsmanagement Fachkraft QMF-TÜV
» Geprüfter Wertanalytiker

Languages

» German (mother-tongue)
» English (fluently)
» French (fair)
» Italian (passive)

Hobbies

» My family
» Mountain-biking
» Hiking
» Traveling
» IT and Technology in General

December 2008